Microstructural analysis using X-ray diffraction

M. Leoni

Università di Trento – Facoltà di Ingegneria
Dipartimento di Ingegneria dei Materiali e Tecnologie Industriali
via Mesiano, 77 – 38050 Trento
E-mail: Matteo.Leoni@unitn.it

Microstructural Analysis using XRD

- X-ray diffraction & materials science/engineering?
  a case of study: materials for gas turbines

- X-ray diffraction for microstructure analysis:
  - what can we measure/obtain?
  - some practical applications

- Additional topics
  - the mathematics behind…

Materials in Engineering

A case of study: materials for jet propulsion engines

Materials in Engineering

A case of study: materials for jet propulsion engines

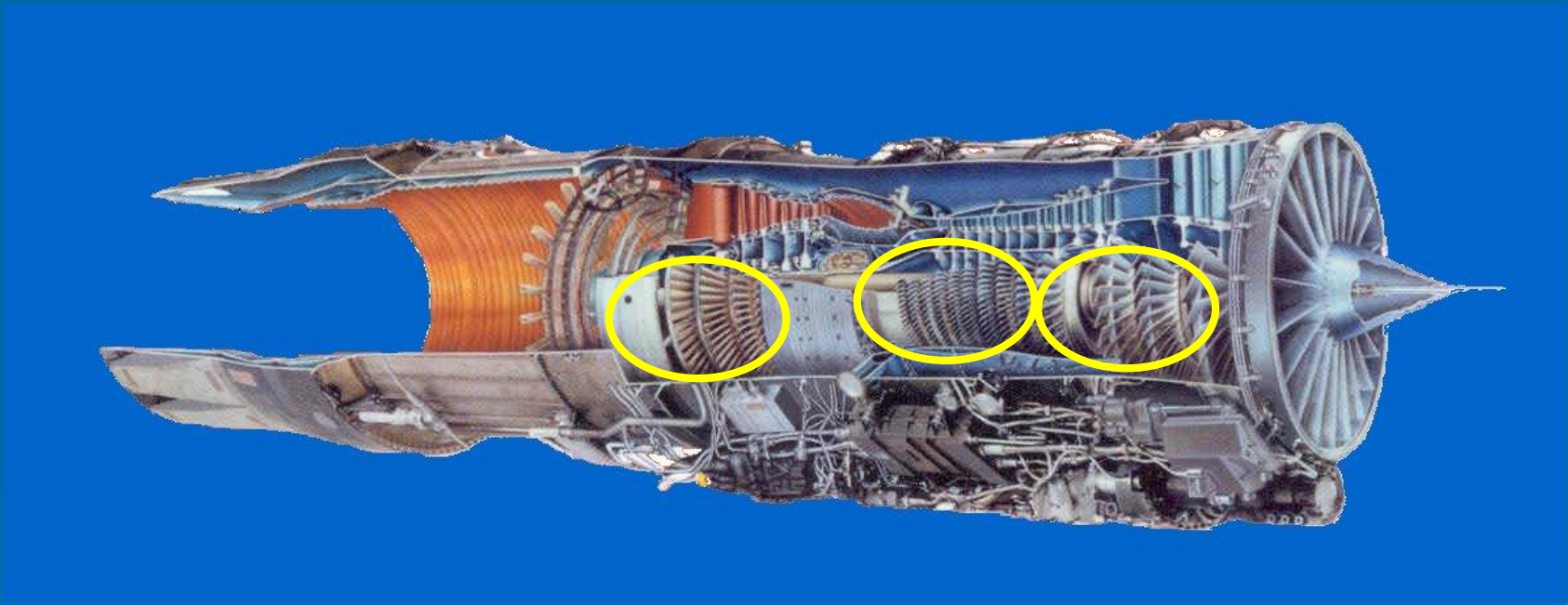

Turbine blades and vanes in different stages

Materials in Engineering

A case of study: materials for jet propulsion engines

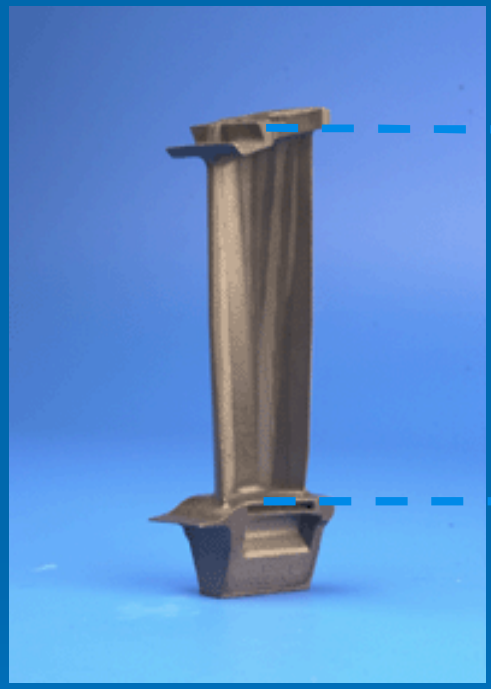

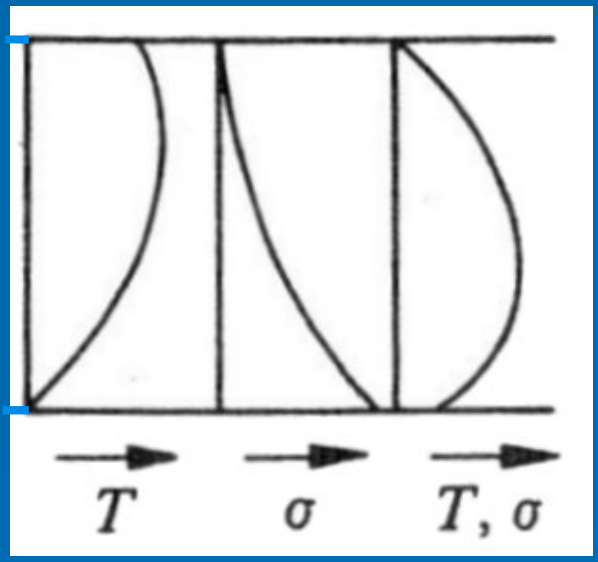

Blades and vanes used in different stages of gas turbines must withstand high mechanical and thermal solicitations in hostile atmosphere (corrosion/oxidation)

The quest for high temperature in gas turbines

High temperature: why?

Power and Fuel efficiency are determined by service temperature

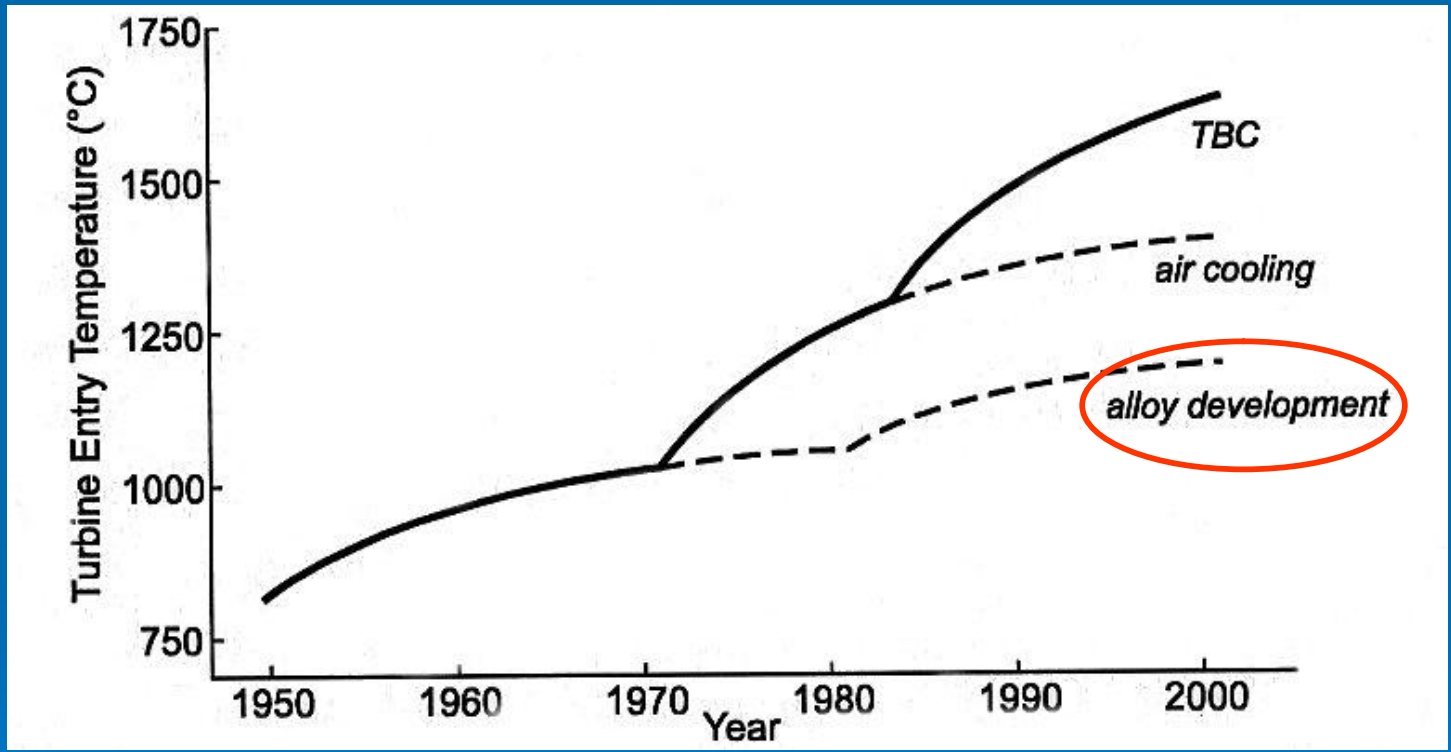

- Jumbo-jet engines: 110°C higher Tgas **à** 20% increase in thrust
- Industrial GTs: 55°C higher gas temp. **à** 8-13% more power
  1-4 % higher efficiency

Turbine blade strengthening phase

The γ-γ' microstructure of Ni-based Superalloys

γ-γ' Ni_3Al

Yield stress vs. temperature

In most metals and alloys, yield stress (s_y) and elastic modulus drastically fall with the temperature

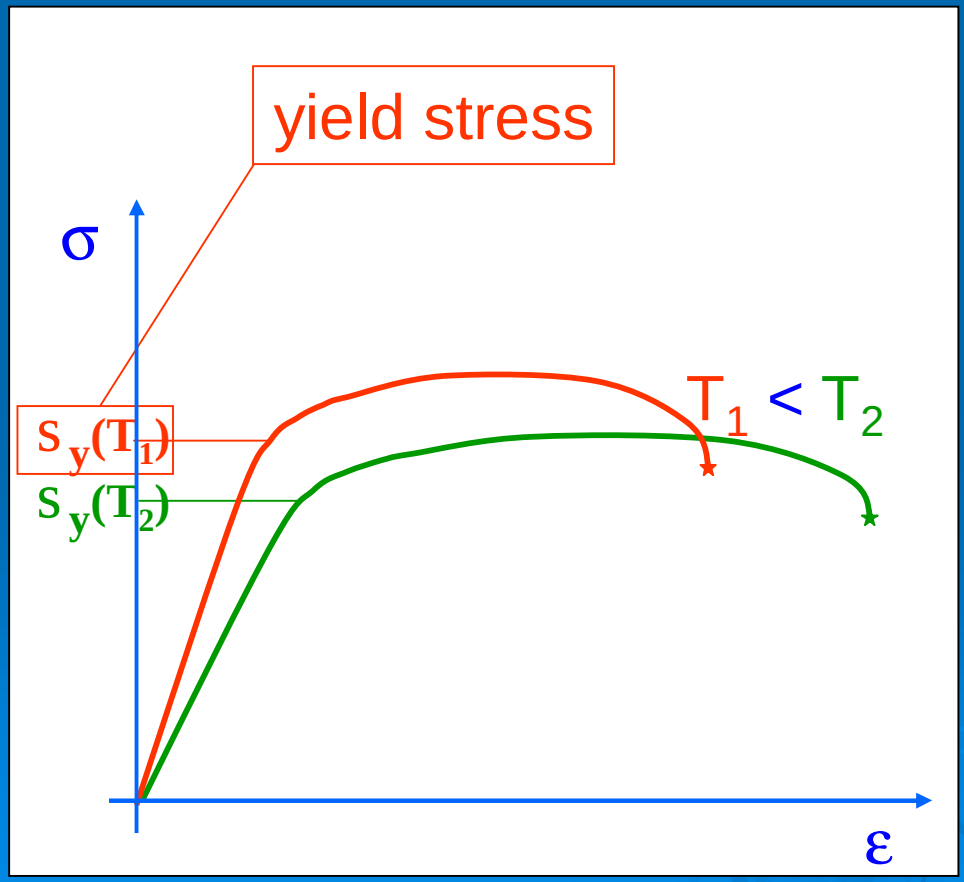

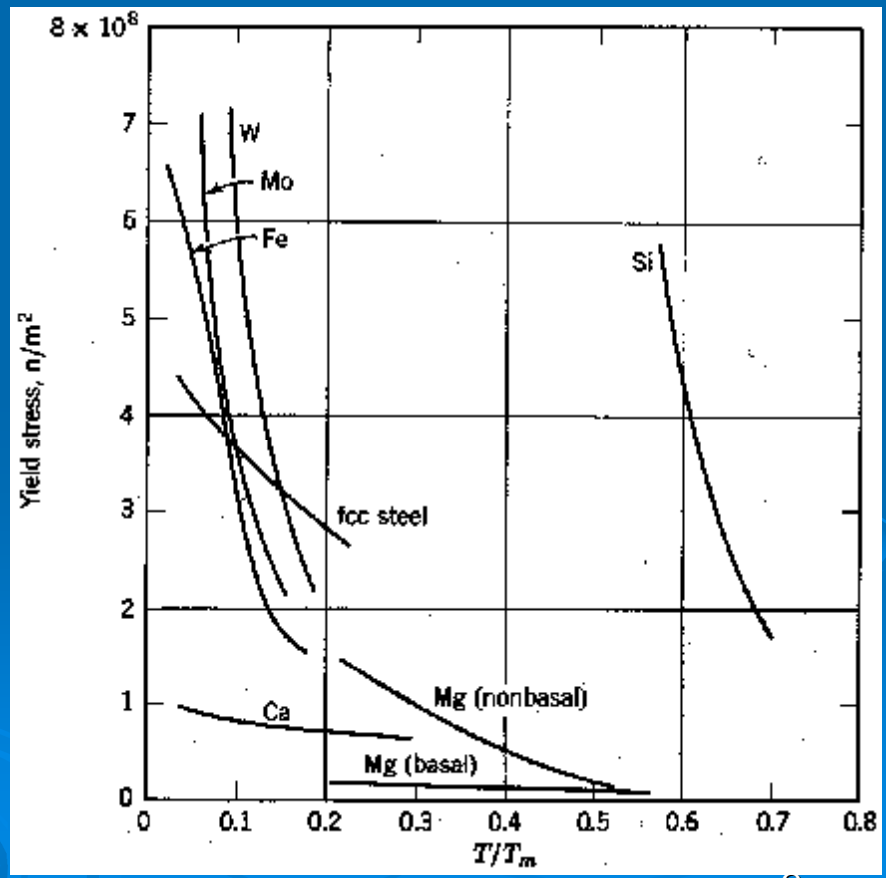

Yield stress anomaly in $L1_2$ phases

Some Ni_3Al-type phases ($L1_2$) exhibit a *Yield Stress anomaly* :

σ_y increases with the temperature

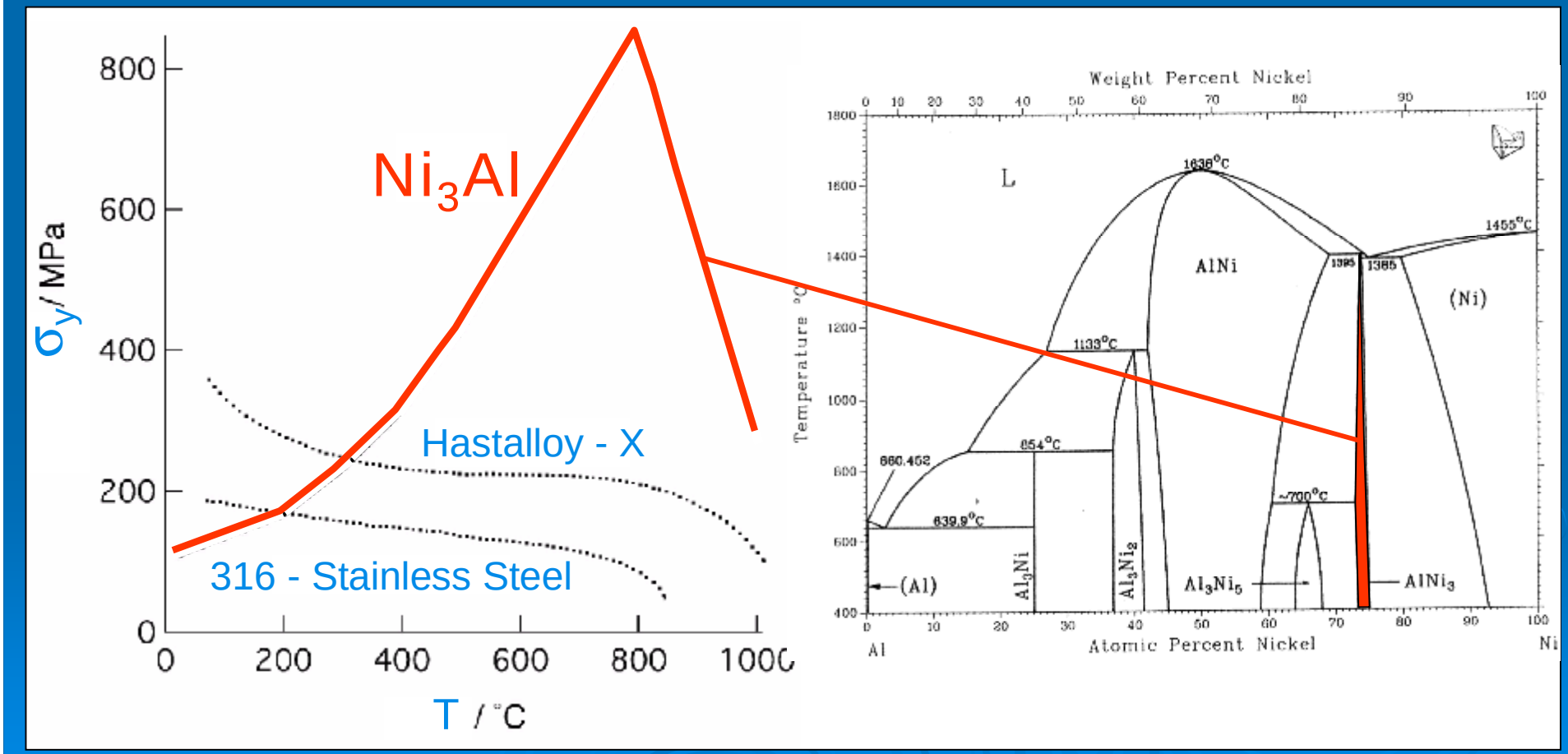

Order-disorder transformation

G=H-TS

Ordered
Low T

T_c

Disordered
High T

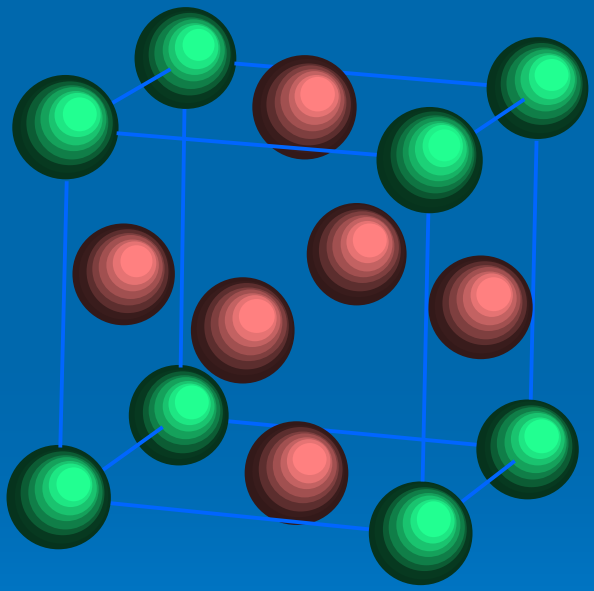

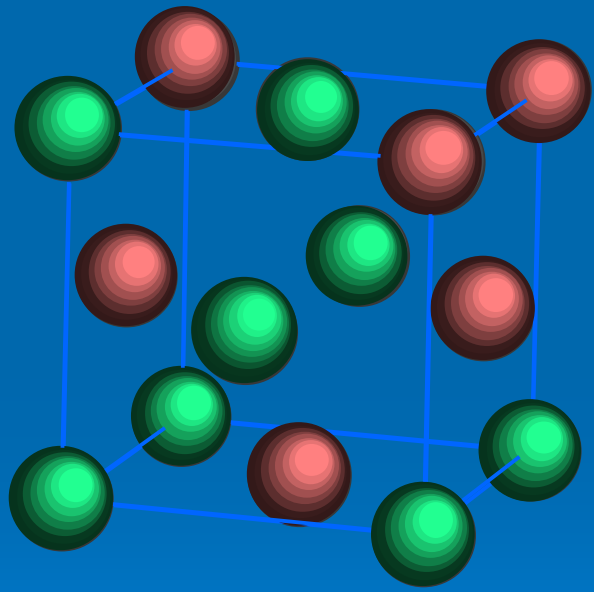

$L1_2$ (Pm3m)

fcc (Fm-3m)

Al

Ni

(0.75) Ni - (0.25) Al

TEM - SAD in γ–γ'

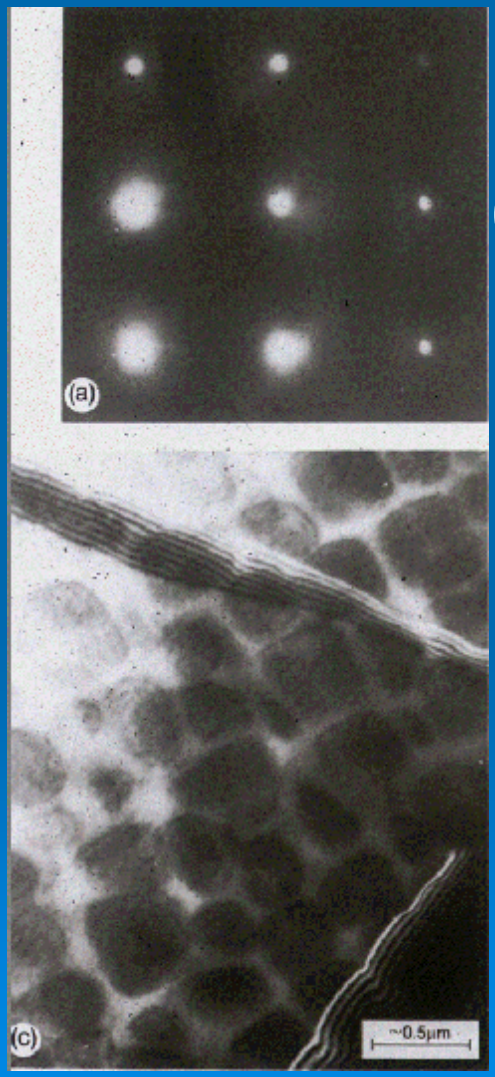

γ-Ni_3Al
(disordered)

γ'-Ni_3Al
(ordered)

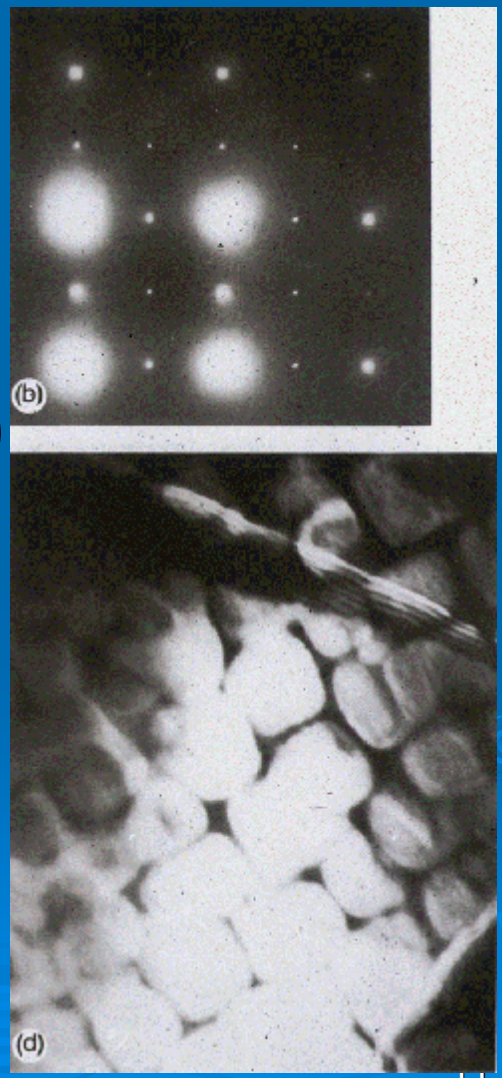

TEM - SAD in γ–γ'

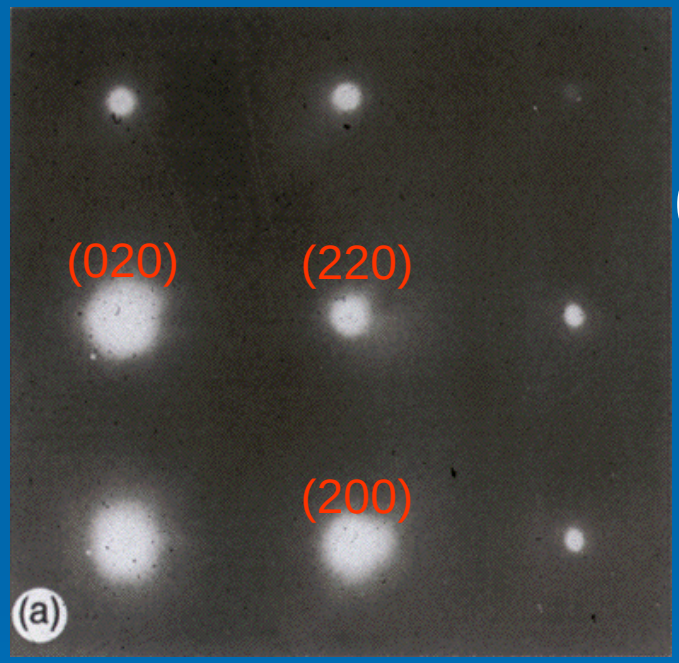

γ-Ni_3Al
(disordered)

superstructure reflections

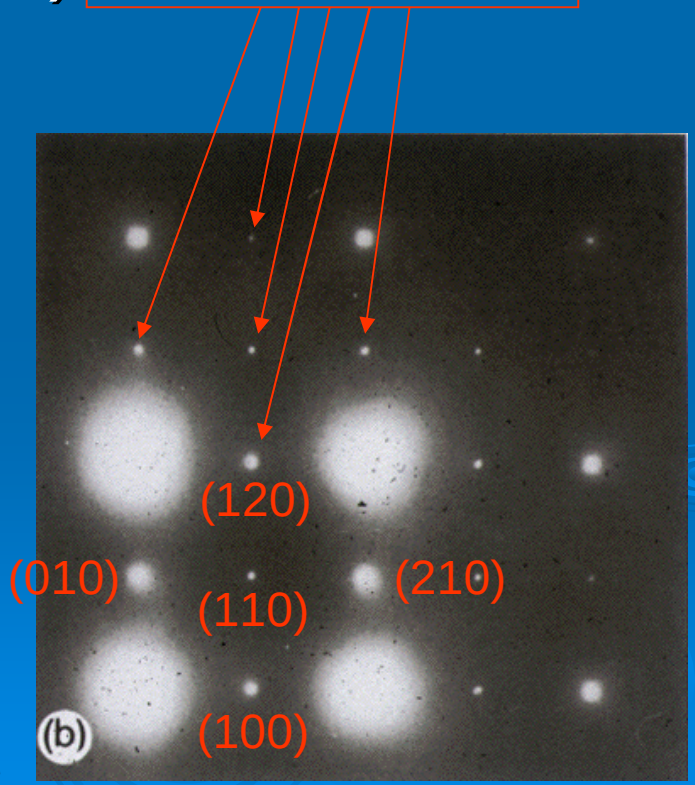

γ'-Ni_3Al
(ordered)

Dislocations in Ni_3Al

Dislocations in Ni_3Al superlattice (b=a<101>) are unstable and dissociate in 4 Shockley partials (b=a/6<211>) in the {111} planes.

Partials are separated by two Complex Stacking Faults (CSF) limiting an Anti-Phase Domain (APD) region

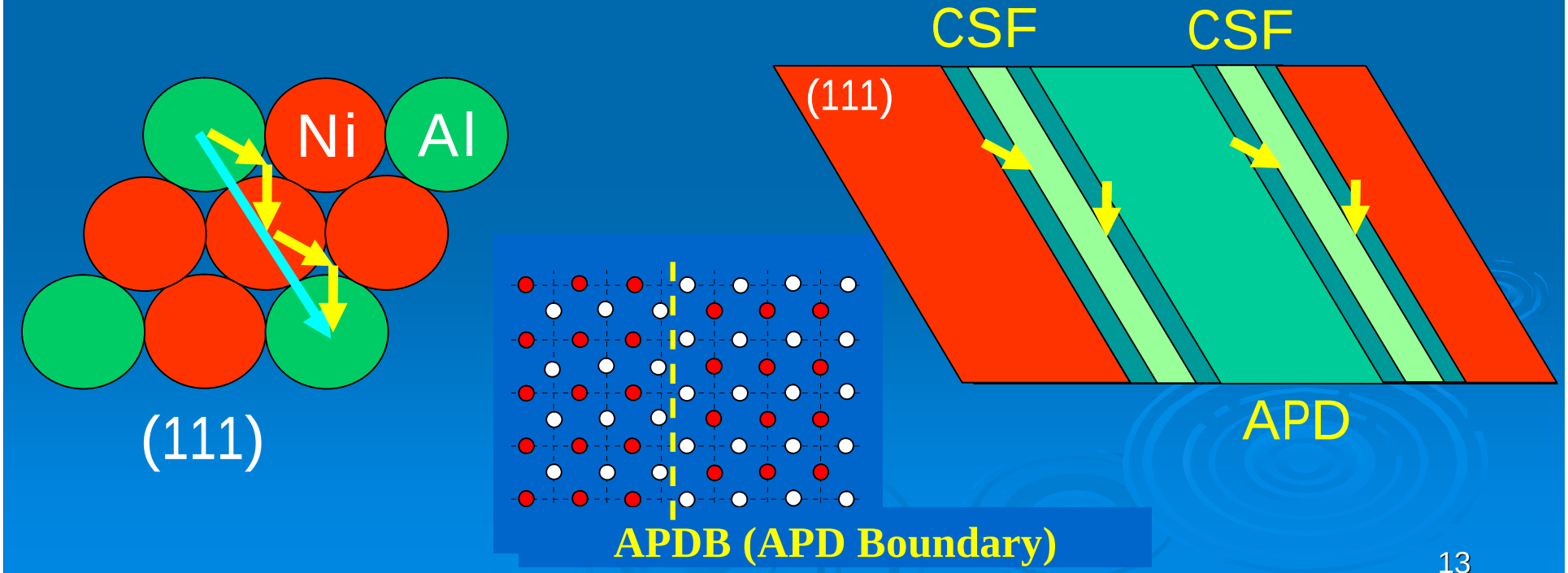

Kear-Wilsdorf lock

APBs have a lower energy on {100} than on {111}. Thermal activation allows cross slip leading to a non-gliding (sessile) configuration

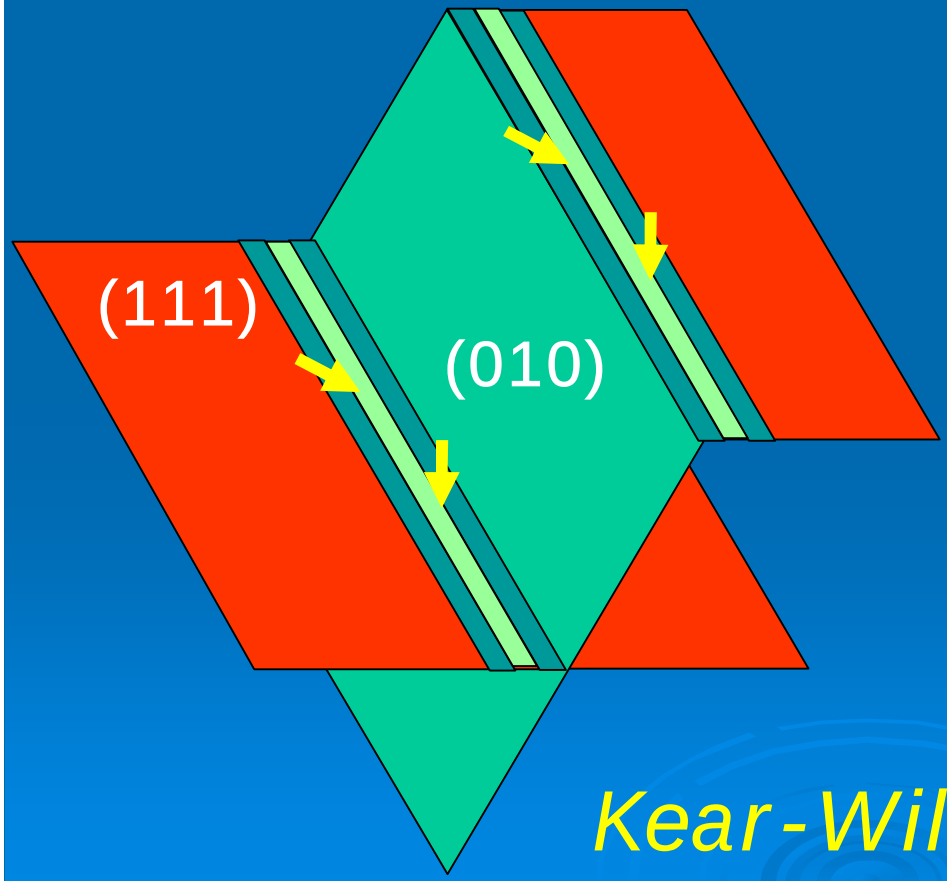

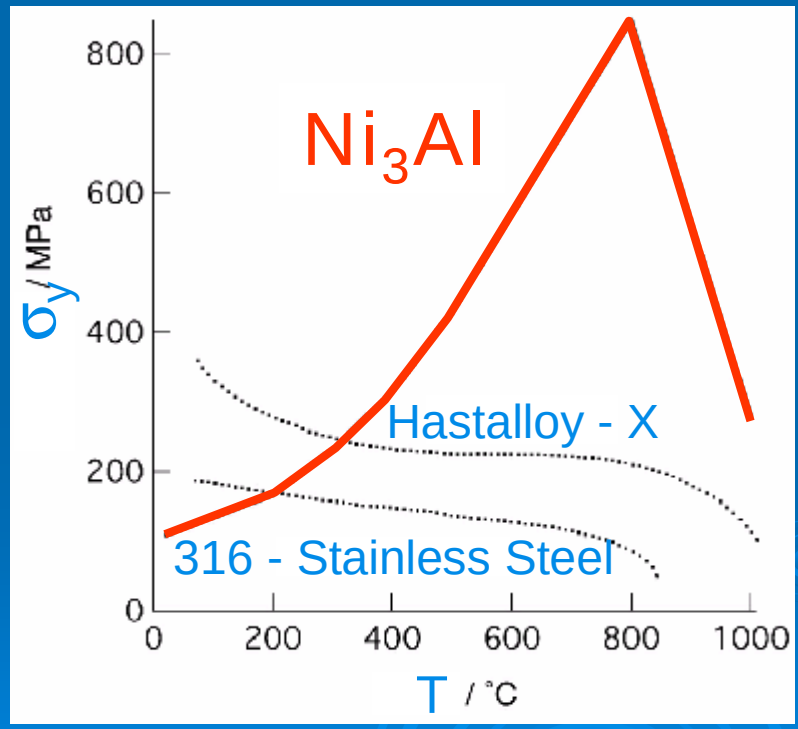

Kear-Wilsdorf lock

XRD Line Profile Analysis

How can we study dislocations, faulting, APB and other features of the microstructure ?

X-ray diffraction Line Profile Analysis

XRD LPA is ideally suited to determine size/shape of crystalline domains and content of lattice defects (e.g., dislocations, faulting, APDs)

The quest for high temperature in gas turbines

High temperature: why?

Power and Fuel efficiency are determined by service temperature

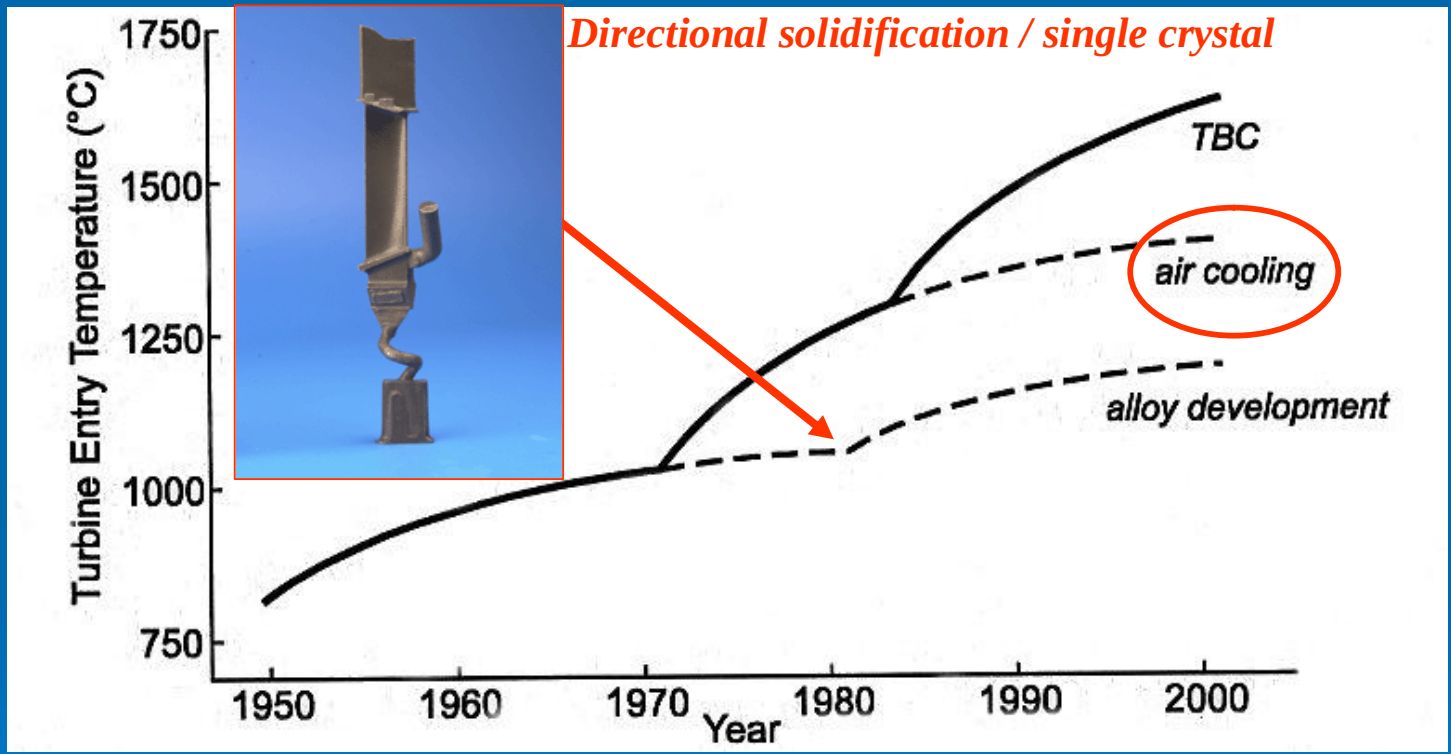

High temperature materials in GT

Power and Fuel efficiency are determined by service temperature

Gas turbine achieve high temperatures by air-cooling

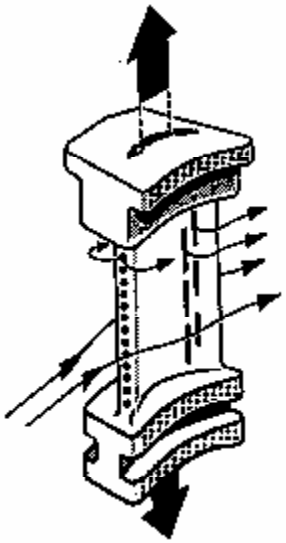

Spera & Grisaffe, Proc. 1972 Gas Turbine Matls. Conf., Wash, DC, p. 99.

The quest for high temperature in gas turbines

Power and Fuel efficiency are determined by service temperature

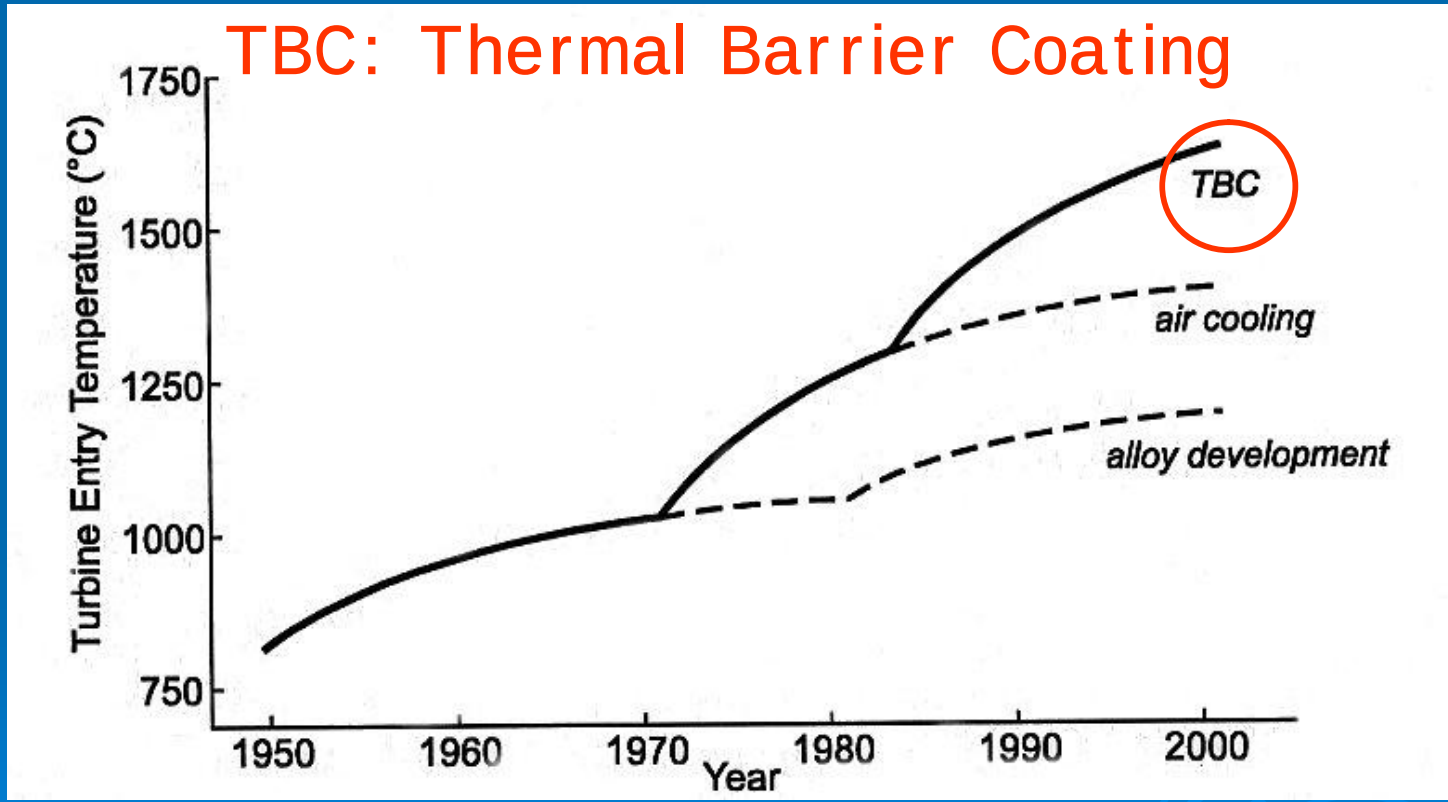

Thermal Barrier Coatings (TBCs)

Blade performance improved by means of ceramic TBCs

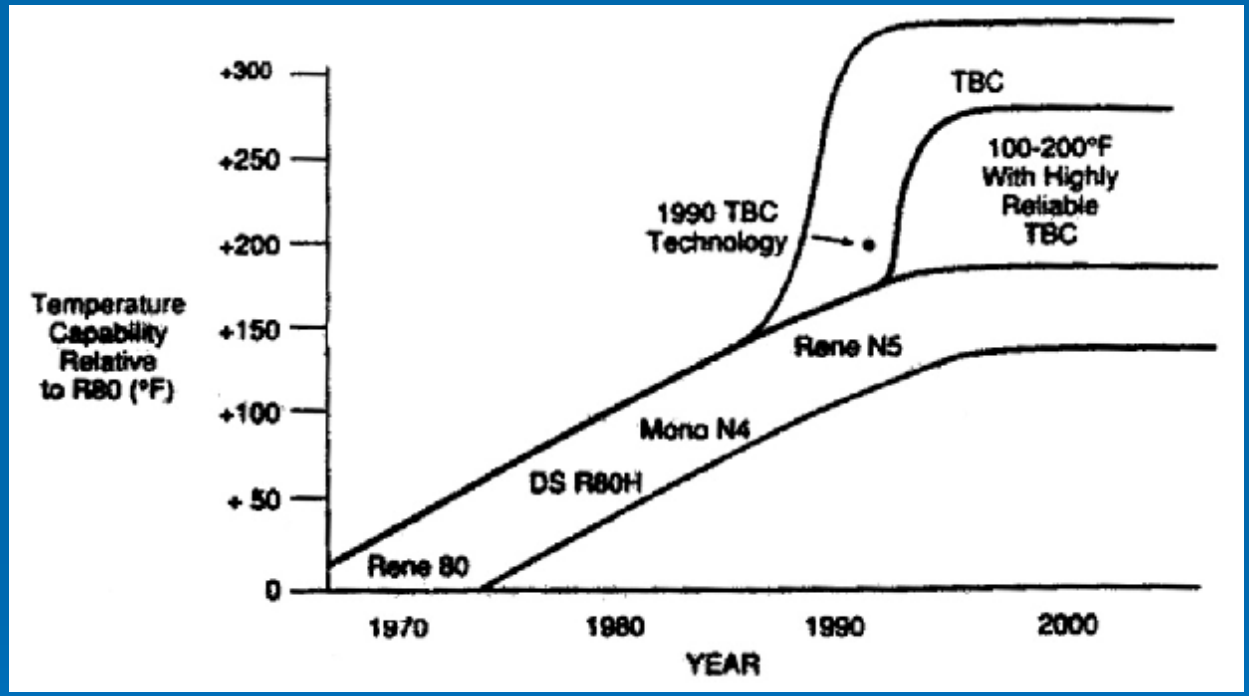

- TBCs on blades **à** 10^7 gals fuel savings per year (250 plane air fleet)
- In aviation engines: **à** 3x longer life (at 1000-3000 US$ per blade)

(data from *R.L. Jones*, formerly at Naval Research Laboratory, USA)

TBC Materials: stabilised zirconia

Partially Stabilised-Zirconia (PSZ) (t/t') or Stabilised Zirconia (c)

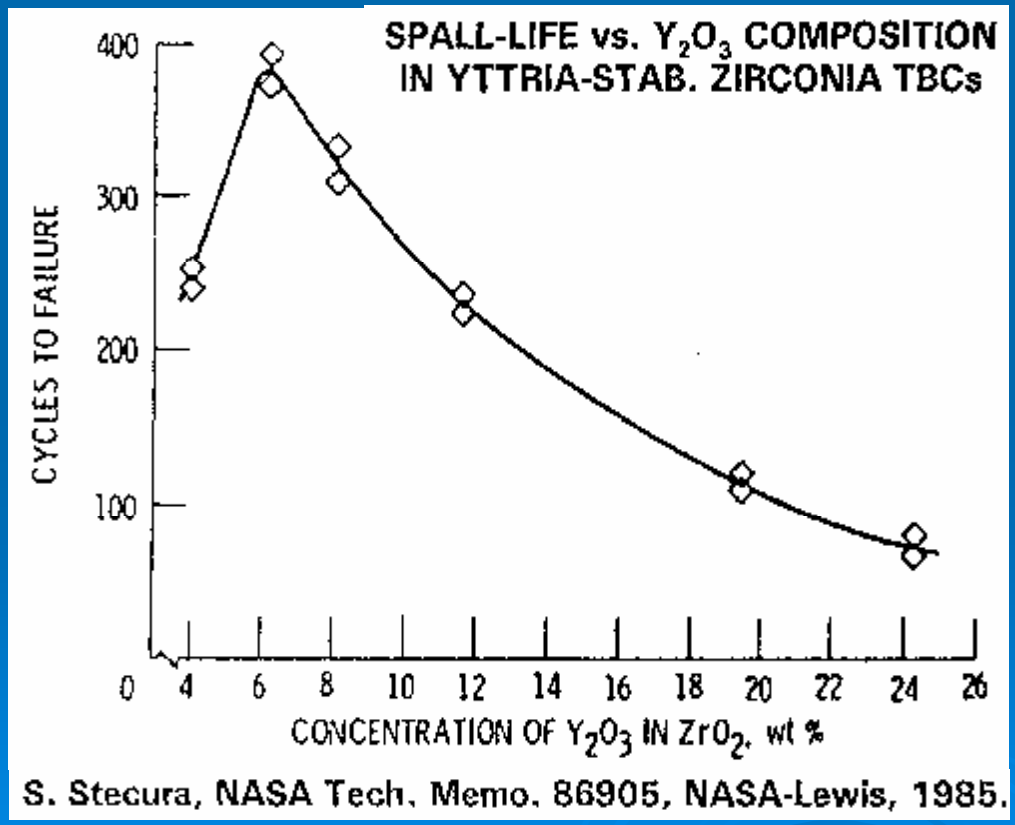

S. Stecura, NASA Tech. Memo. 86905, NASA-Lewis, 1985.

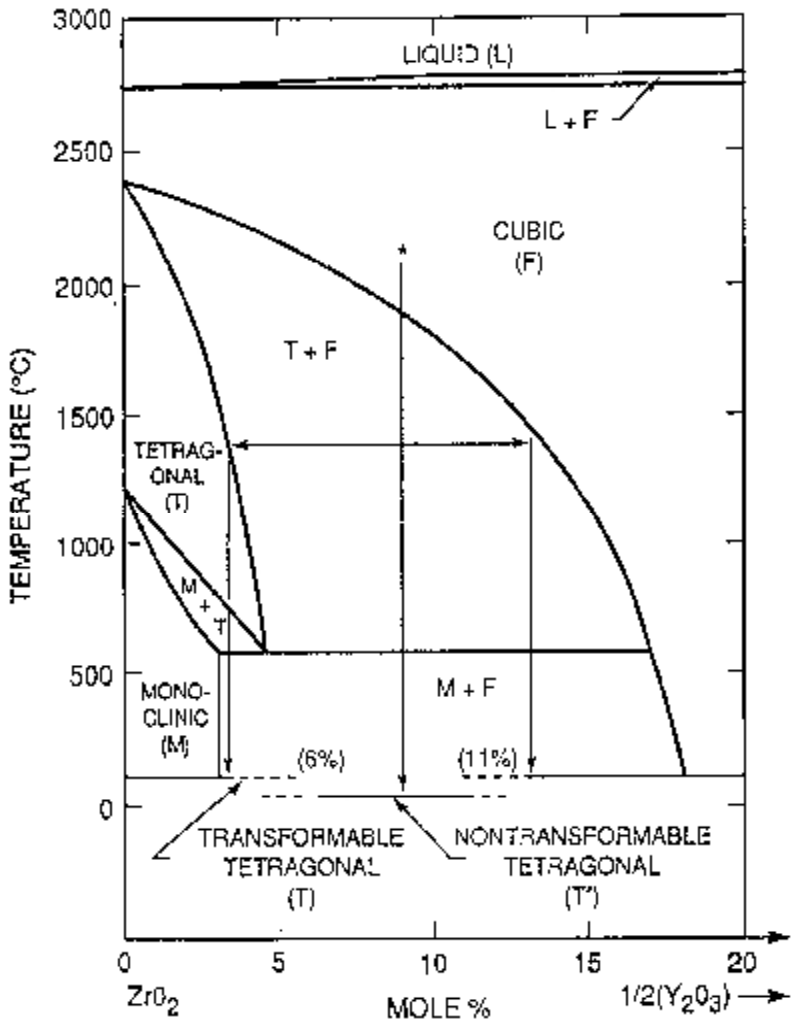

Y_2O_3-ZrO_2

Partially-stabilised Zirconia TBC

Quantitative Phase Analysis (QPA) of Zirconia polymorphs by X-ray Diffraction (XRD) (*Rietveld method*)

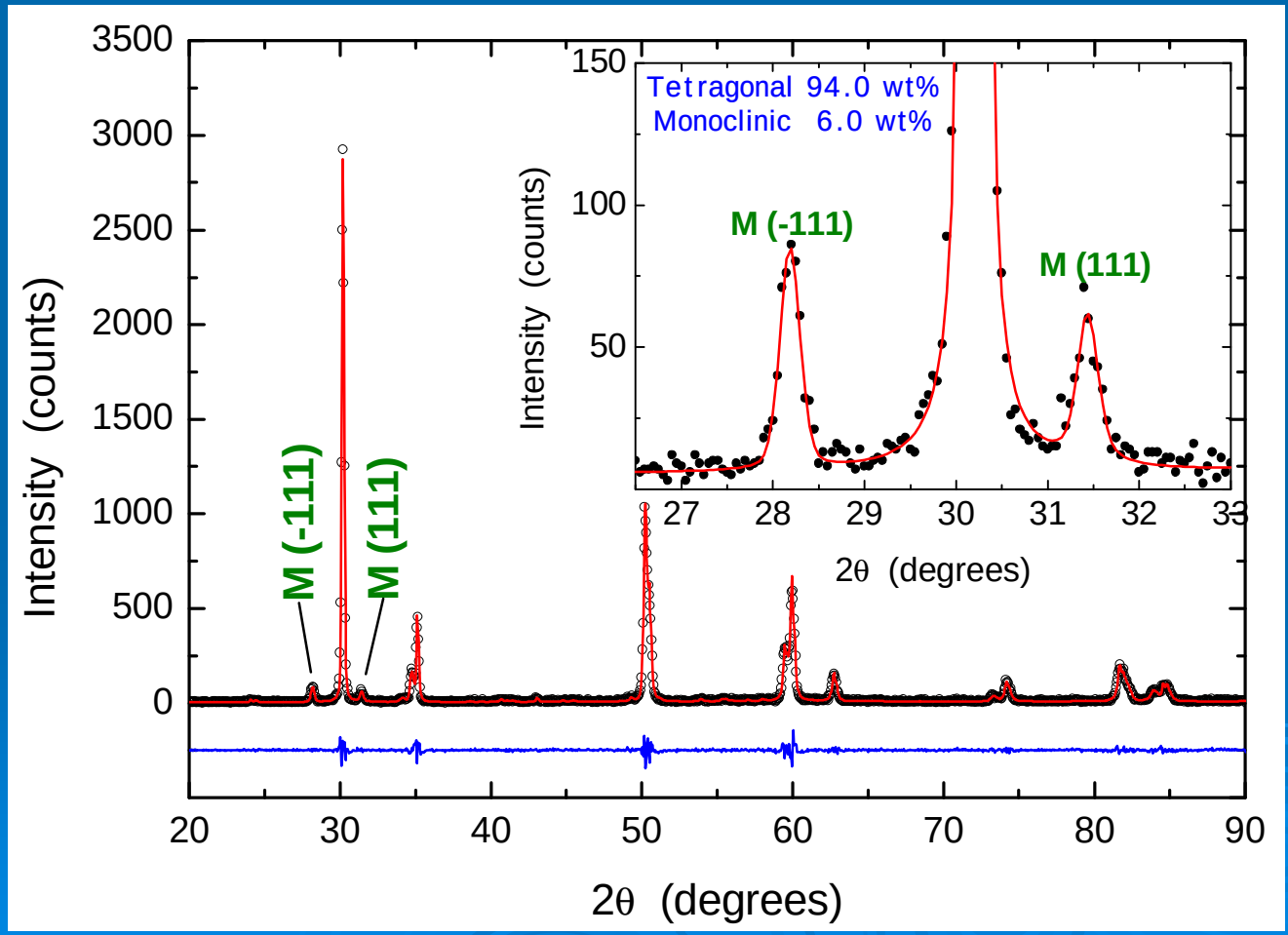

Air Plasma Spray (APS)

Plasma Torch

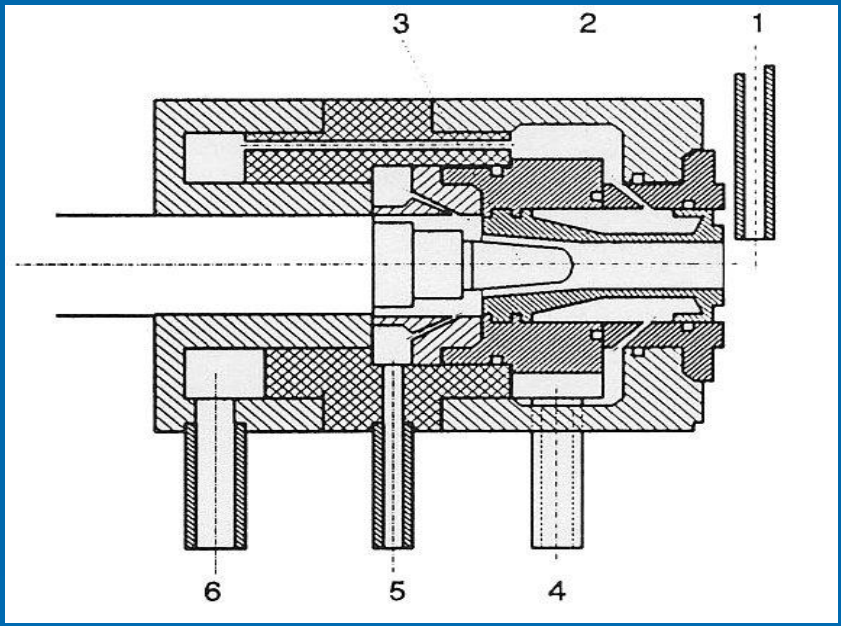

1. Powder injection
2. Tubolar anode
3. Catode
4,6. Cooling system
5. Plasma gas inlet

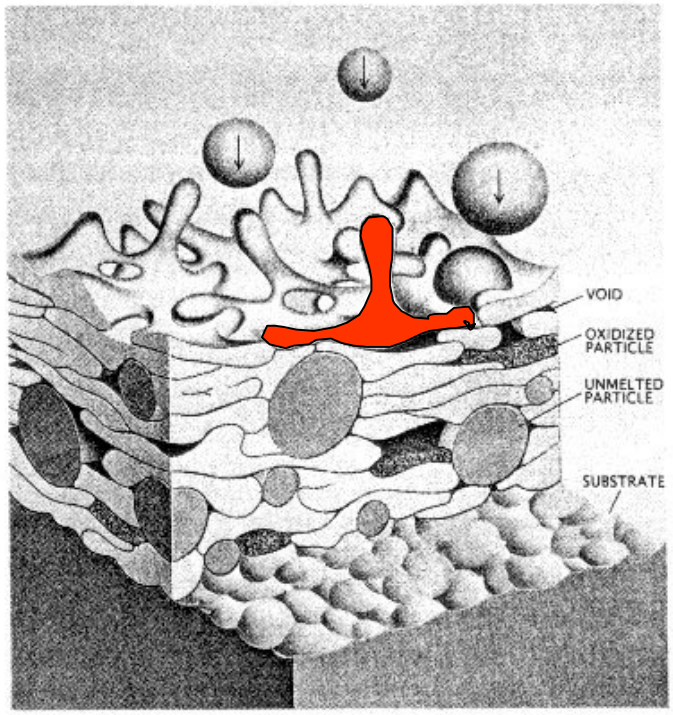

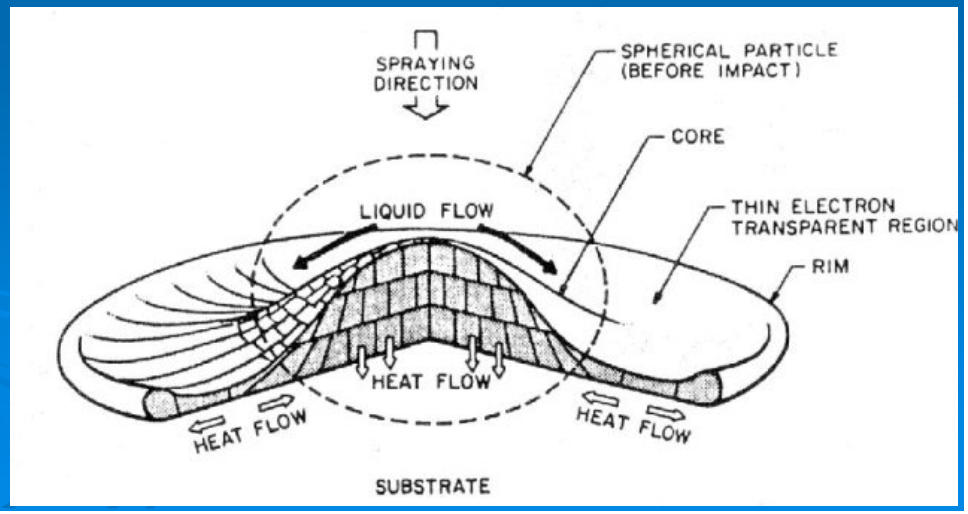

New TBCs: APS vs. EB-PVD

State-of-art: APS (Plasma Spray)

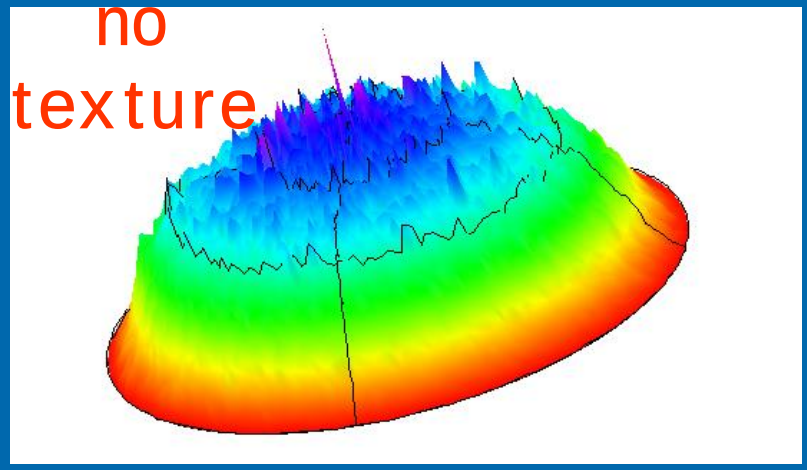

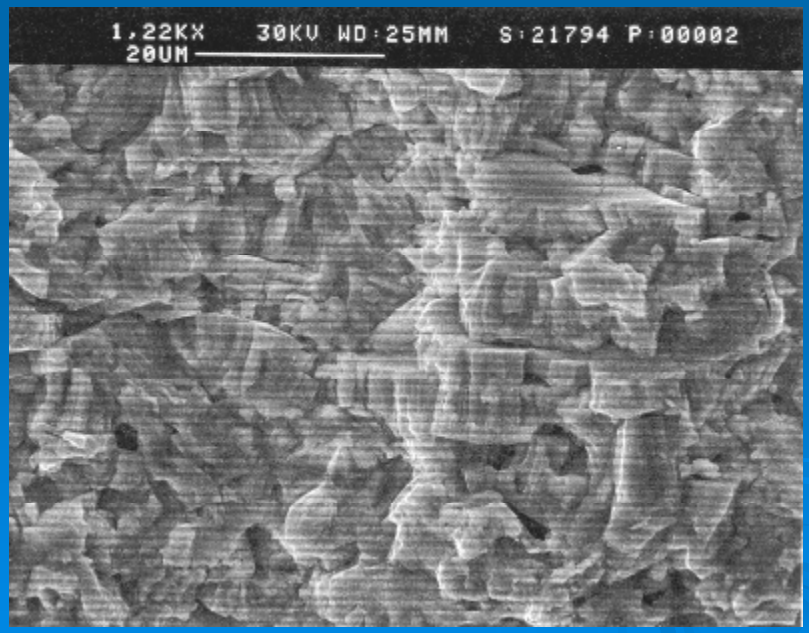

New: Electron Beam-PVD

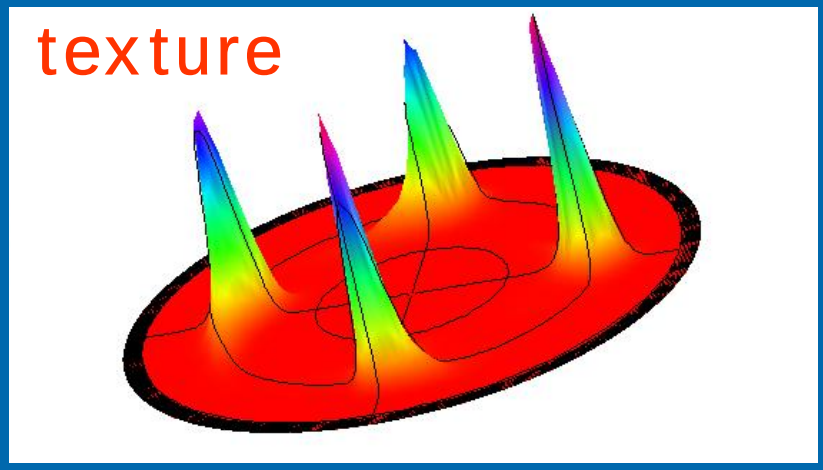

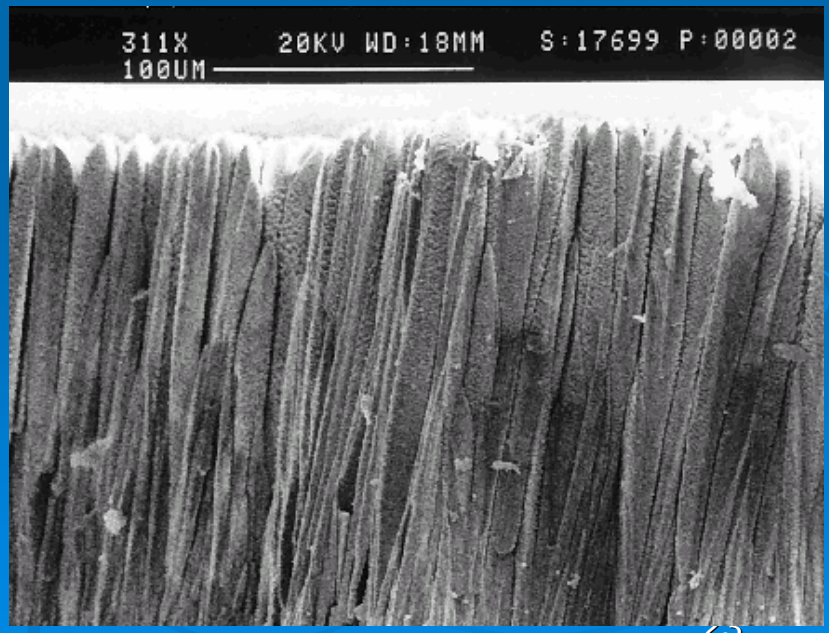

Textured TBCs

Microstructure of yttria partially stabilised zirconia TBC deposited by EB-PVD: evidence of highly *textured columnar grains*

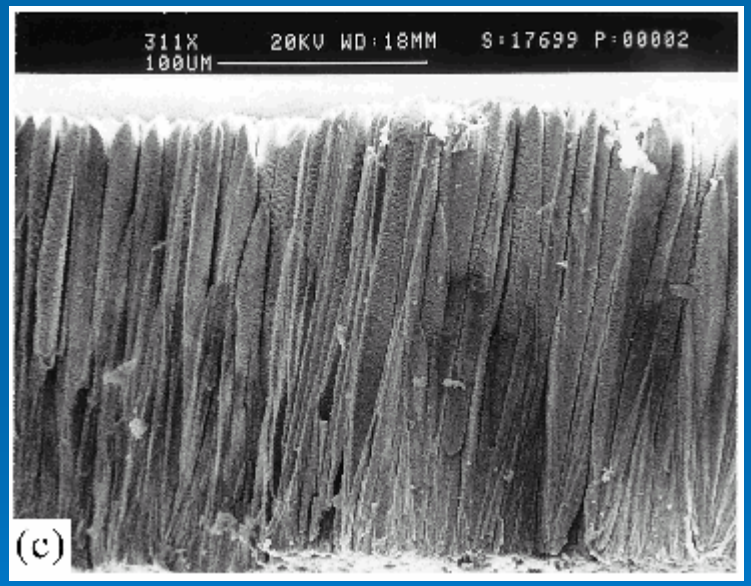

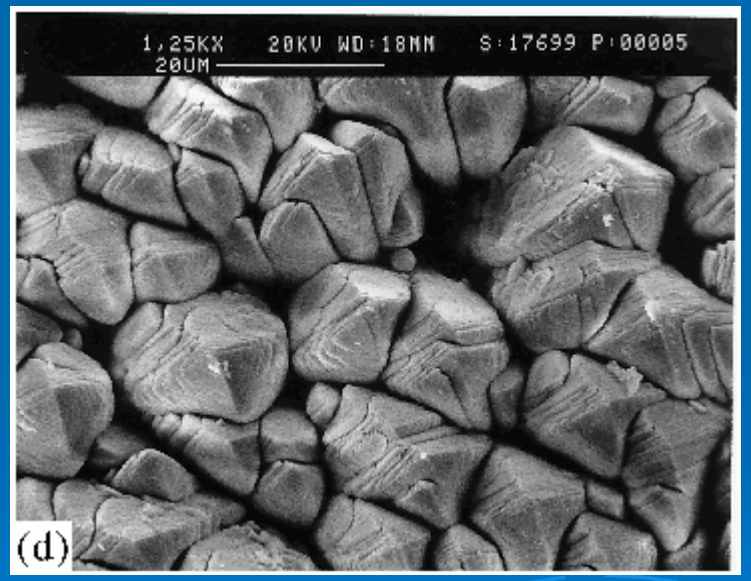

Thermal as well as intrinsic (growth) stresses need be considered in coating design and production process

Residual stress and texture

How can we evaluate
residual stress and texture in thin films?

X-ray diffraction is ideally suited for non-destructive evaluation of residuals stress and texture in thin films and coatings.

Structural information must be properly considered in the modelling of the elastic behaviour of textured coatings.

LINE PROFILE ANALYSIS

LPA Applications typically concern the study of:

- crystalline domain size and shape (and distribution)
- generalised line defects, e.g., dislocations, disclinations
- planar faults, e.g., twin and deformation faults
- anti-phase domain boundaries (in ordered phases)
- residual (micro)strain (e.g. by misfitting inclusions)
- grain surface effects (e.g. grain surface relaxation)
- impurities (--> lattice parameter fluctuation from grain to grain)
- ……..

Line Profile Analysis: history

Starting from the pioneering work of *Scherrer* (1918), LPA developed during the '40s and '50s (*Wilson*, *Warren*, *Bertaut*), with further significant contributions by *Krivoglaz* and *Wilkens* during the '60s.

Profile fitting techniques in the '80s/'90s had quite an impact on LPA; however, present day traditional LPA methods are still mostly based on those early studies.

Traditional methods are usually grouped as:

- Line Breadth 'simplified' methods
  (e.g., *Scherrer* formula, *Williamson-Hall* plot)
- Fourier methods
  (e.g., *Warren-Averbach* method)

Line Breadth 'simplified' methods

Profile information is typically extracted as FWHM or Integral Breadth (β) – ratio between peak area and maximum intensity

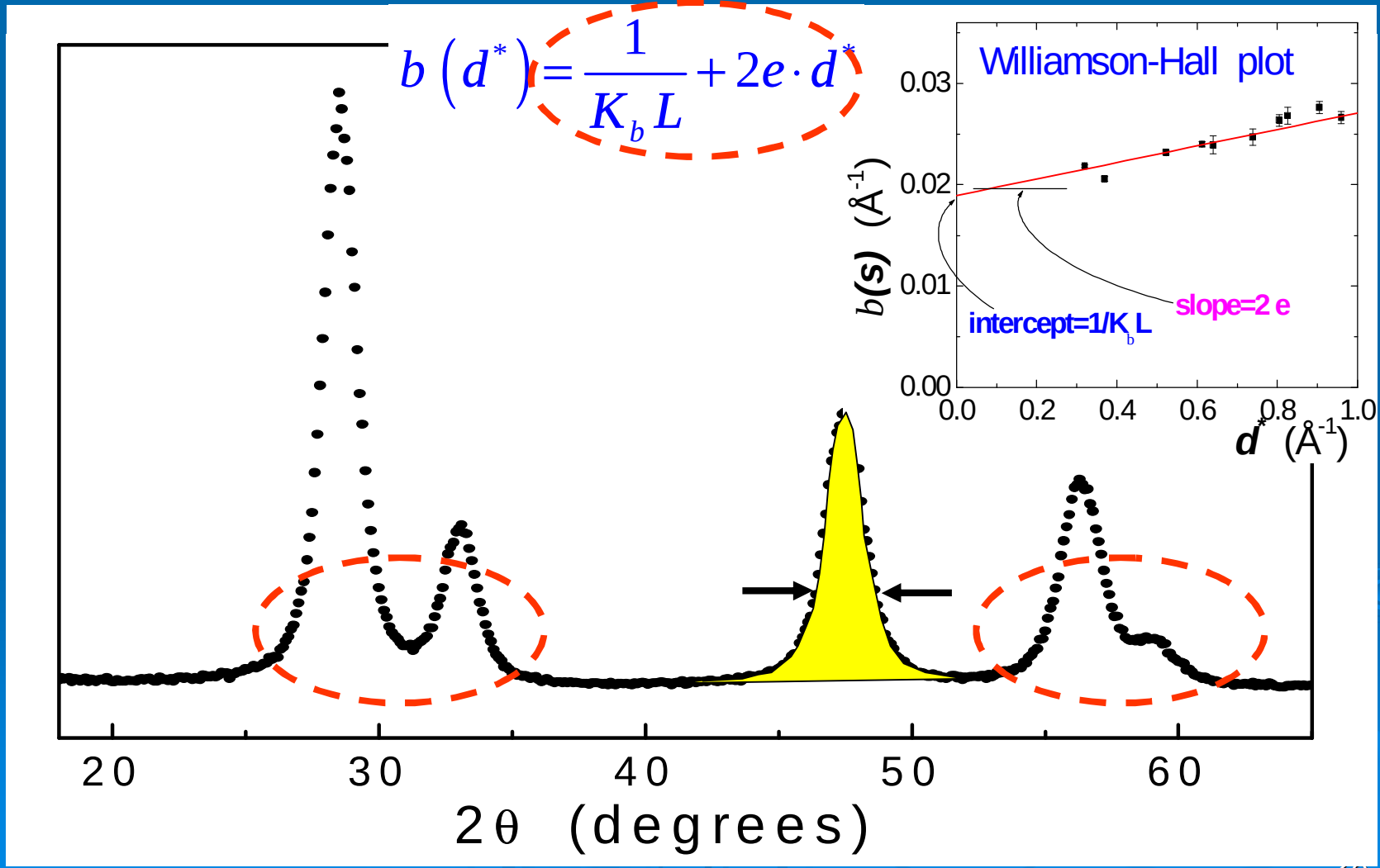

Pattern Decomposition + LPA

Pattern decomposition (profile fitting) is frequently used to extract peak profile parameters by fitting suitable (but arbitrary !!) analytical functions, like, e.g., Voigt, pseudo-Voigt or PVII.

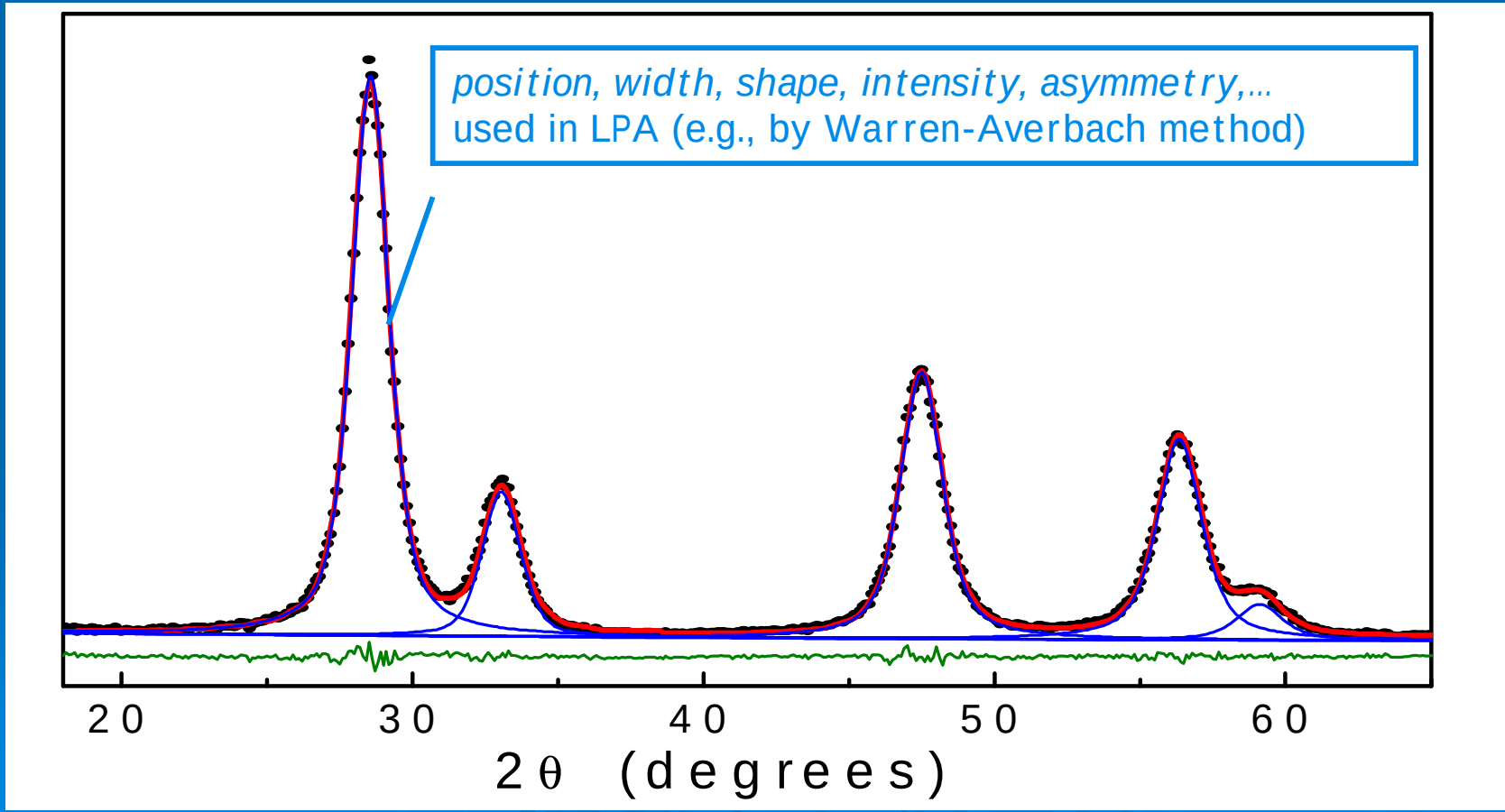

Traditional Line Profile Analysis

Most traditional methods are based on a multiple-step procedure:

1. Correction of line profiles for the instrumental component/backgr.
2. Extraction of line profile data (FWHM, β, Fourier coefficients, …), typically by analytical profile fitting
3. Application of physical models to parameters *extracted* from the experimental pattern.

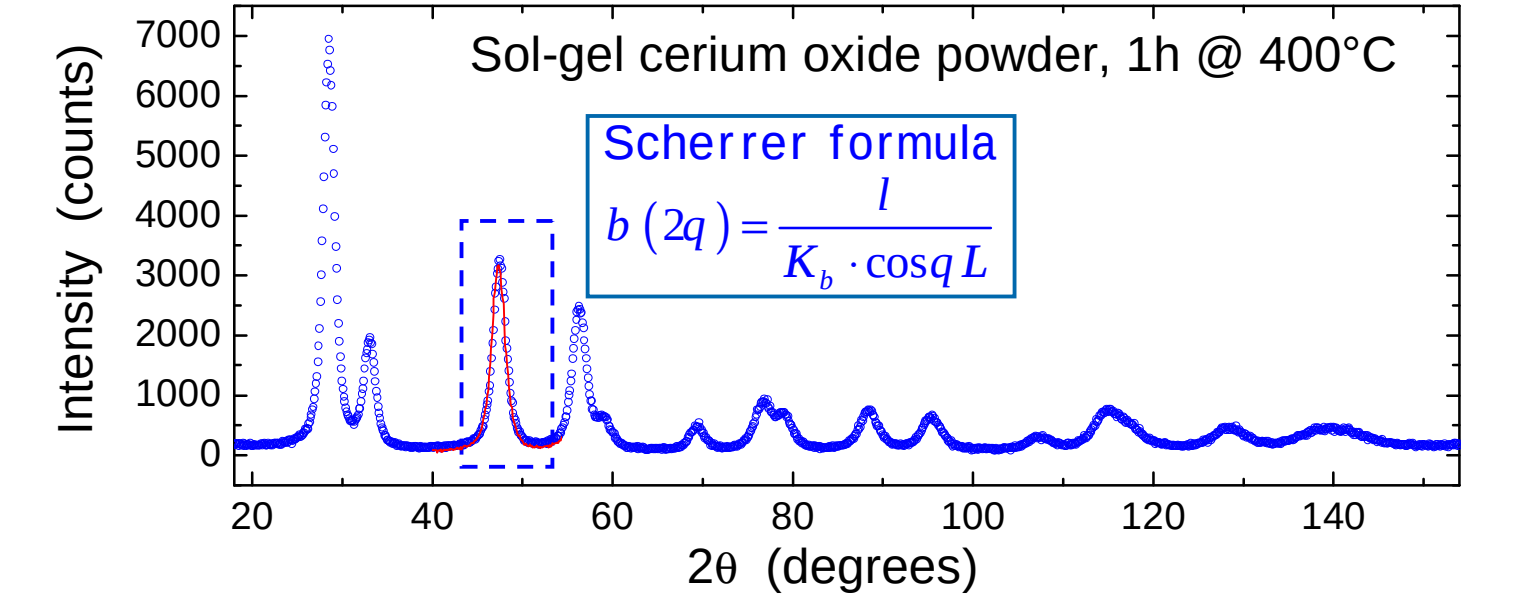

Traditional Line Profile Analysis

Most traditional methods are based on a multiple-step procedure:

1. Correction of line profiles for the instrumental component/backgr.
2. Extraction of line profile data (FWHM, β, Fourier coefficients, ...), typically by analytical profile fitting
3. Application of physical models to parameters *extracted* from the experimental pattern.

Whole Powder Pattern Modelling

WPPM is based on a direct modelling of the experimental pattern, based on physical models of the microstructure and lattice defects:

Diffraction Pattern

WPPM

Physical Model

Microstructural Parameters

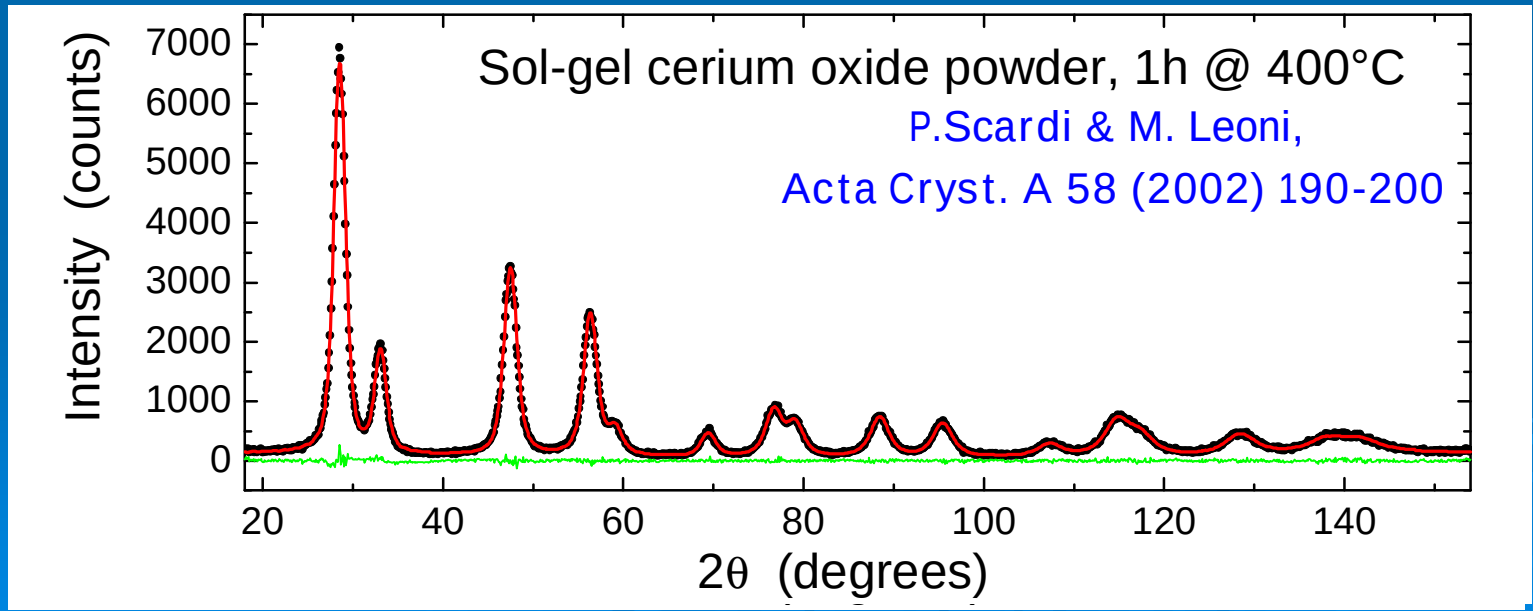

References

Diffraction Analysis of Materials Microstructure
E.J. Mittemeijer & P. Scardi, editors.
Berlin: Springer-Verlag, 2004.

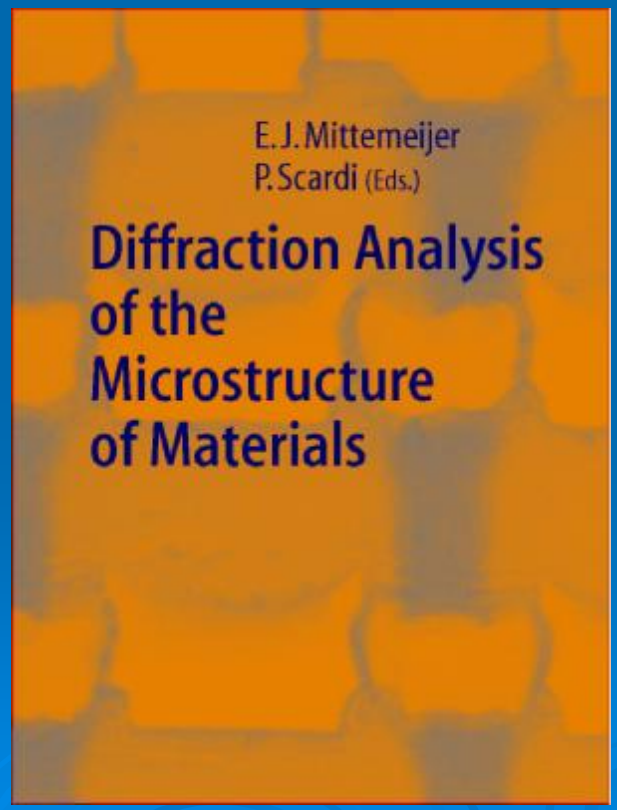

WPPM APPLICATIONS

- Ball milled Fe-Mo powder
- Ball milled nickel powder
- Nanocrystalline cerium oxide
- Cu-Be alloy wear debris
- Anti-Phase Domains in Cu_3Au

WPPM application: Ball milled Fe-Mo

Main sources of broadening in this case are dislocations and domain size. Corresponding fitting parameters are:

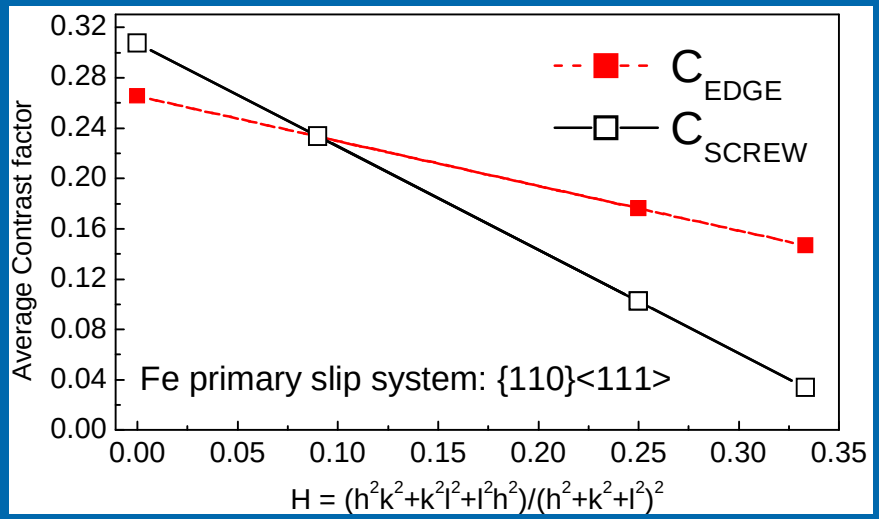

- average dislocation density *r*,
- effective outer cut-off radius *Re*,
- fraction of Edge/Screw dislocations, *fE* . Average contrast factor from Fe elastic constant, for primary slip system {110}<111>: $\overline{C}_{hkl} = \overline{C}_{EDGE} f_E + \overline{C}_{SCREW}(1 - f_E)$
- mean *m* and variance *s* of a lognormal distribution of (spherical) domains

In addition: peak intensities, background coefficients (Chebyshev polynomial), lattice parameter and sample displacement. Data corrected for Lorentz-Polarization effect.

WPPM application: Ball milled Fe-Mo

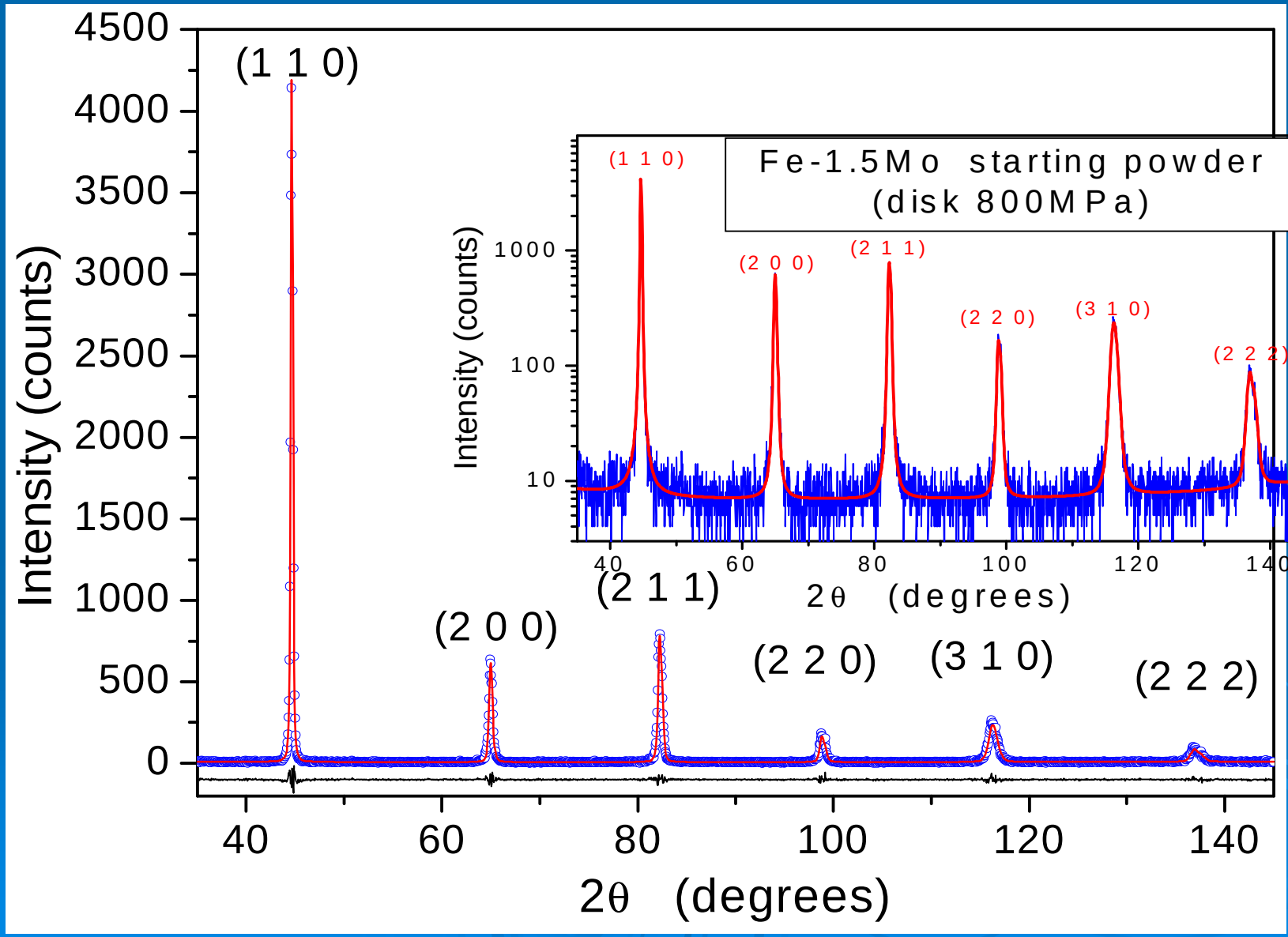

WPPM application: Ball milled Fe-Mo

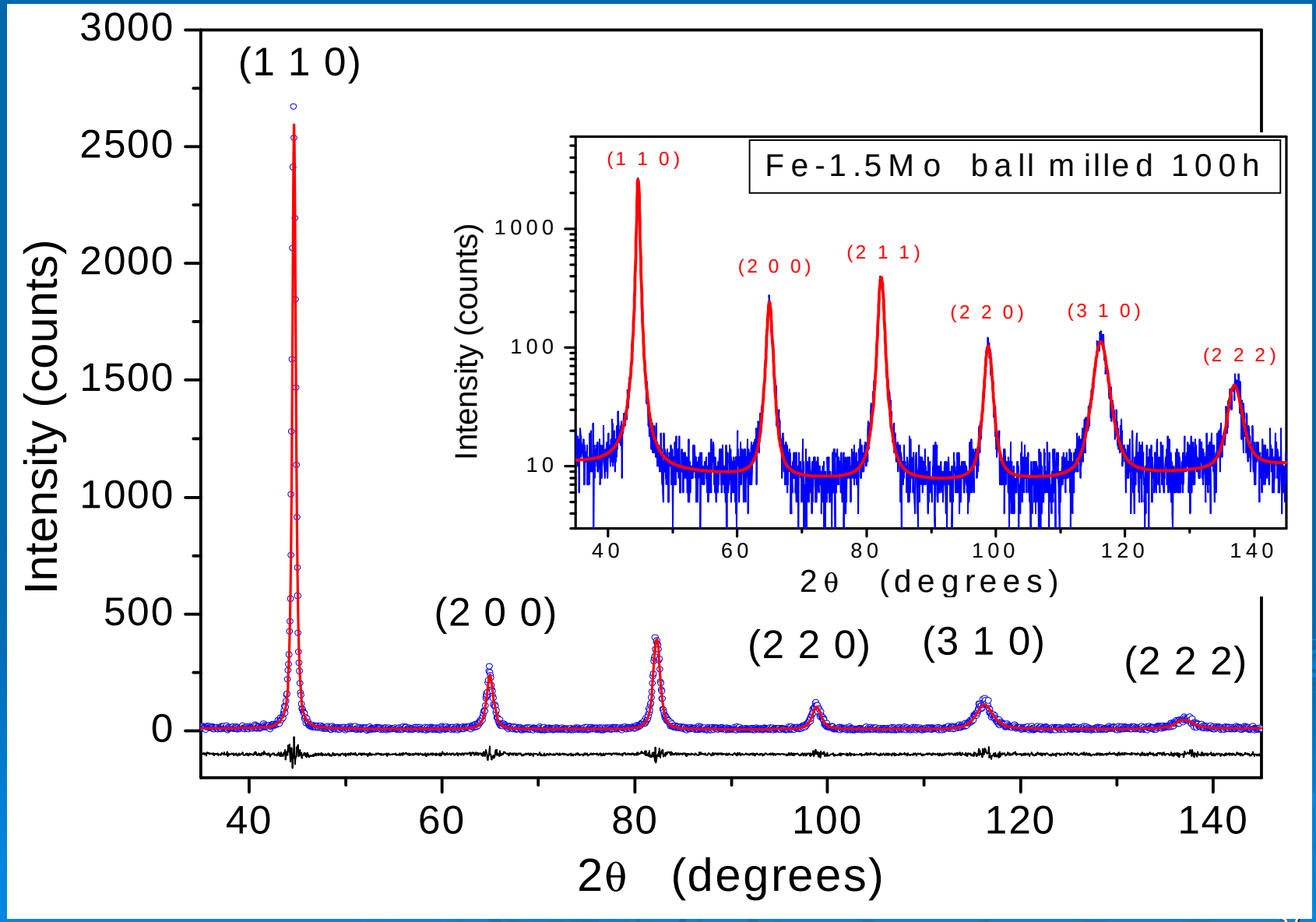

WPPM application: Ball milled Fe-Mo

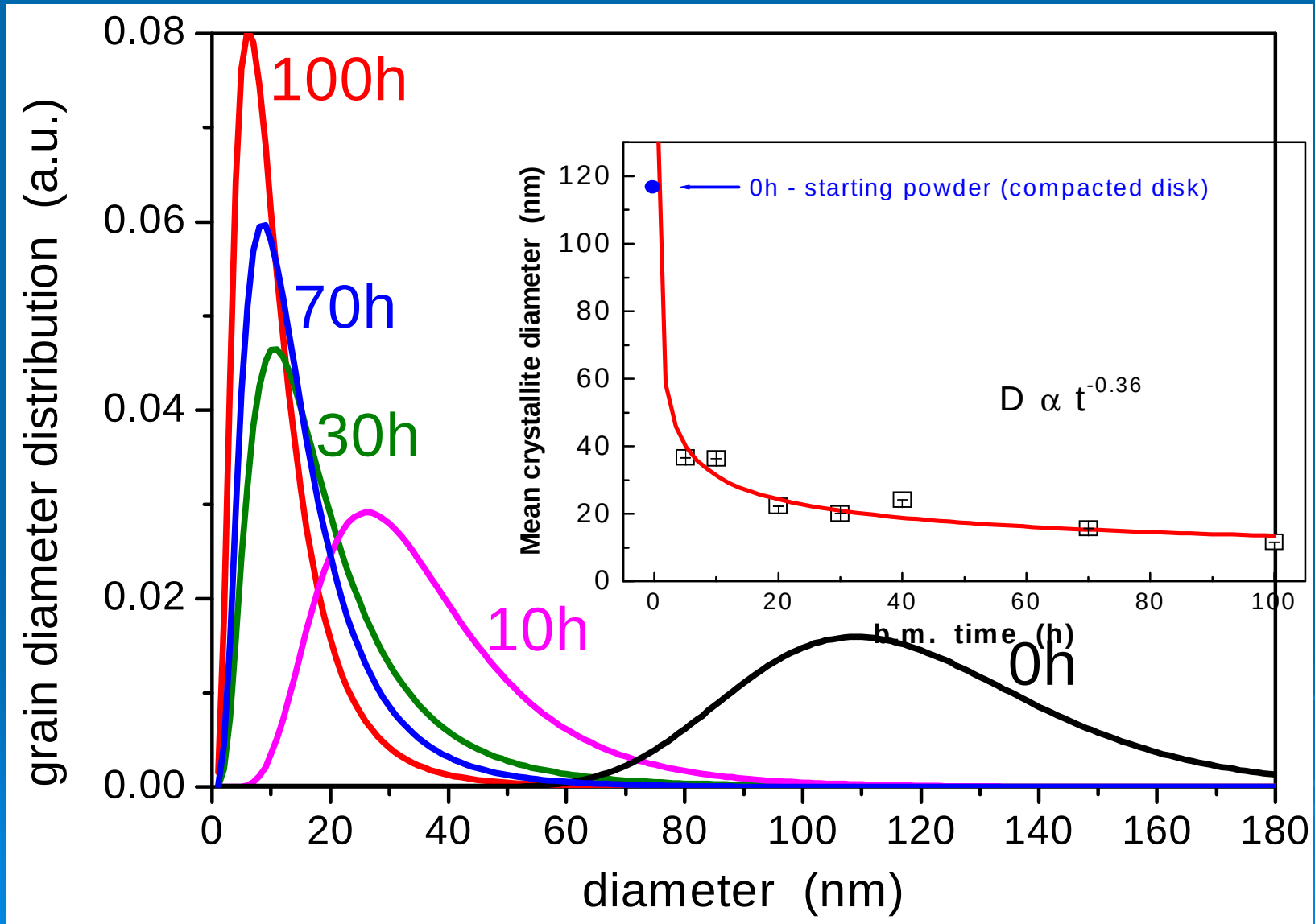

WPPM application: Ball milled Fe-Mo

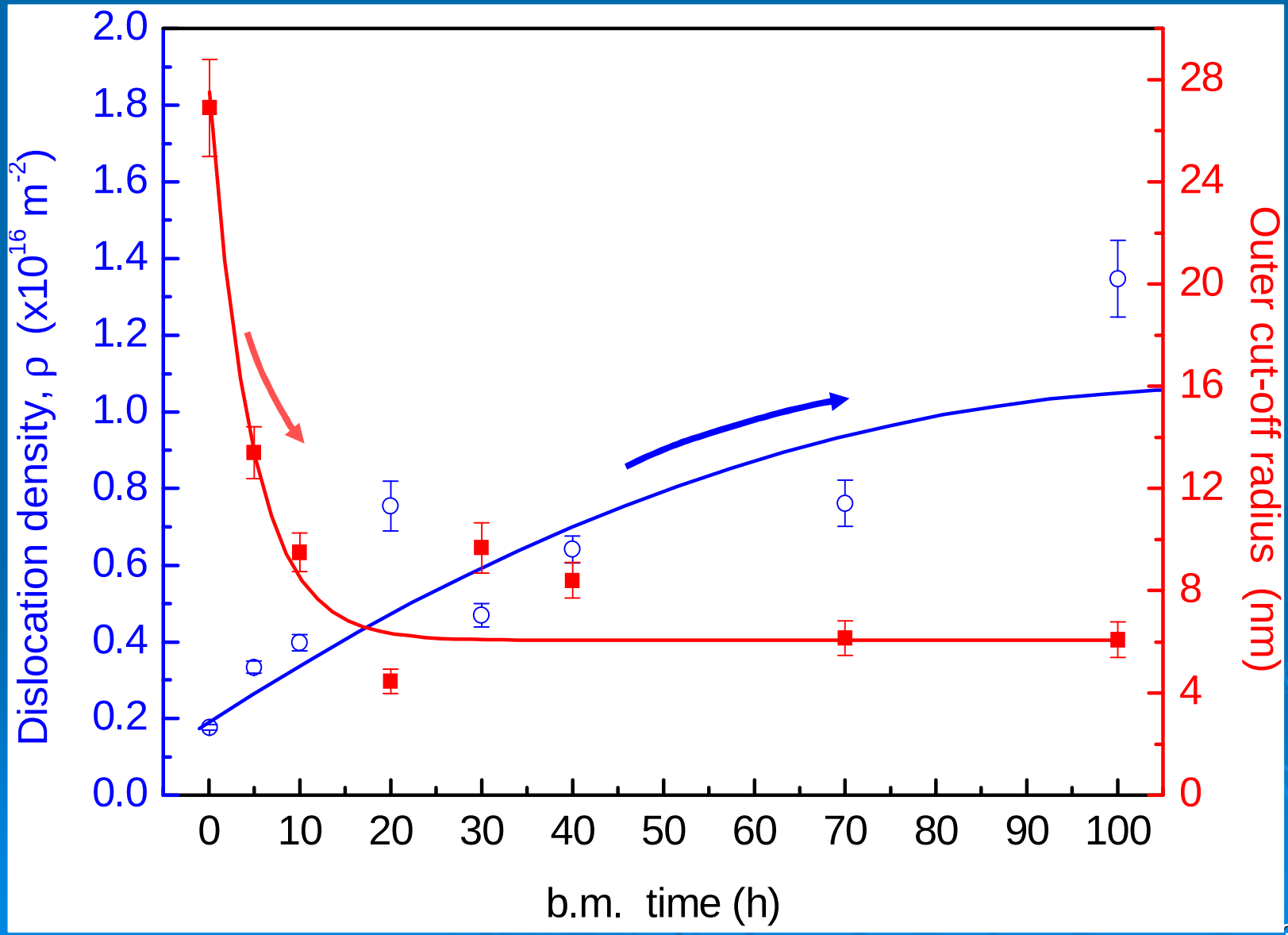

WPPM application: Ball milled Fe-Mo

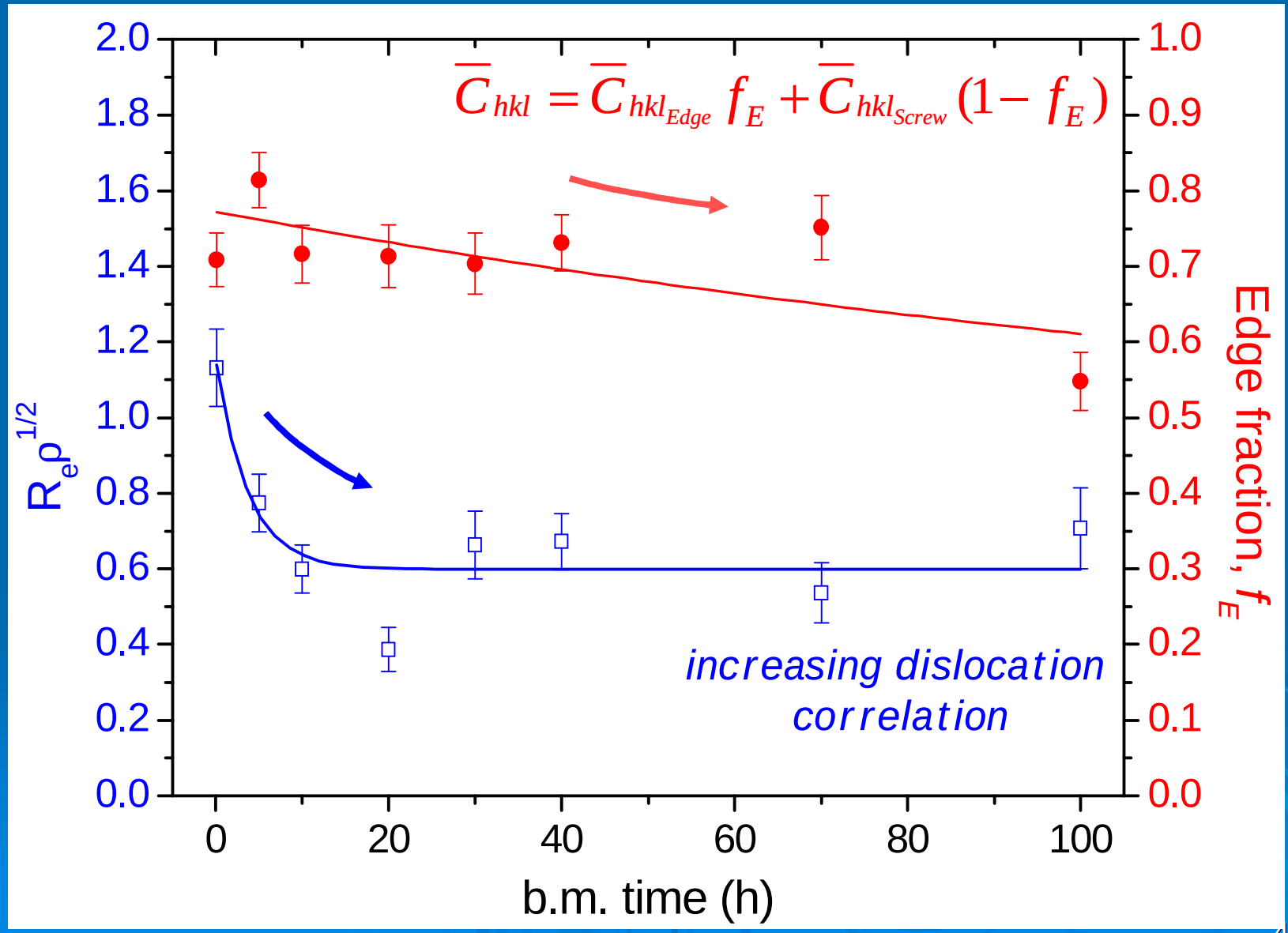

WPPM: Applications

- Ball milled Fe-Mo powder
- Ball milled nickel powder
- Nanocrystalline cerium oxide
- Cu-Be alloy wear debris
- Anti-Phase Domains in Cu_3Au

WPPM Application: Ball-Milled Nickel

Ni patterns at increasing ball milling time

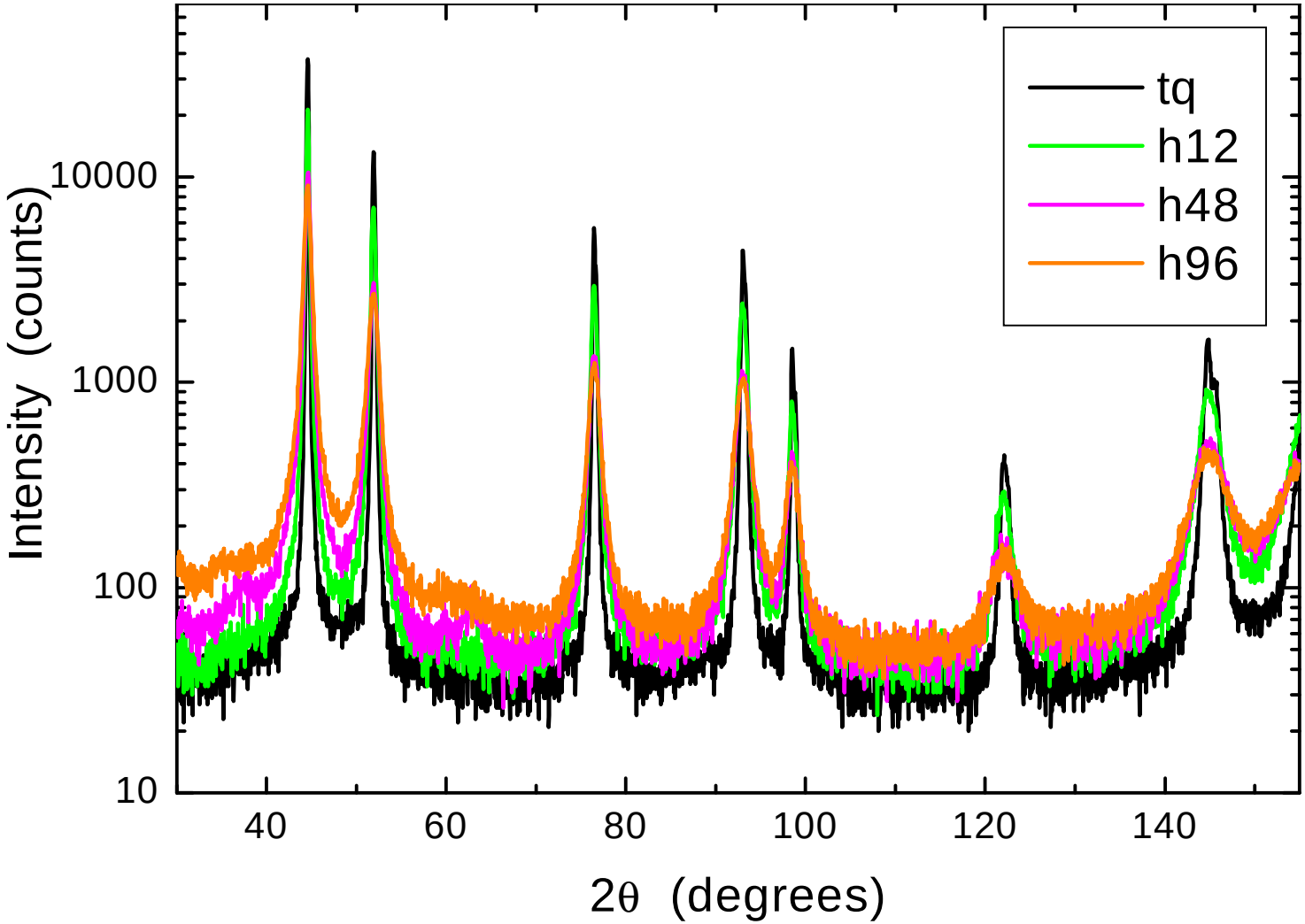

WPPM Application: Ball-Milled Nickel

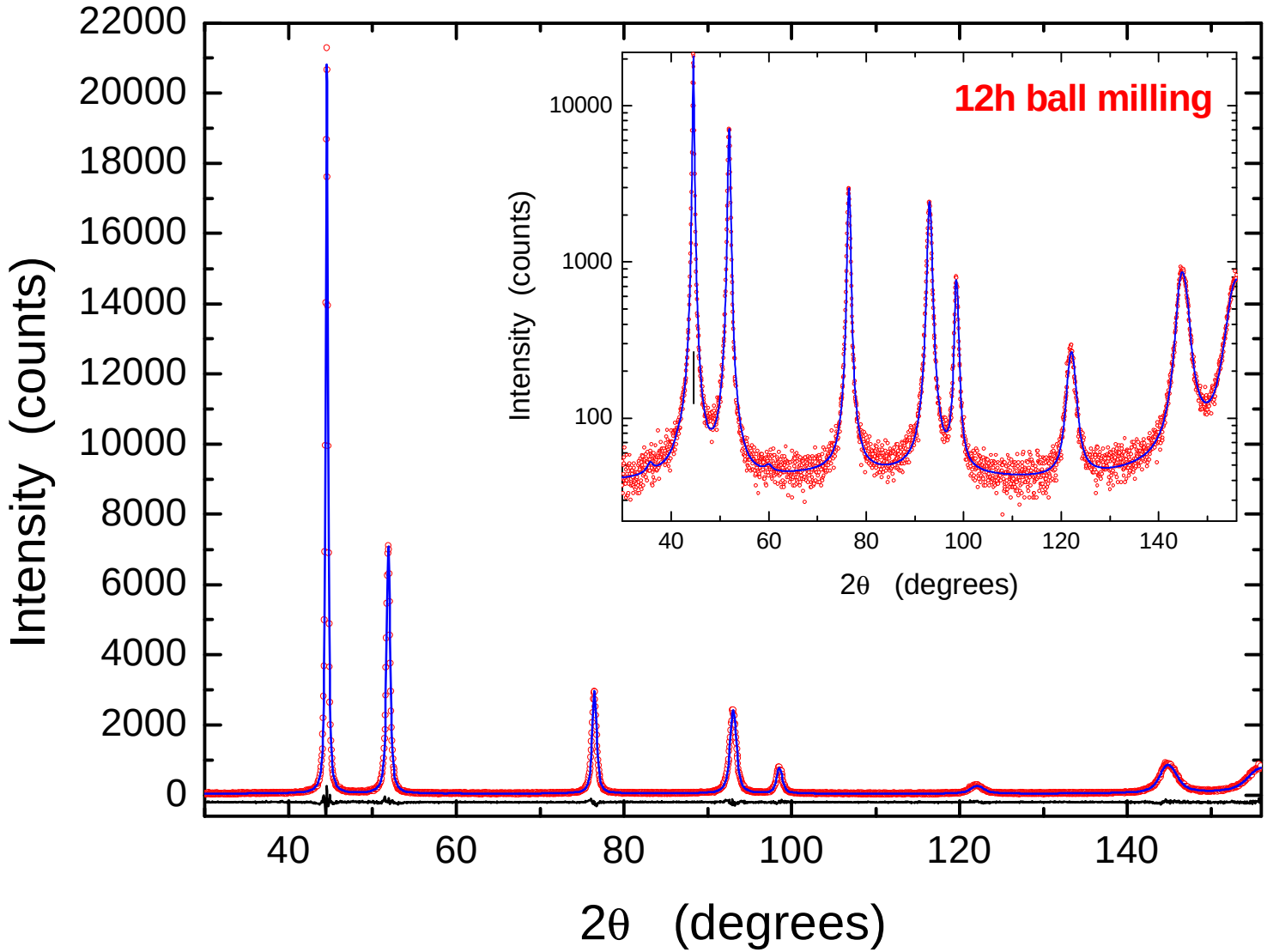

WPPM Application: Ball-Milled Nickel

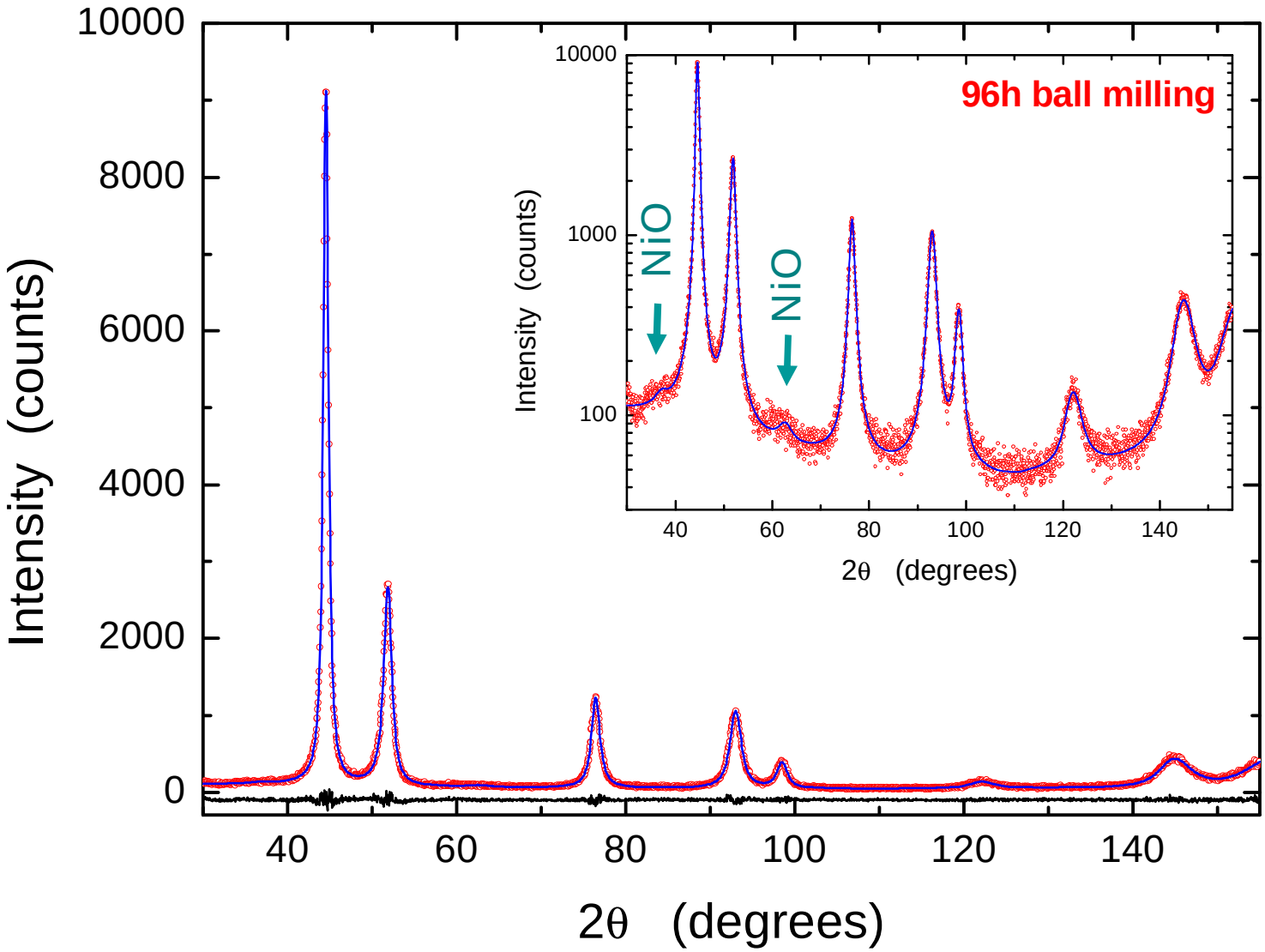

WPPM Application: Ball-Milled Nickel

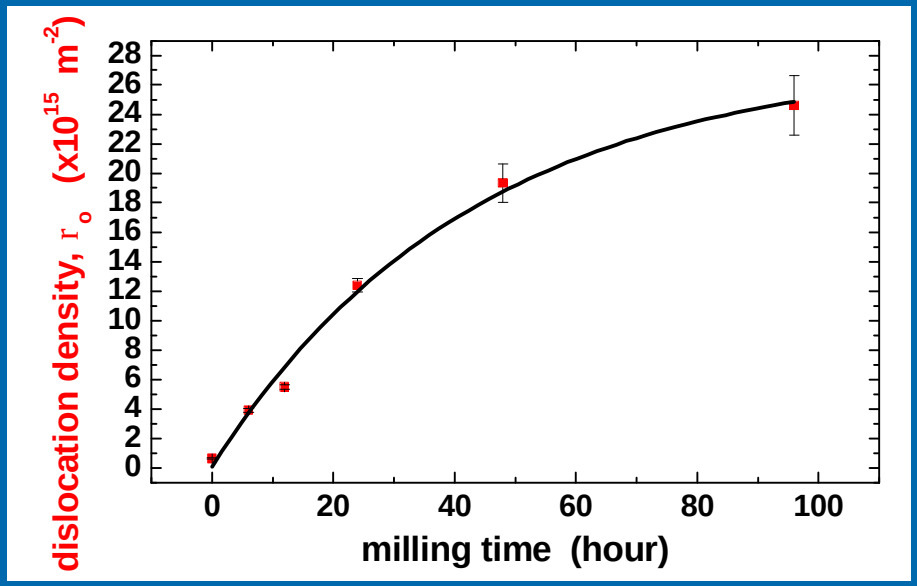

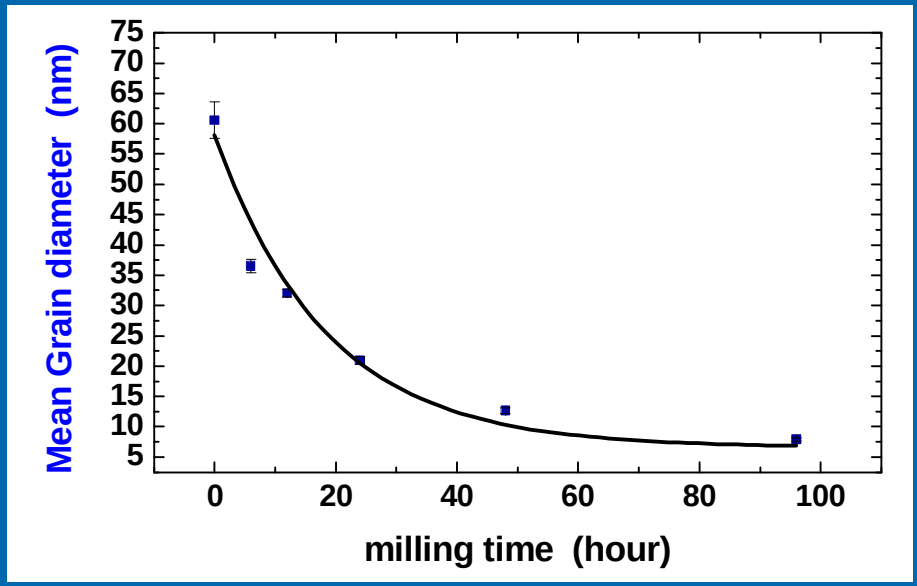

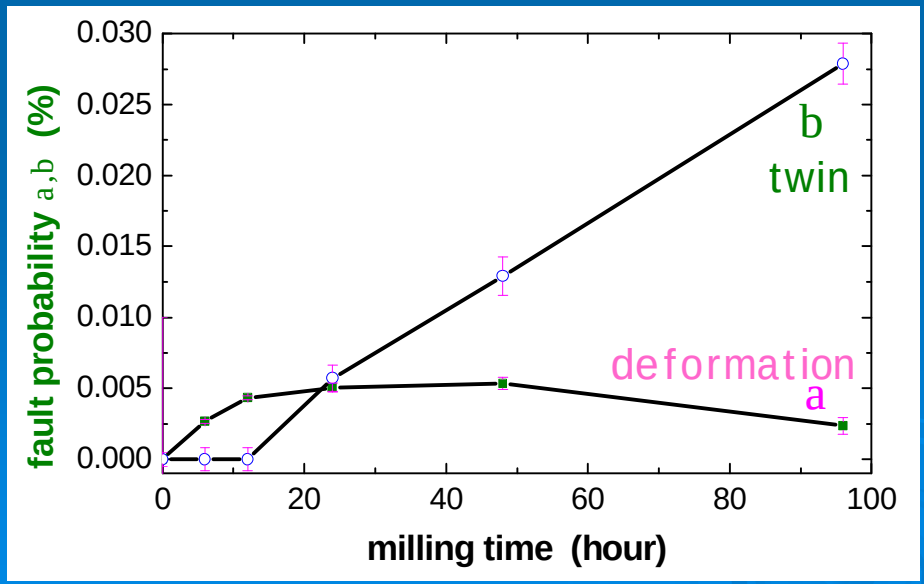

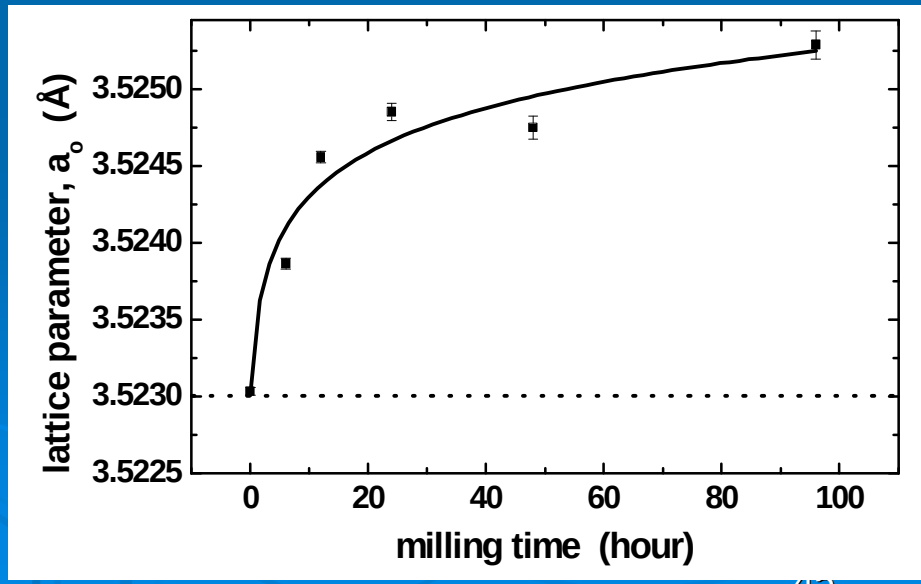

WPPM Application: Ball-Milled Nickel

96h ball milling

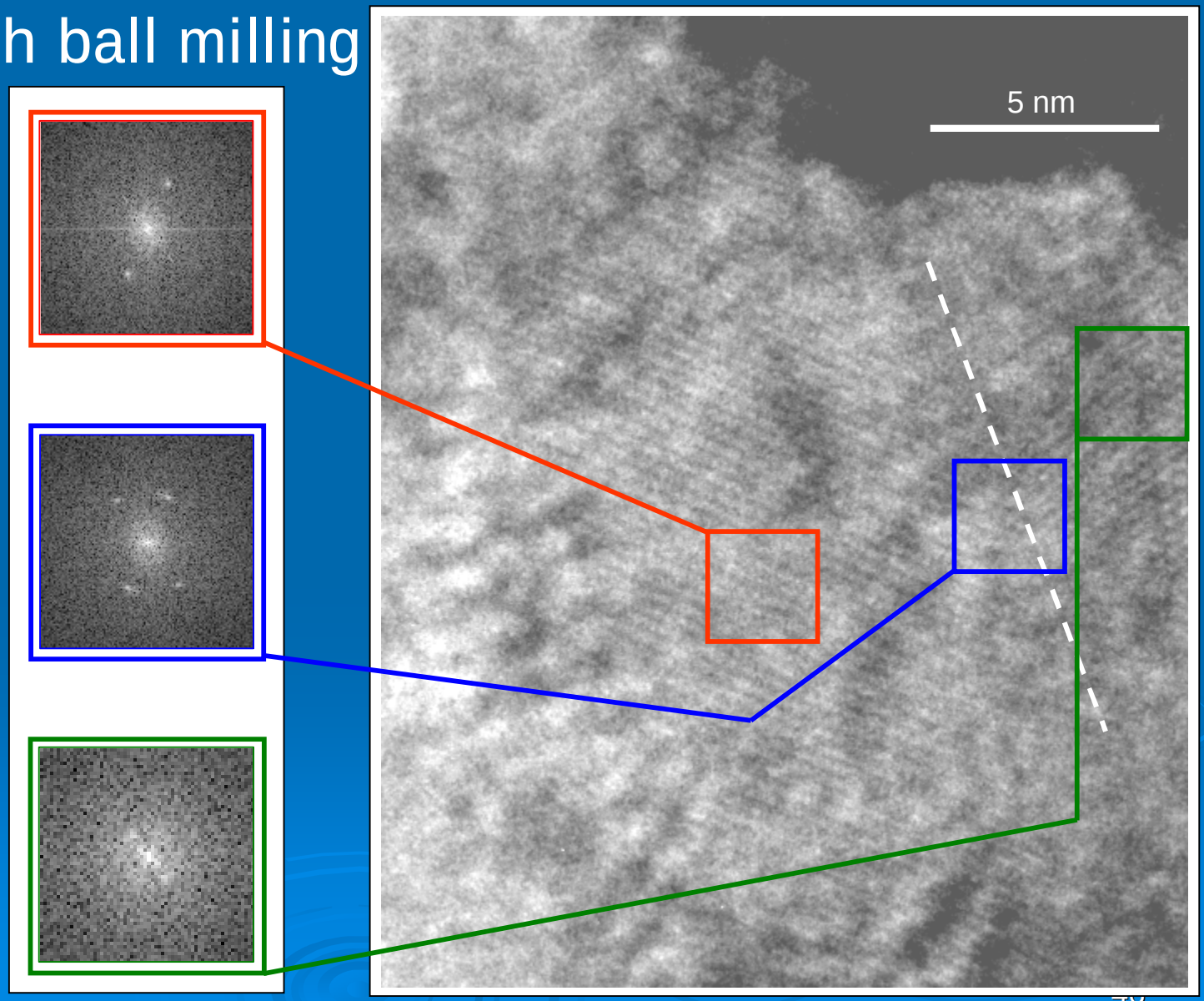

WPPM Application: Ball-Milled Nickel

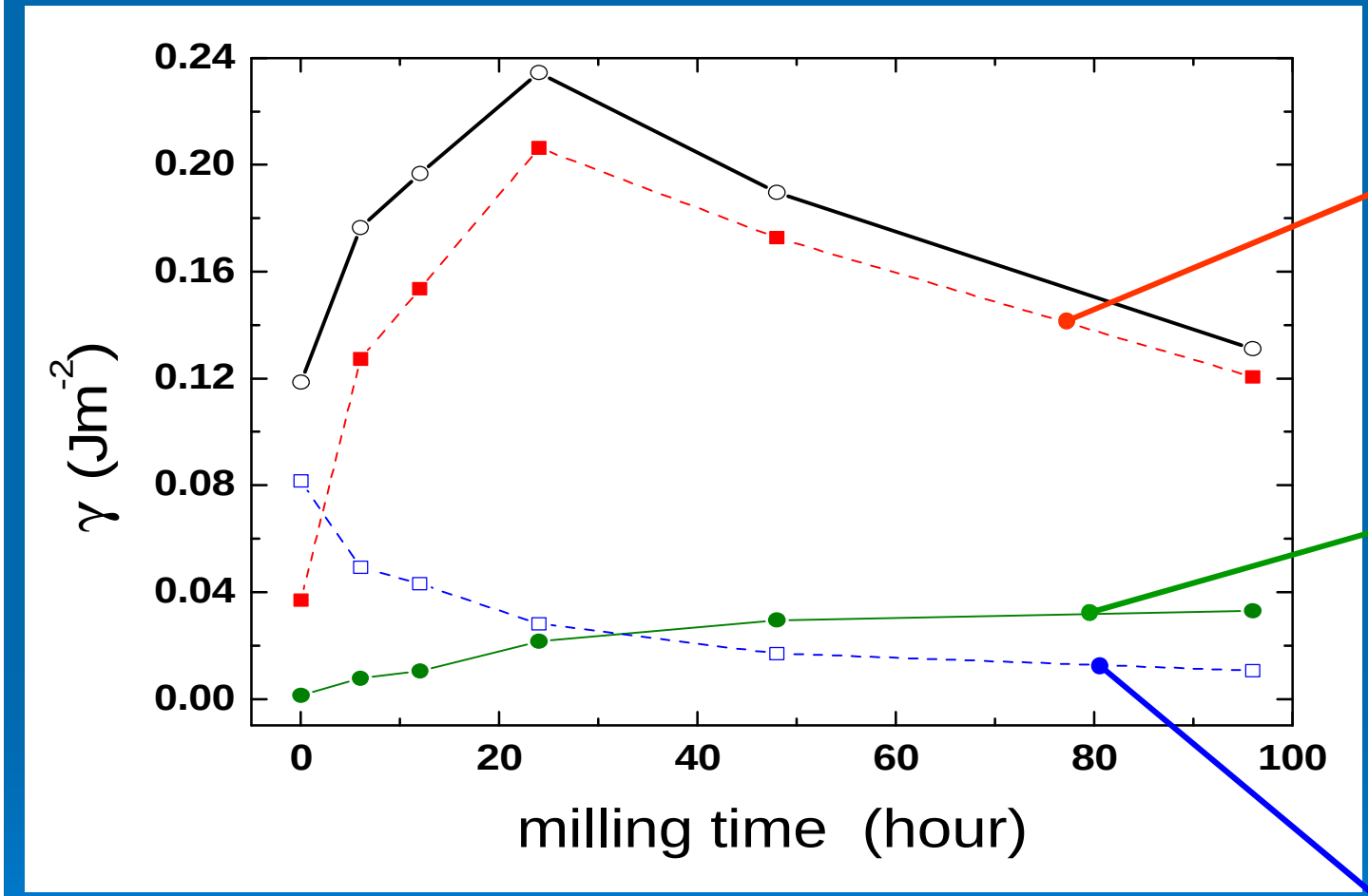

GB Dislocations

$$g_{Disl} = \frac{Gb^2 r D}{12p(1-n)} \ln\left(\frac{D}{b}\right)$$

RD Dislocations

$$g_{RD} = AGb^2 r \ln\left(\frac{R_e}{b}\right)$$

$$g_{Disc} = \frac{G\langle\Omega^2\rangle D \ln 2}{16p(1-n)}$$

Disclinations

WPPM Application: Ball-Milled Nickel

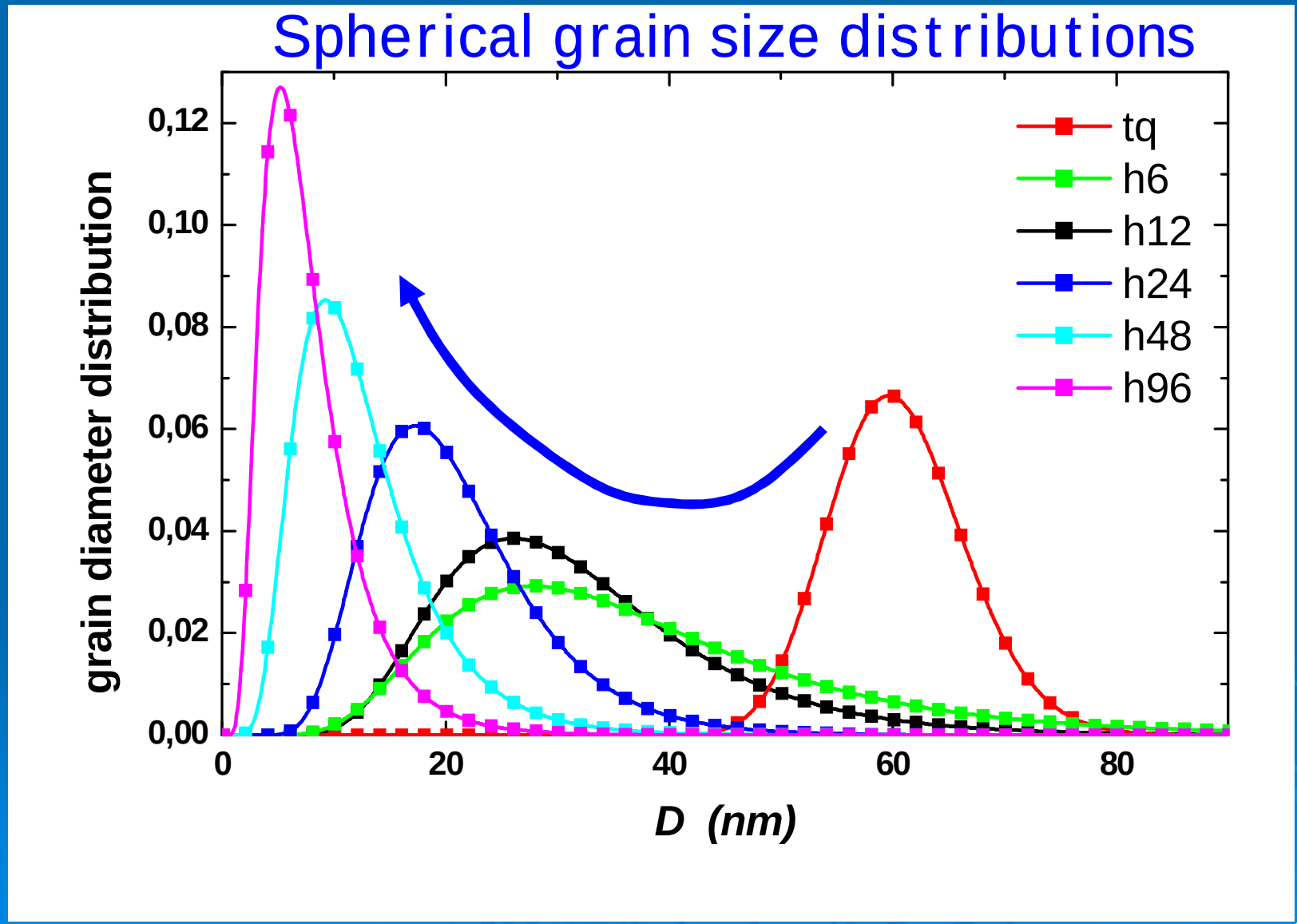

WPPM Application: Ball-Milled Nickel

Nickel powder ball milled for 96 h

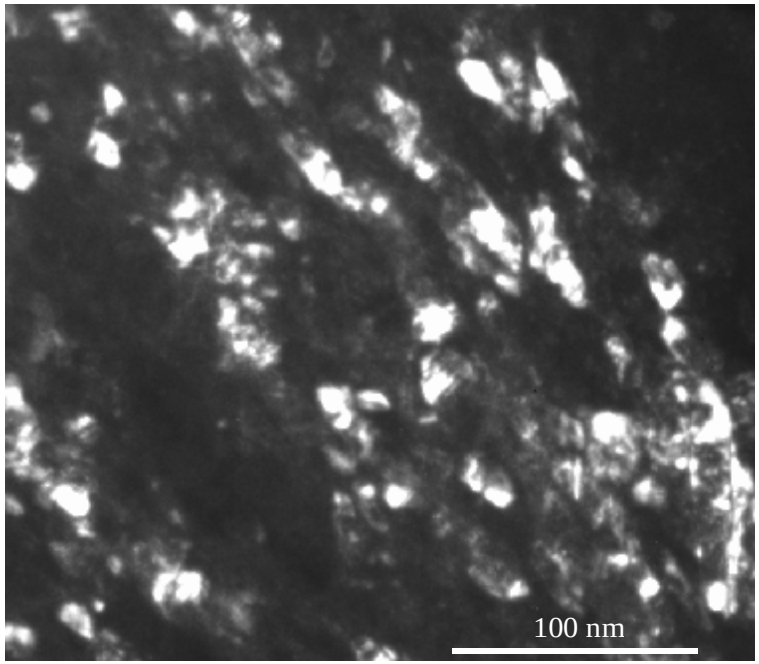

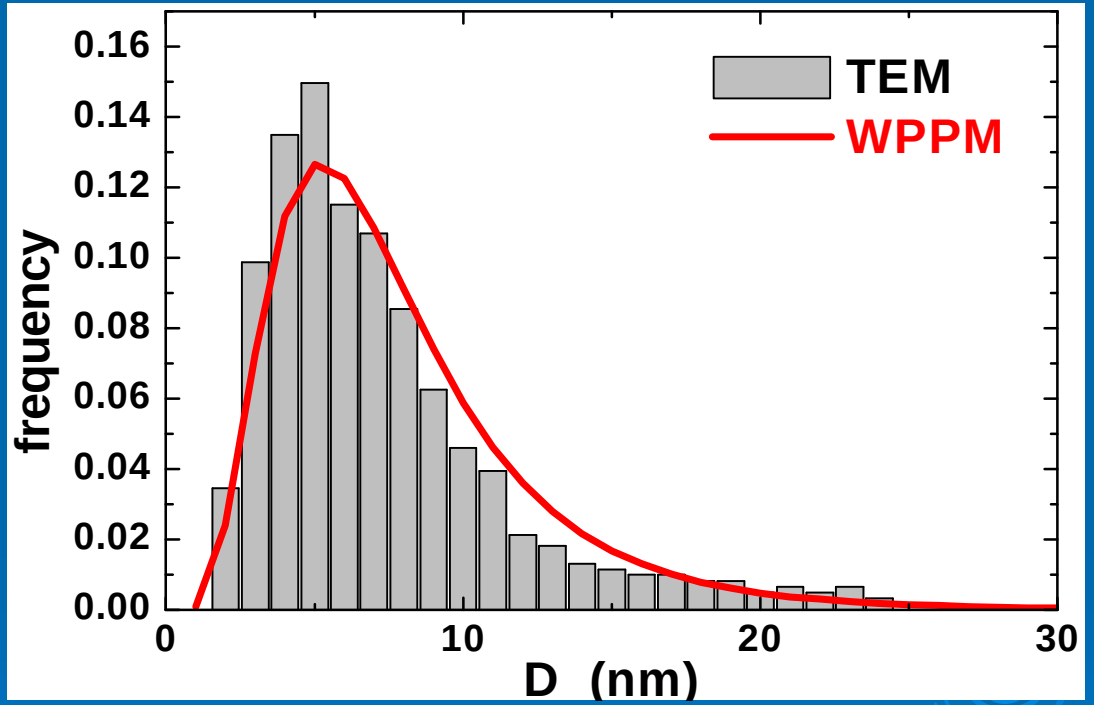

WPPM: Applications

- Ball milled Fe-Mo powder
- Ball milled nickel powder
- Nanocrystalline cerium oxide
- Cu-Be alloy wear debris
- Anti-Phase Domains in Cu_3Au

WPPM: Application - Nanocrystalline Ceria

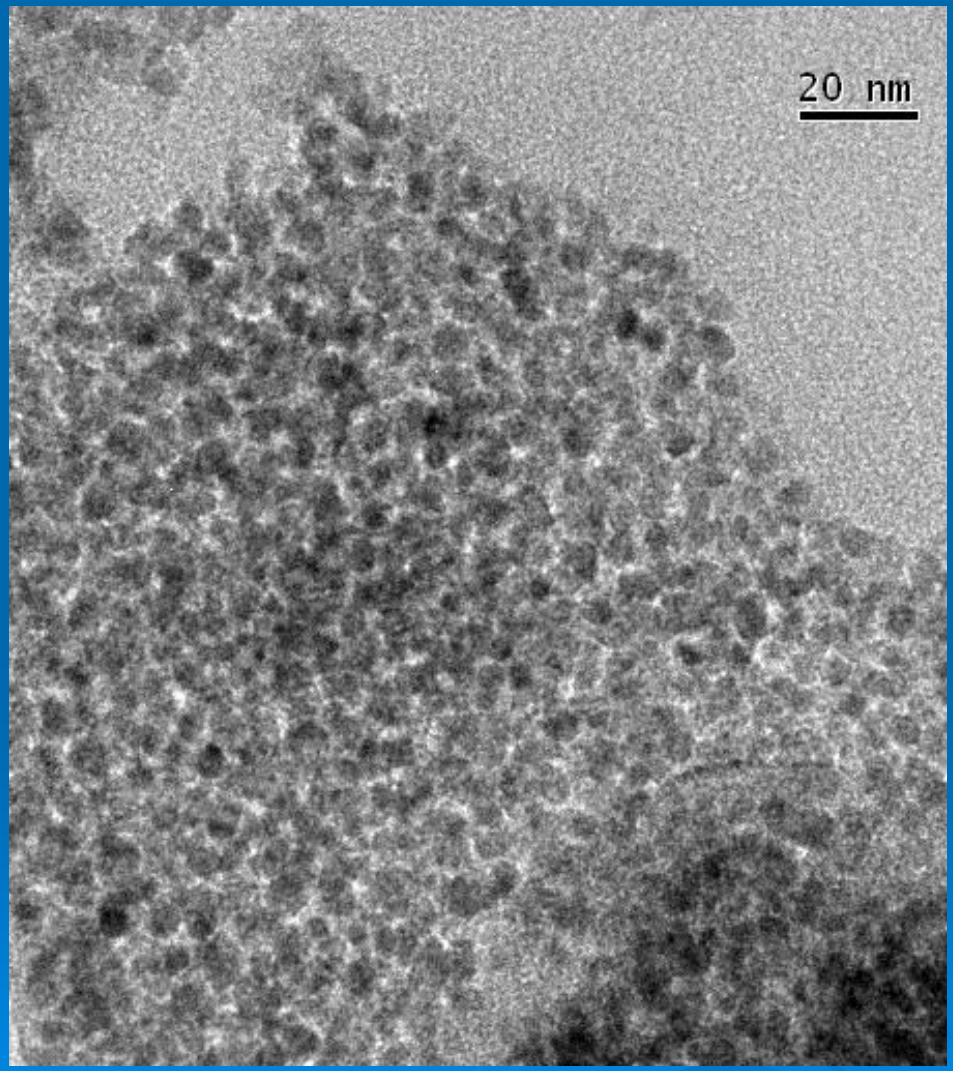

CeO_2 calcinated at 400°C for 1h

Grains are almost spherical and well separated

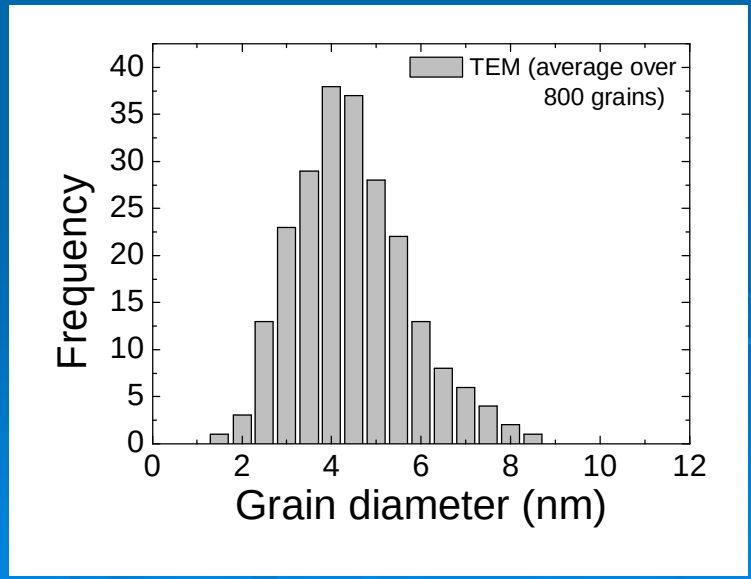

WPPM Application: nanocrystalline oxides

Nanocrystalline cerium oxide from sol-gel route

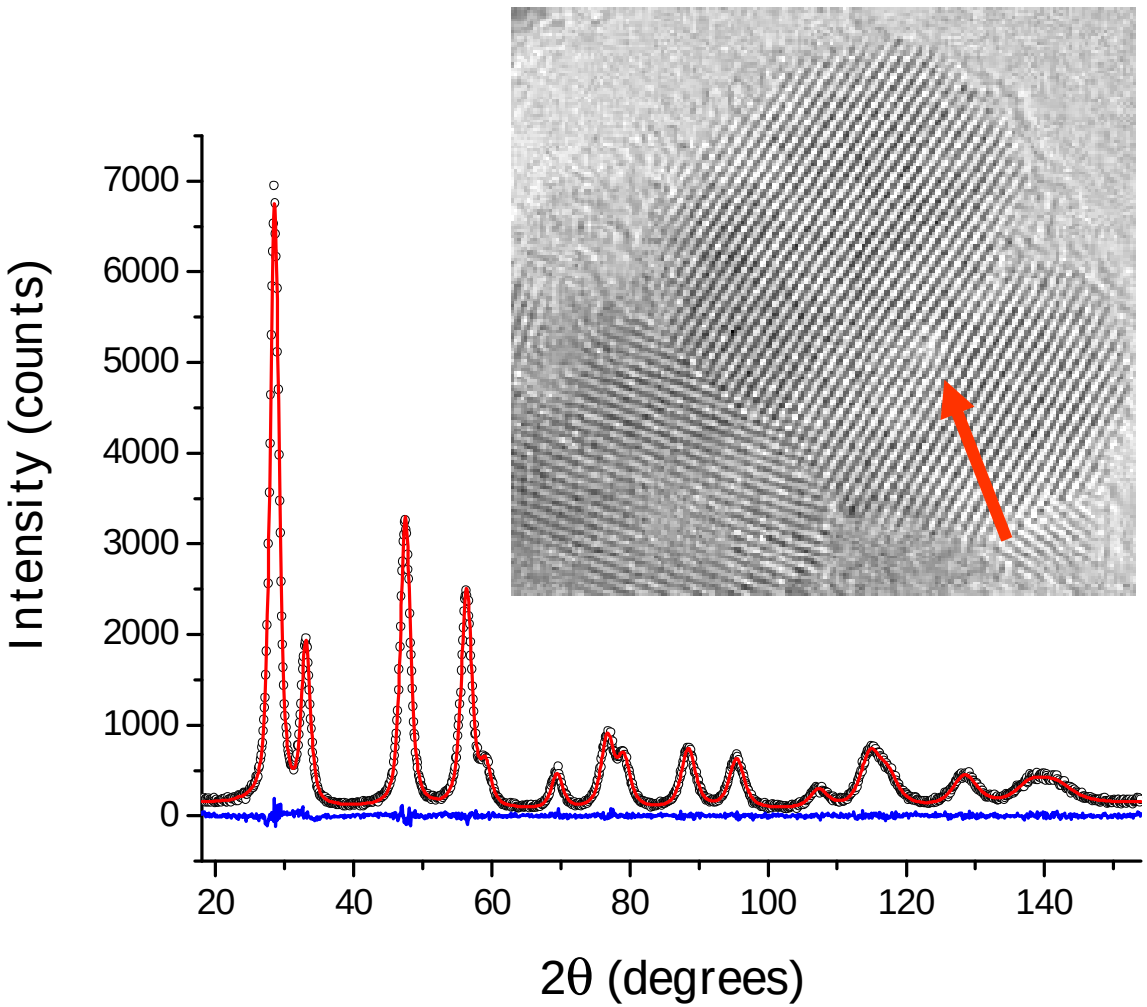

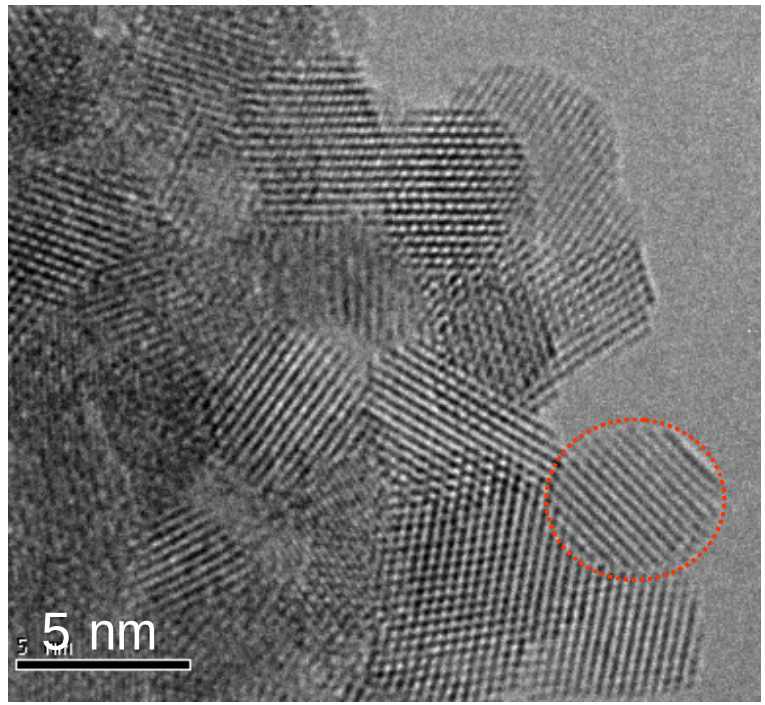

- P.Scardi, Z. Kristallogr 217 (2002)
- M. Leoni & P.Scardi, in *Diffraction Analysis of Materials Microstructure.* E.J. Mittemeijer & P. Scardi, editors. Berlin: Springer-Verlag. 2003

WPPM Application: nanocrystalline oxides

Nanocrystalline cerium oxide from sol-gel route

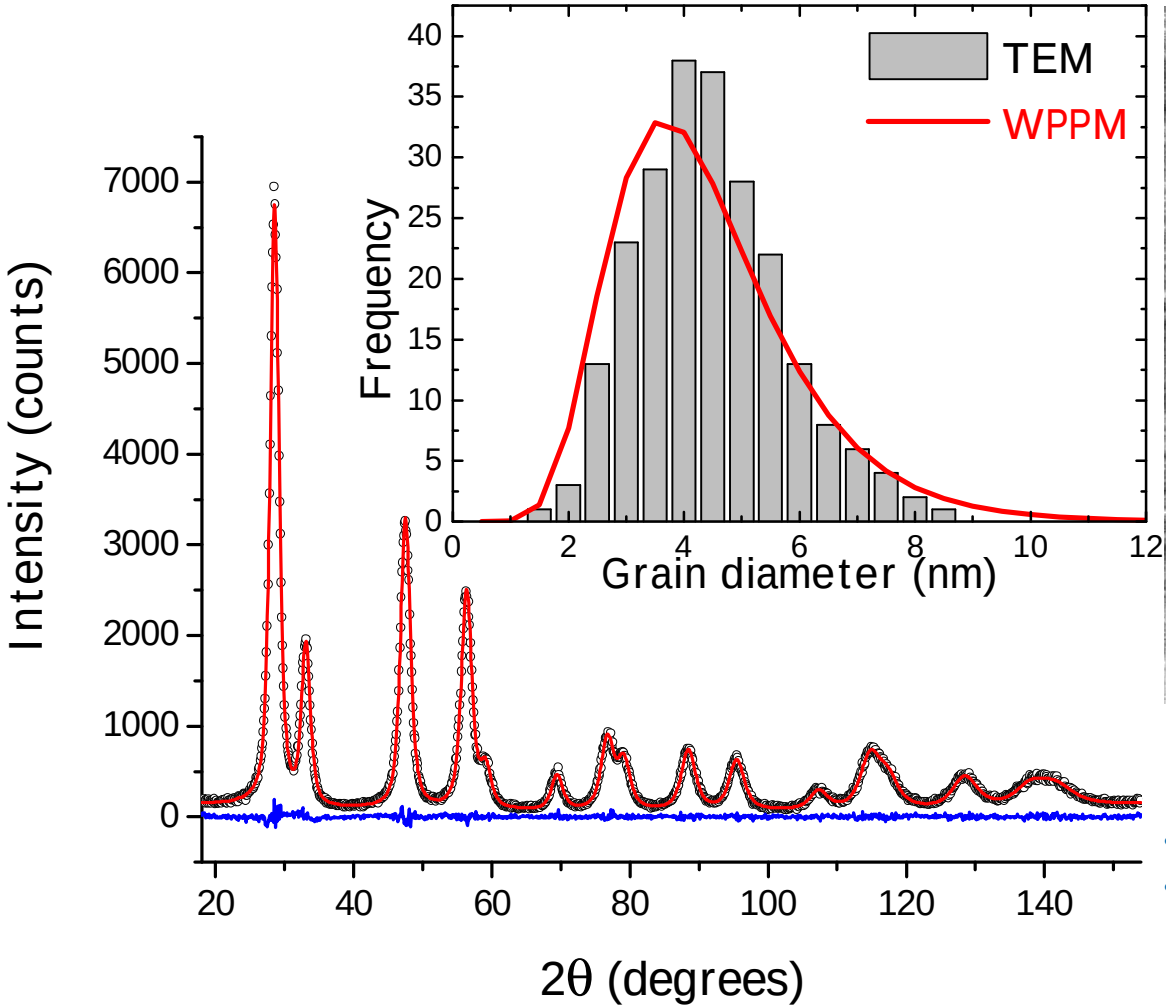

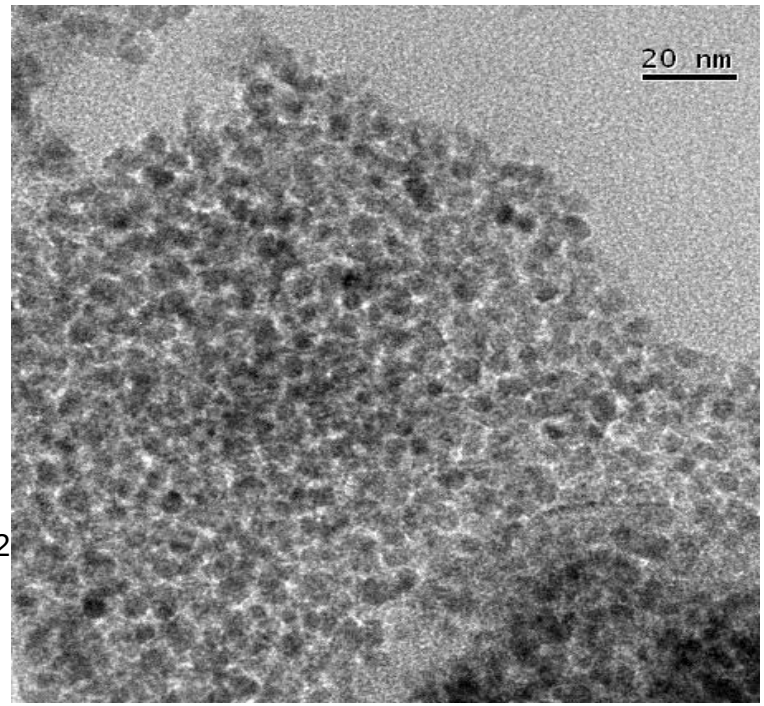

- P.Scardi, Z. Kristallogr 217 (2002)
- M. Leoni & P.Scardi, in *Diffraction Analysis of Materials Microstructure.* E.J. Mittemeijer & P. Scardi, editors. Berlin: Springer-Verlag. 2003

WPPM: Application - Nanocrystalline Ceria

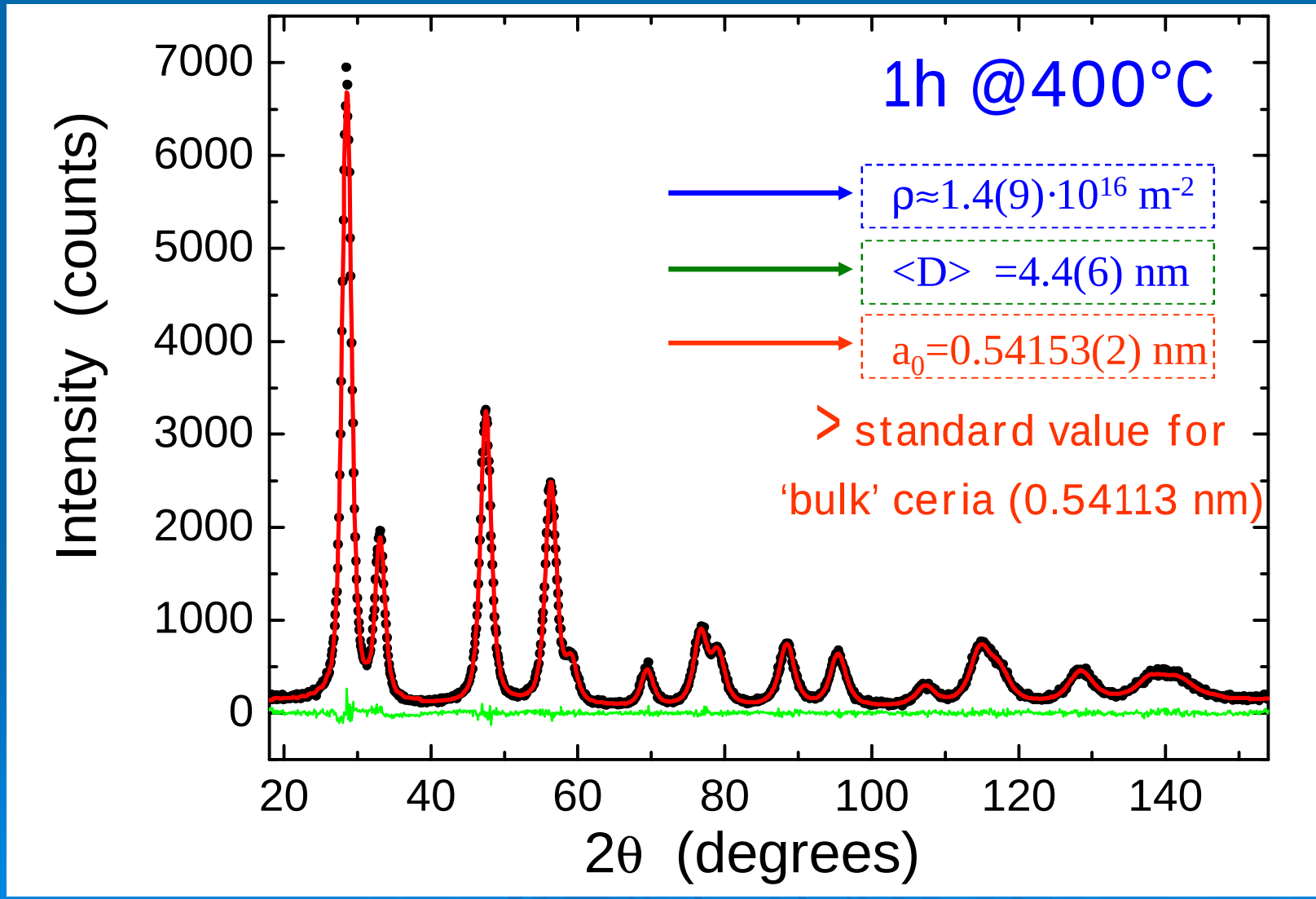

WPPM: Application - Nanocrystalline Ceria

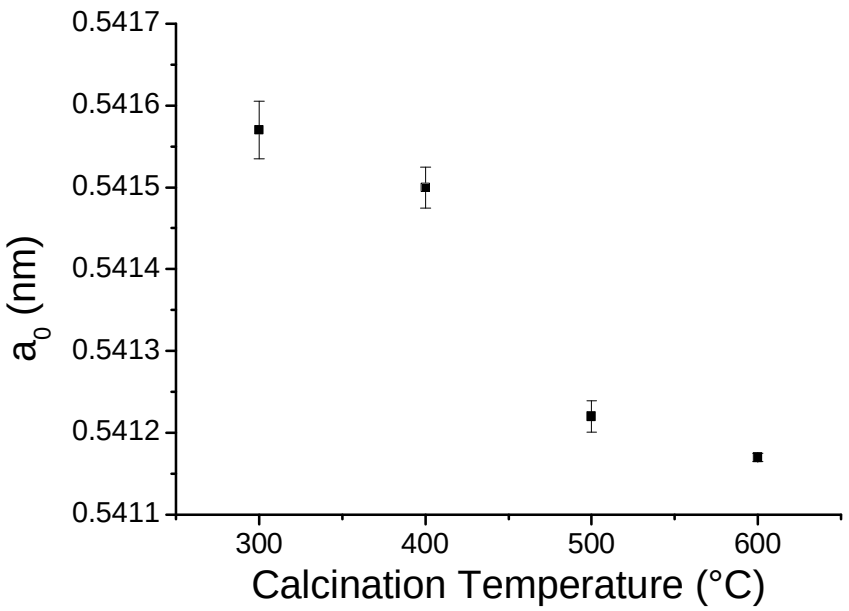

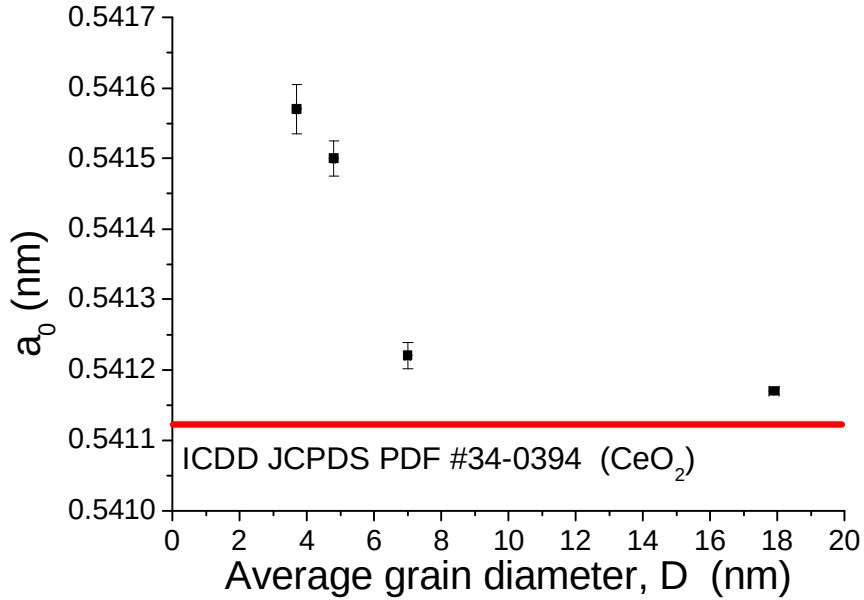

Refined cell parameters increase with decreasing average grain diameter

A core-surface grain model

grain in polycrystalline sample grain of powder

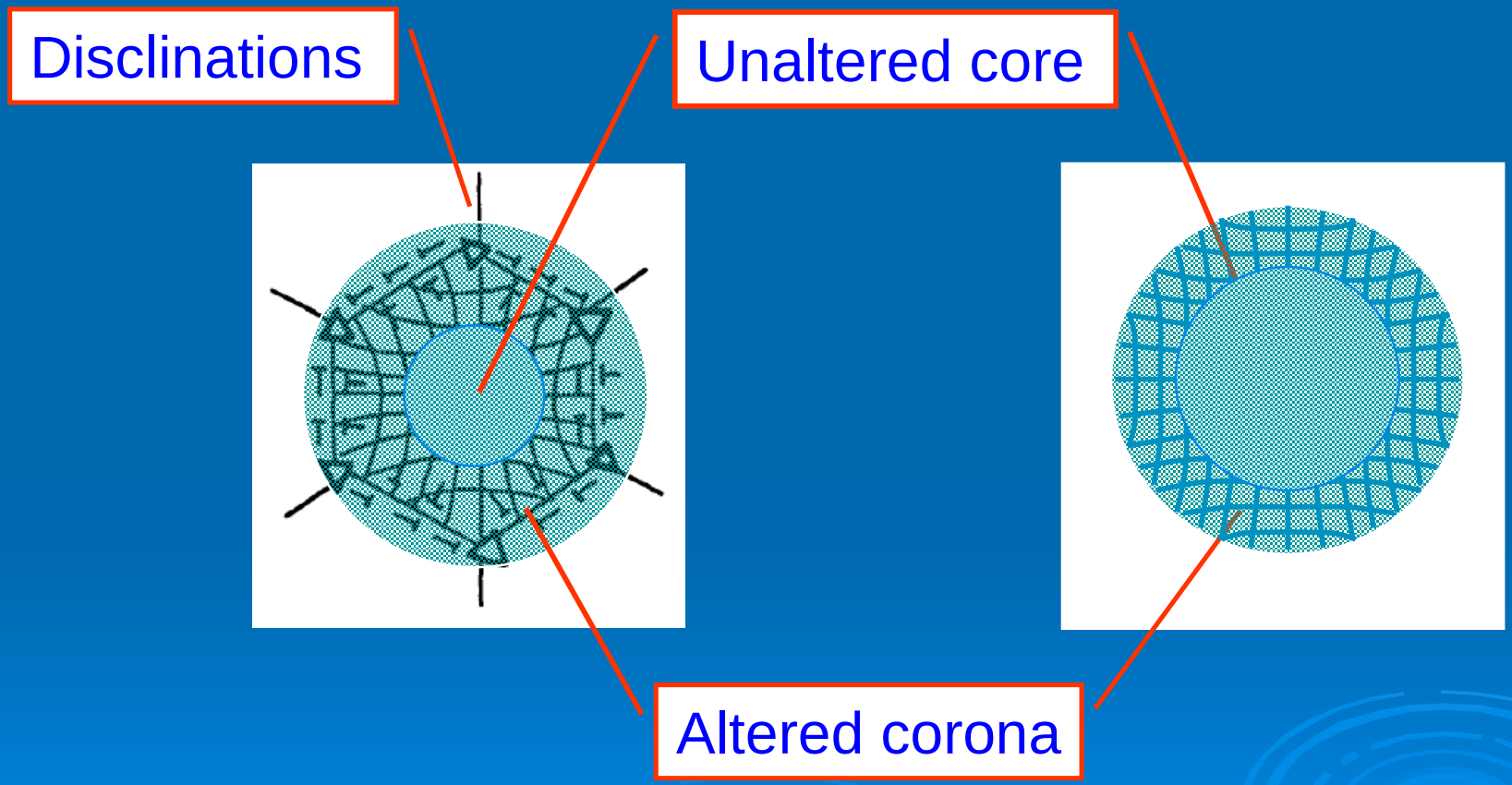

Grain surface relaxation

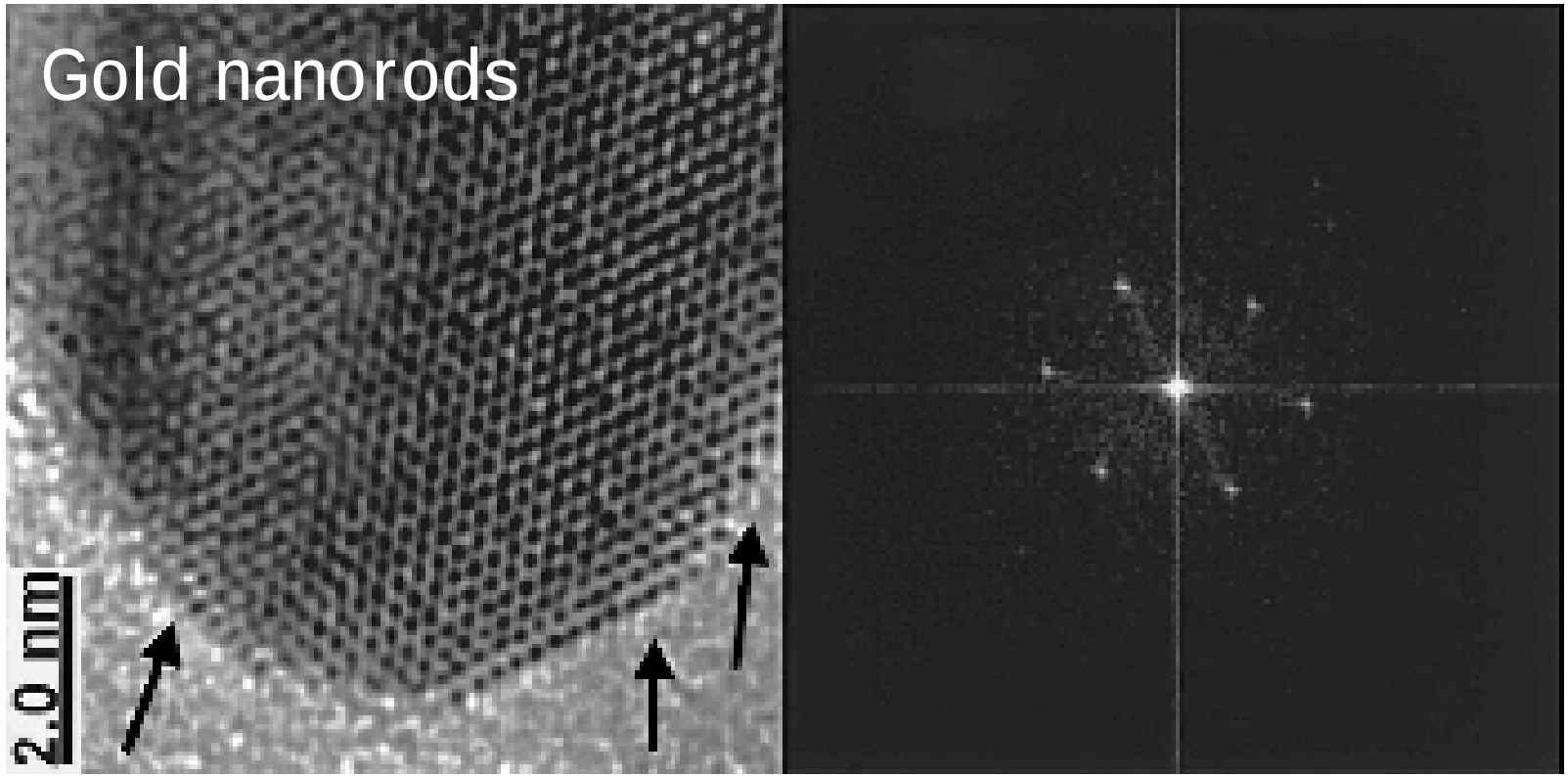

Fig. 2. High resolution image of a tip of a nanorod taken in the "black atom" condition. The (1 1 1) surfaces indicated by an arrow show expansion. The short (1 1 0) facet indicated by a double arrow shows (1 × 2) reconstruction.

Yacaman *et al.*, *Surf. Sci.* 486 (2001) L449-L453

A core-surface grain model

$$\Delta d = \frac{\Delta a}{\sqrt{h^2 + k^2 + l^2}}$$

$$\Delta a = x \frac{x}{|x|} e^{-\frac{R-|x|}{k}}$$

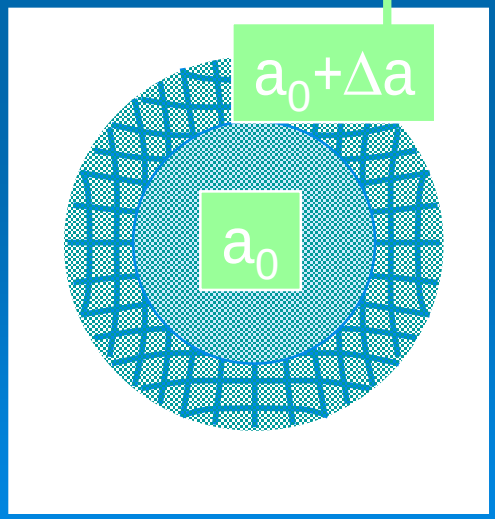

Shift of atomic layers in the outer corona

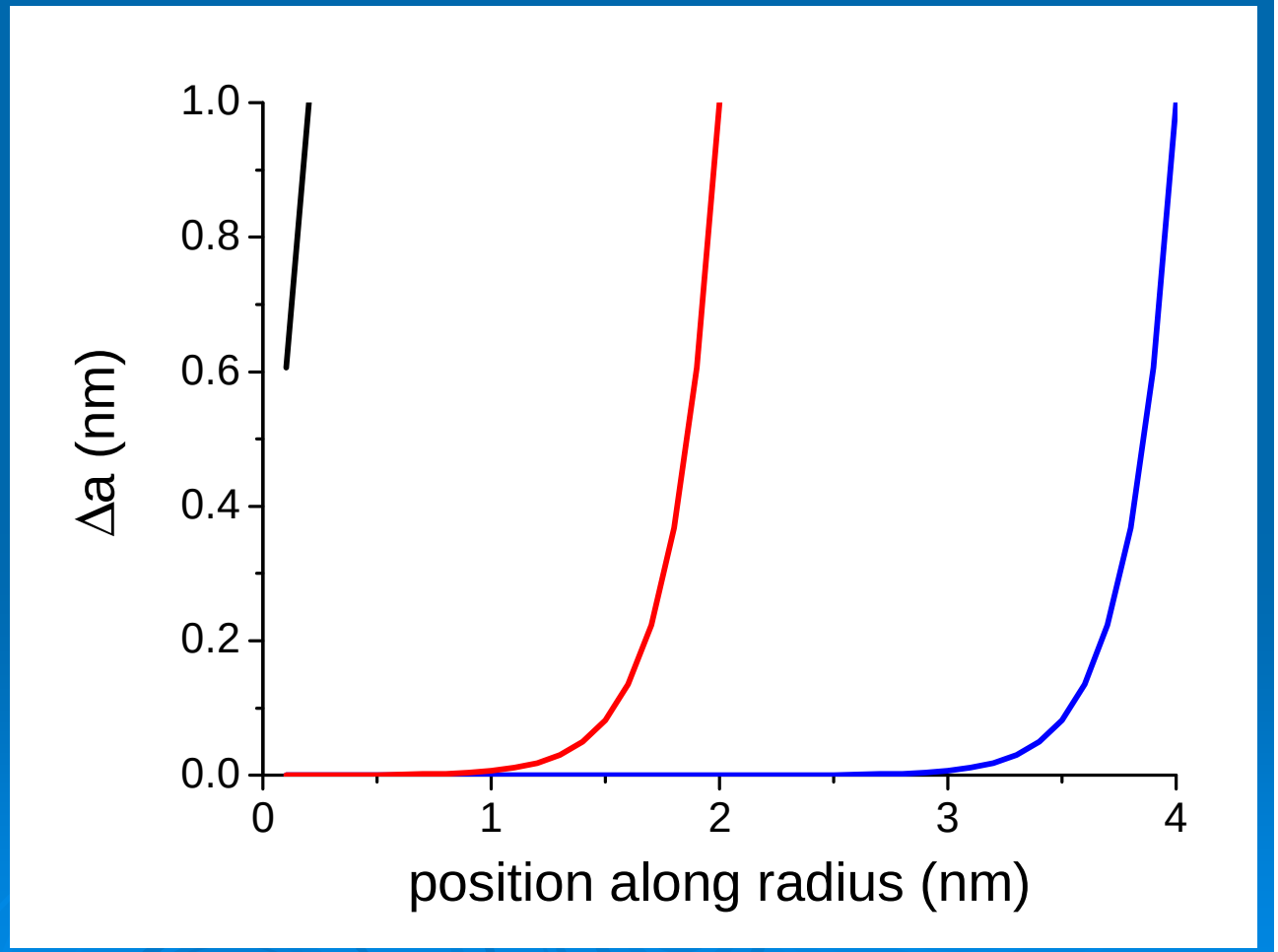

WPPM and grain surface relaxation

Simulation for CeO_2, lognormal distribution of spheres (average 3nm, lognormal variance 0.3), surface relaxation (A=0.05nm, affected zone B=0.3 nm), dislocations (10^{16} m^{-2}, R_e=3nm), twins (1%) and stacking faults (2%)

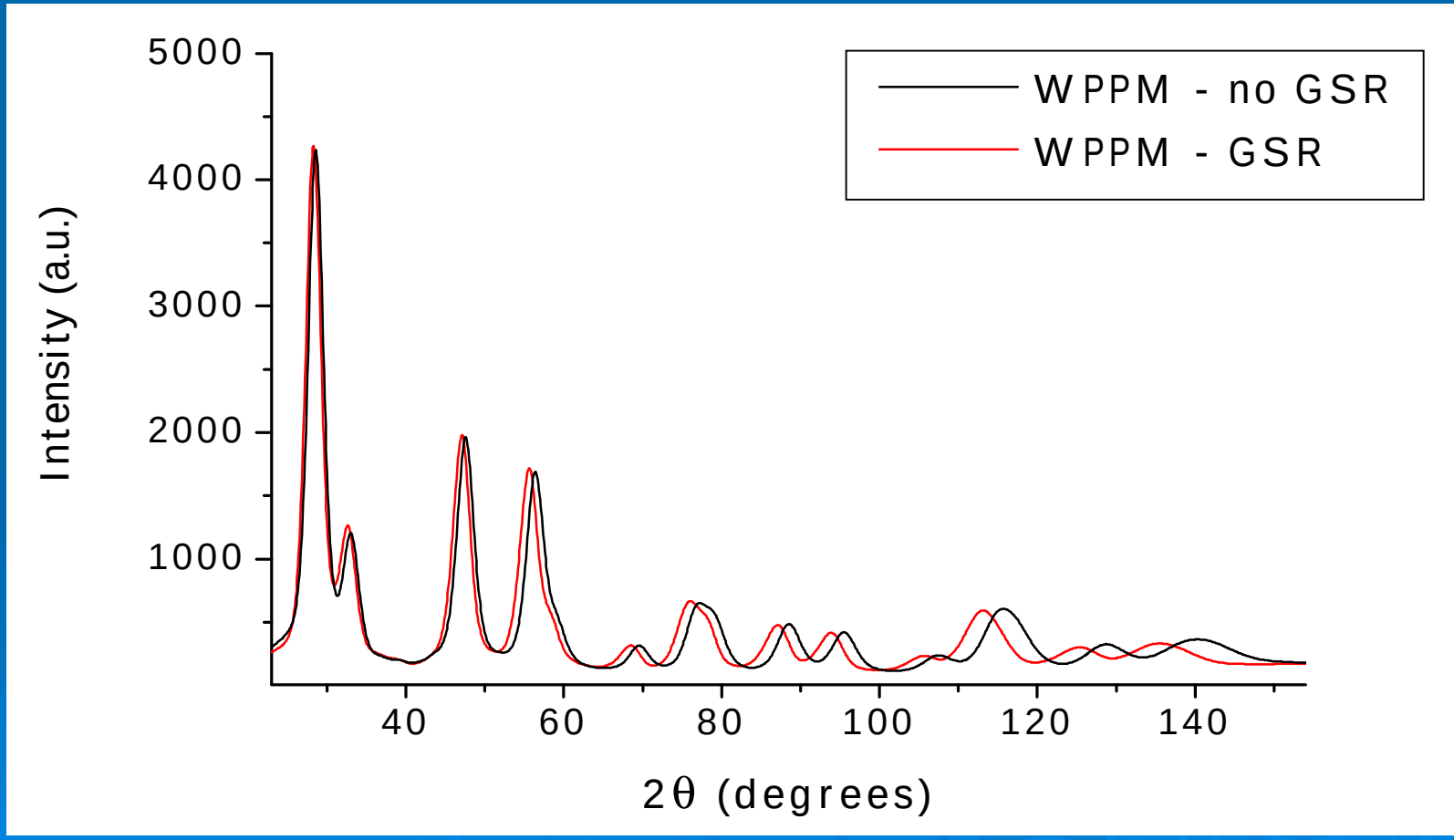

Main effect of GSR is peak shift (a_o changes)

WPPM and grain surface relaxation

		WPPM	GSR - WPPM°
CELL PARAMETER			
cell parameter	(nm)	0.54153(3)	0.541134
SIZE DISTRIBUTION (spherical grains)			
lognormal μ		1.41(2)	1.42(1)
lognormal σ		0.355(7)	0.364(6)
average diameter	(nm)	4.37(1)	4.40(6)
DISLOCATIONS			
dislocation density	(m^{-2})	1.4(10) 10^{16}	1.08(4) 10^{16}
edge dislocations content	(%)	50	50
cutoff radius R_e	(nm)	2(1)	3(1)
A (from elastic constants)		0.1187	0.1187
B (from elastic constants)		0.1618	0.1618
Wilkens parameter M		0.25(1)	0.31(3)
GRAIN SURFACE RELAXATION			
relaxation factor ξ	(nm)		0.008(3)
decay constant κ	(nm)		0.16(4)
STATISTICAL ESTIMATORS			
Rwp		5.51	5.58
Rexp		4.67	4.67
GOF		1.18	1.20

fixed !

(°) Rietveld

WPPM and grain surface relaxation

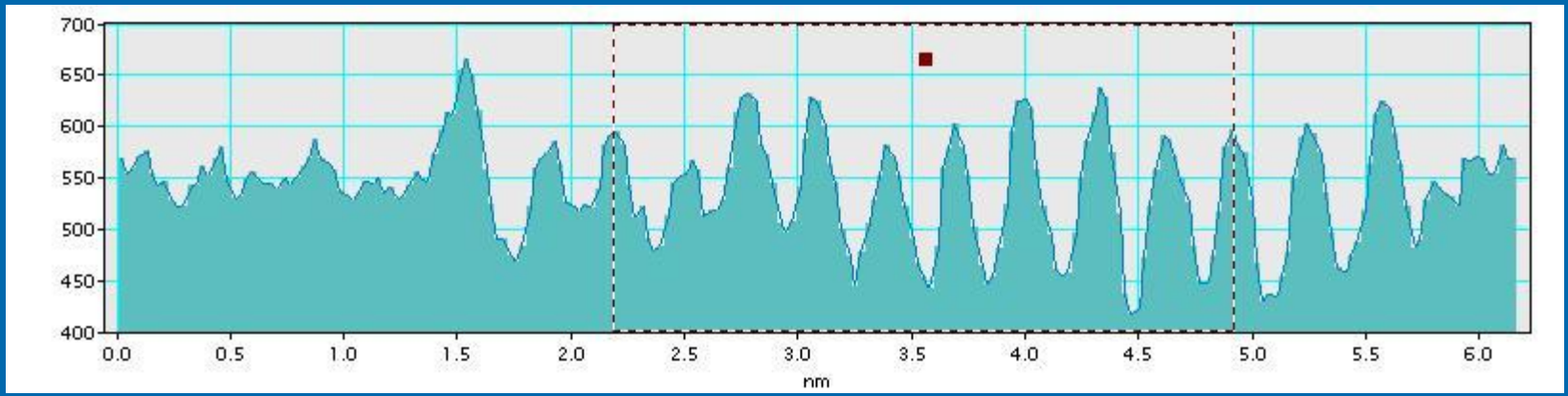

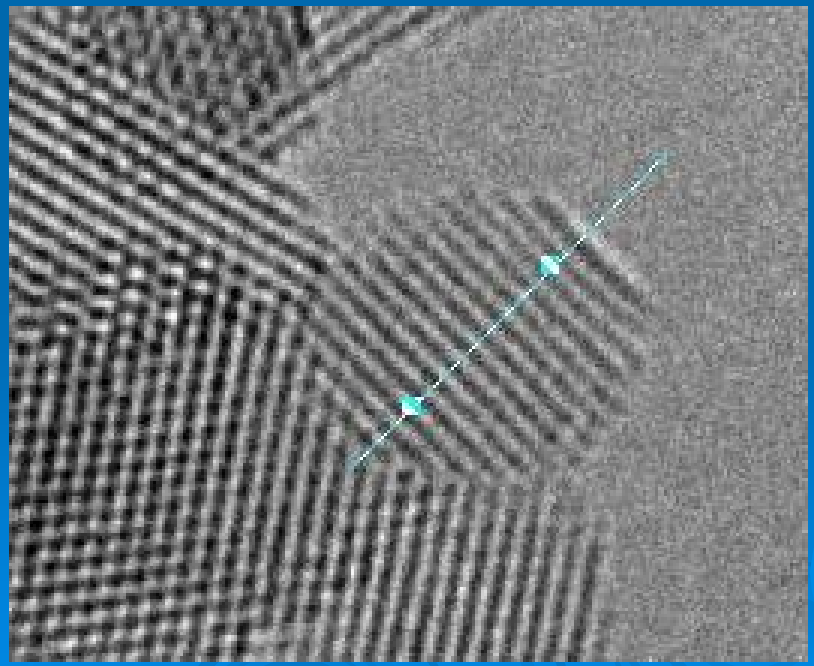

WPPM and grain surface relaxation

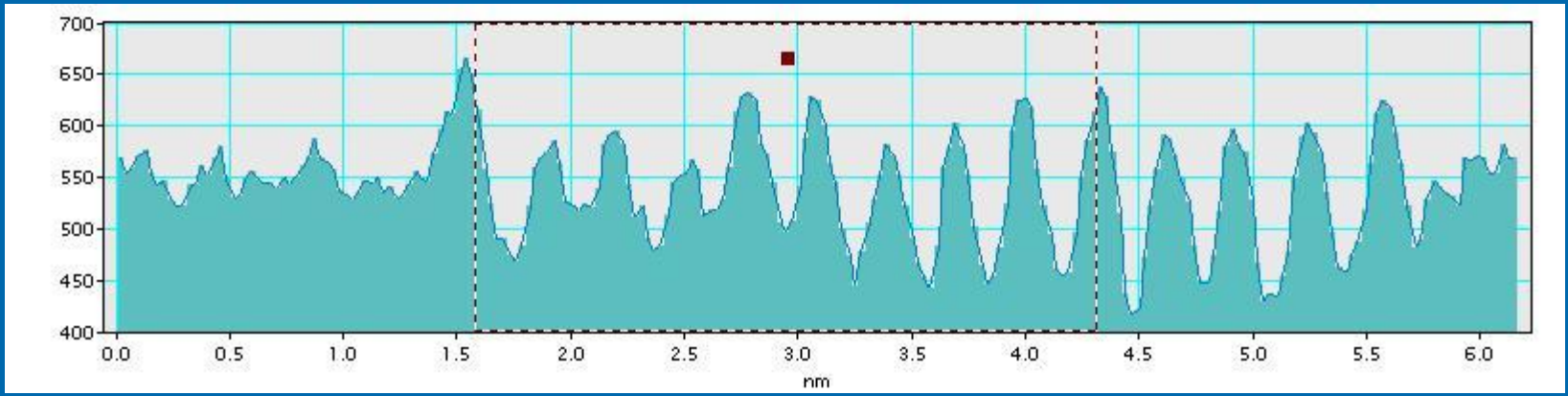

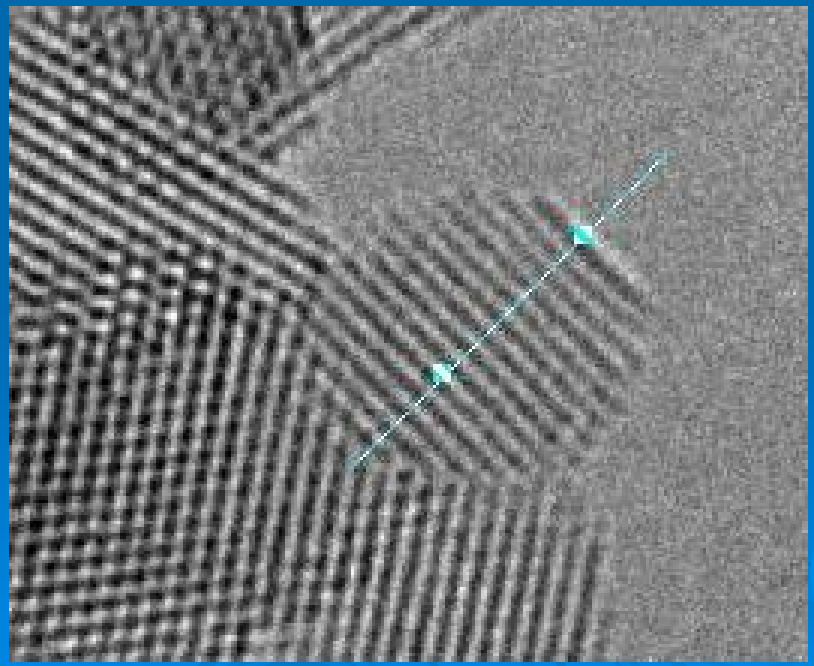

WPPM and grain surface relaxation

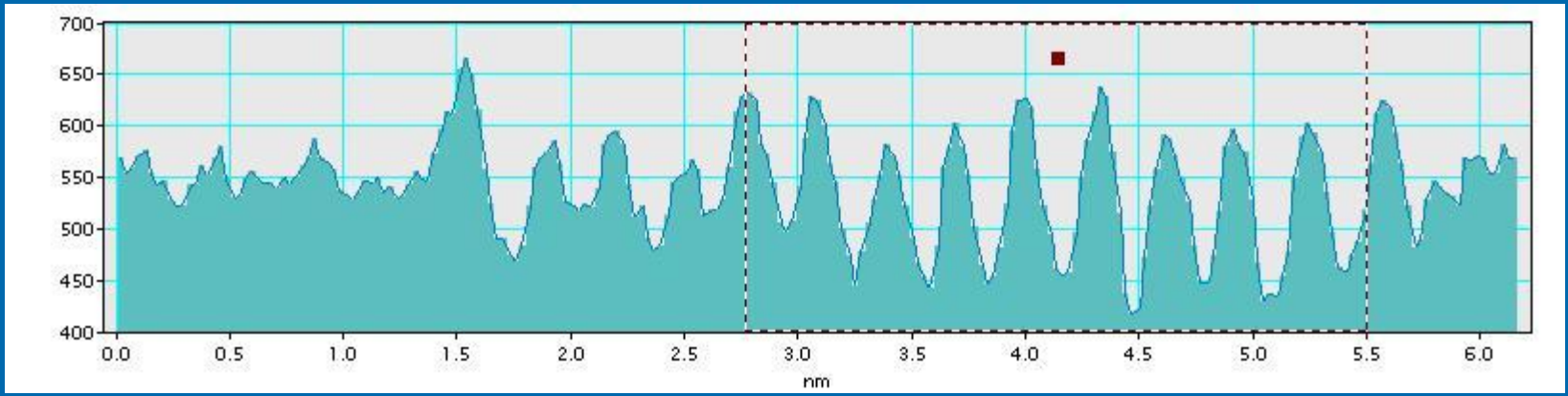

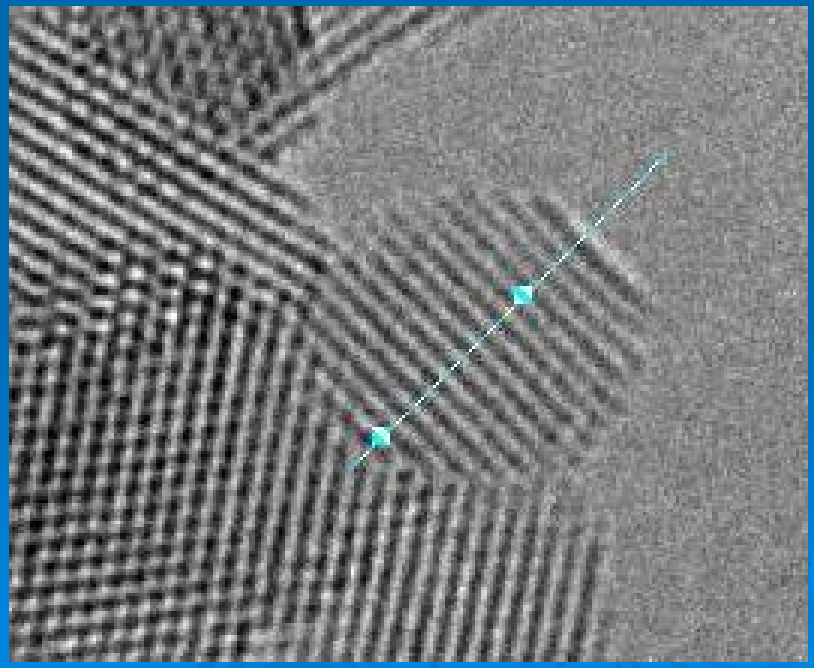

WPPM - GSR - Rietveld

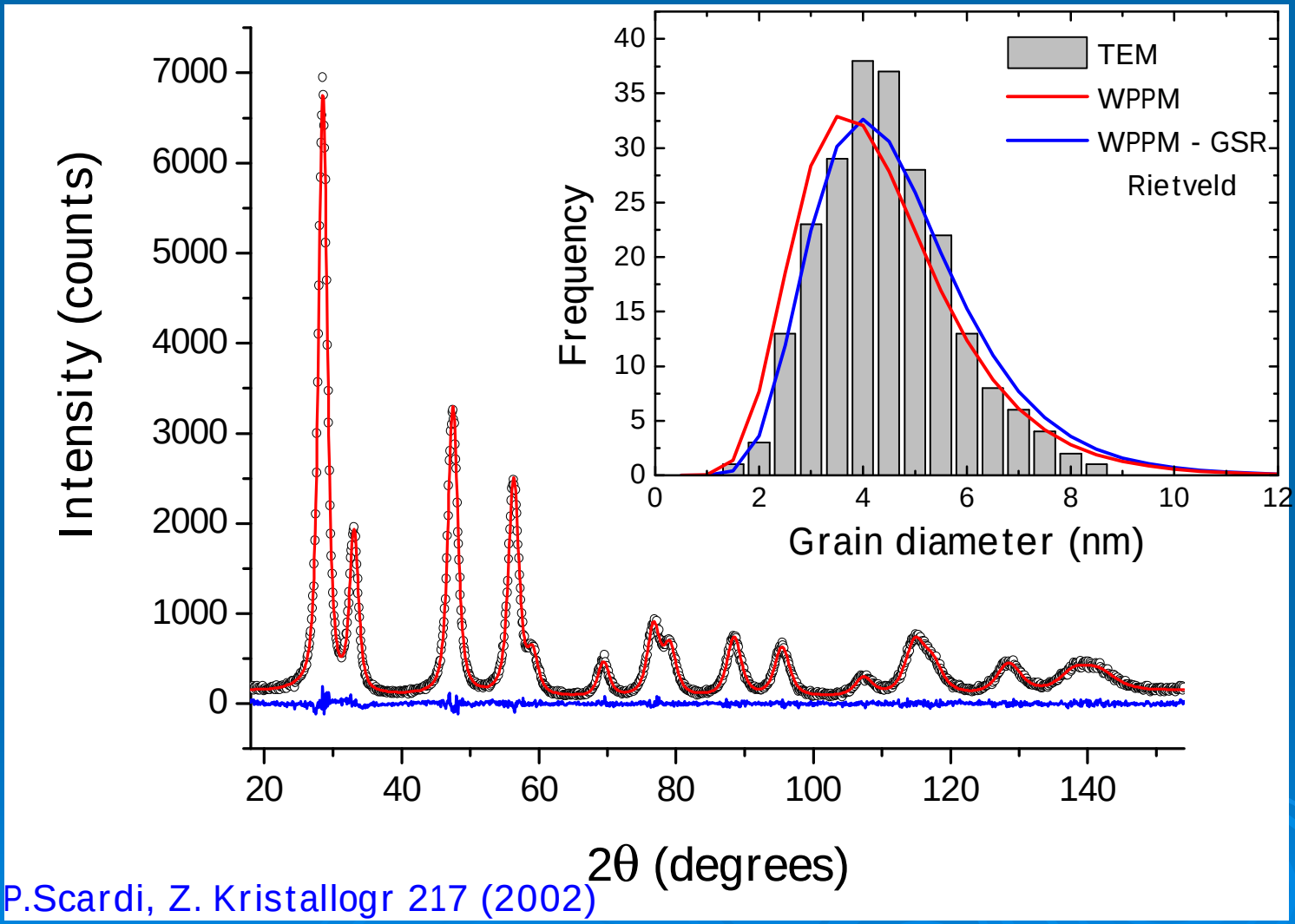

P.Scardi, Z. Kristallogr 217 (2002)

Structure + Microstructure refinement

WPPM: Applications

- Ball milled Fe-Mo powder
- Ball milled nickel powder
- Nanocrystalline cerium oxide
- Cu-Be alloy wear debris
- Anti-Phase Domains in Cu_3Au

WPPM Application: Cu-Be alloy

Applications: wherever good wear resistance or high mechanical properties are desired coupled with a good electrical or thermal conductivity, such as flash welding dies or parts for electrical components

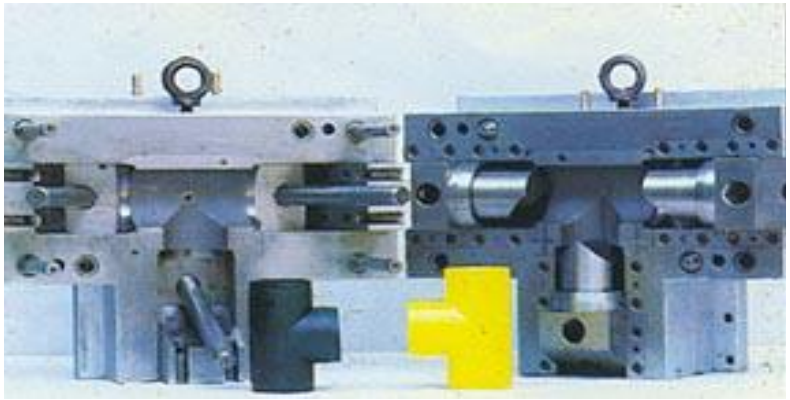

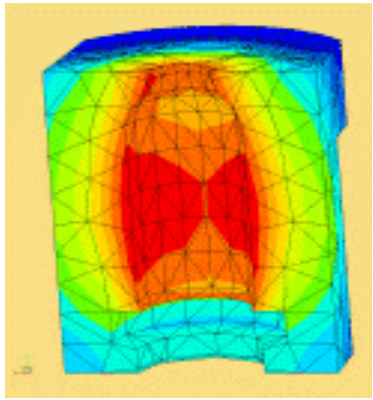

Pin-on-disk wear test:

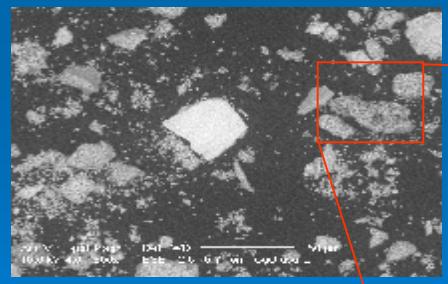

Wear debris

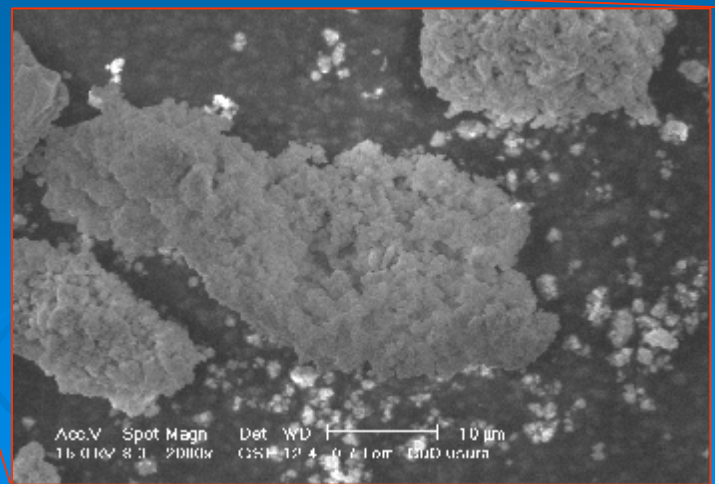

WPPM Application: Cu-Be alloy

Fracture tends to become unlikely in small grains (below Griffith critical length) that tend to store high deformation energy. Analogous behaviour is observed in ball milled ceramics. Cu_2O has a very low specific dislocation energy (≈1/3 of MgO, 1/30 of Fe_3O_4), so a high dislocation density is possible. Shear modulus is just G=10.3 GPa **à** $E \propto Gb^2$

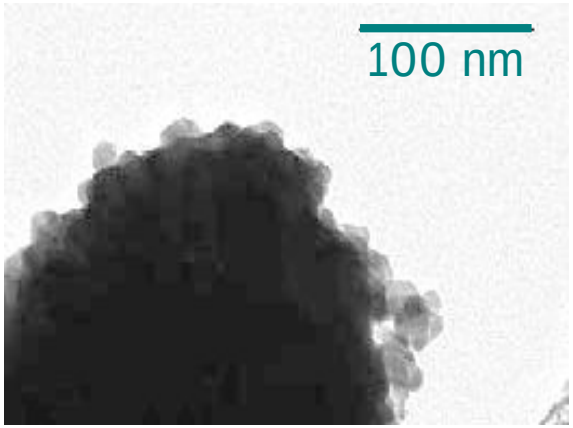

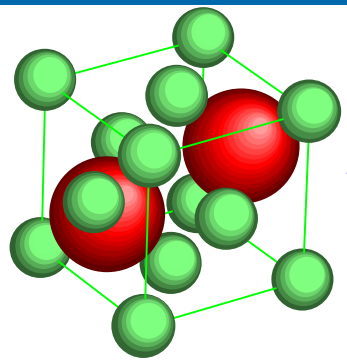

WPPM modelled phases

Cu_2O - Pn-3m

Cu - Fm-3m

(CuO - Cc)

Wear debris are made of Cu_2O (with Cu metal particles).

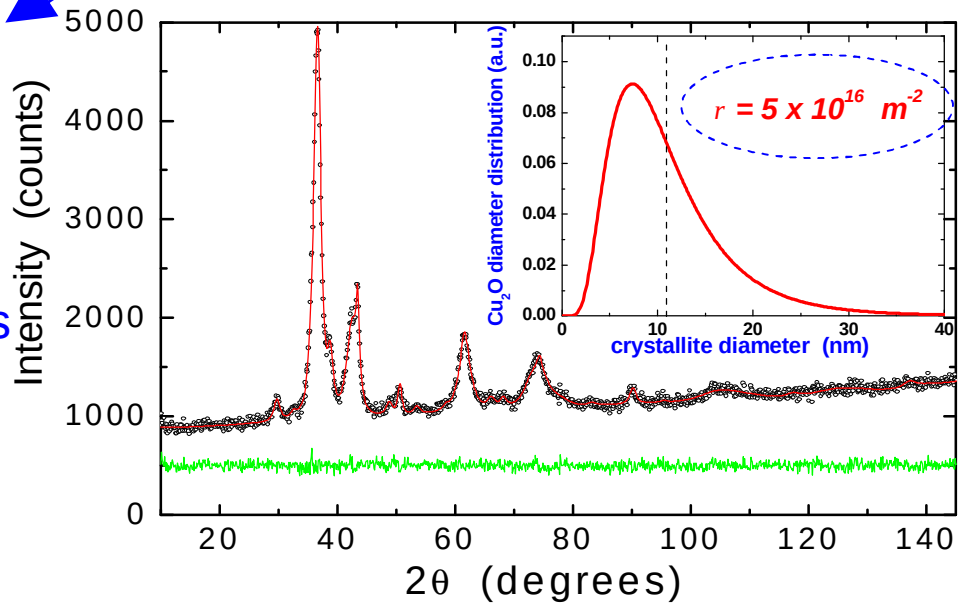

- Cu_2O is stabilised by the very small domain size (<25 nm)
- High angle reflections are so broad owing to the very high dislocation density (≈10^{16} m^{-2}).

Palkar et al. Phys. Rev. B53 (1996) 2167

WPPM: Applications

- Ball milled Fe-Mo powder
- Ball milled nickel powder
- Nanocrystalline cerium oxide
- Cu-Be alloy wear debris
- Anti-Phase Domains in Cu_3Au

WPPM Application: APDs in Cu_3Au

Anti Phase Domains form during the ordering process in Cu_3Au. The o/d process can be thermally activated

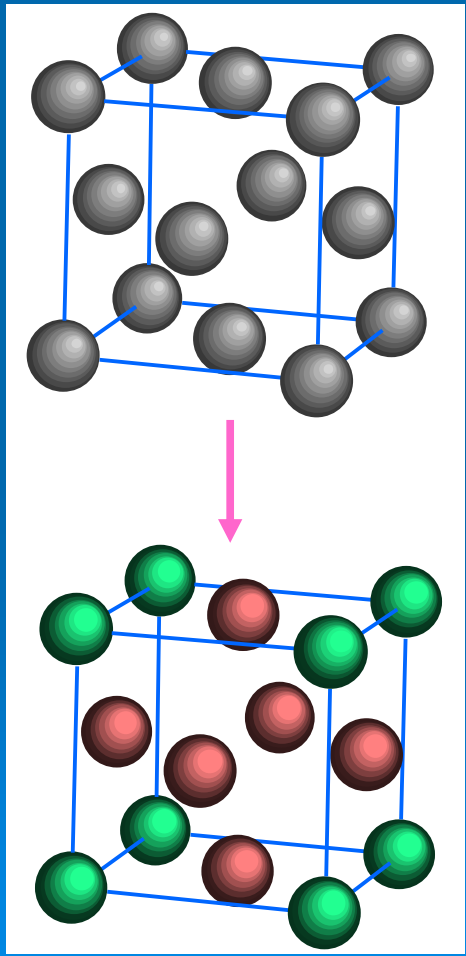

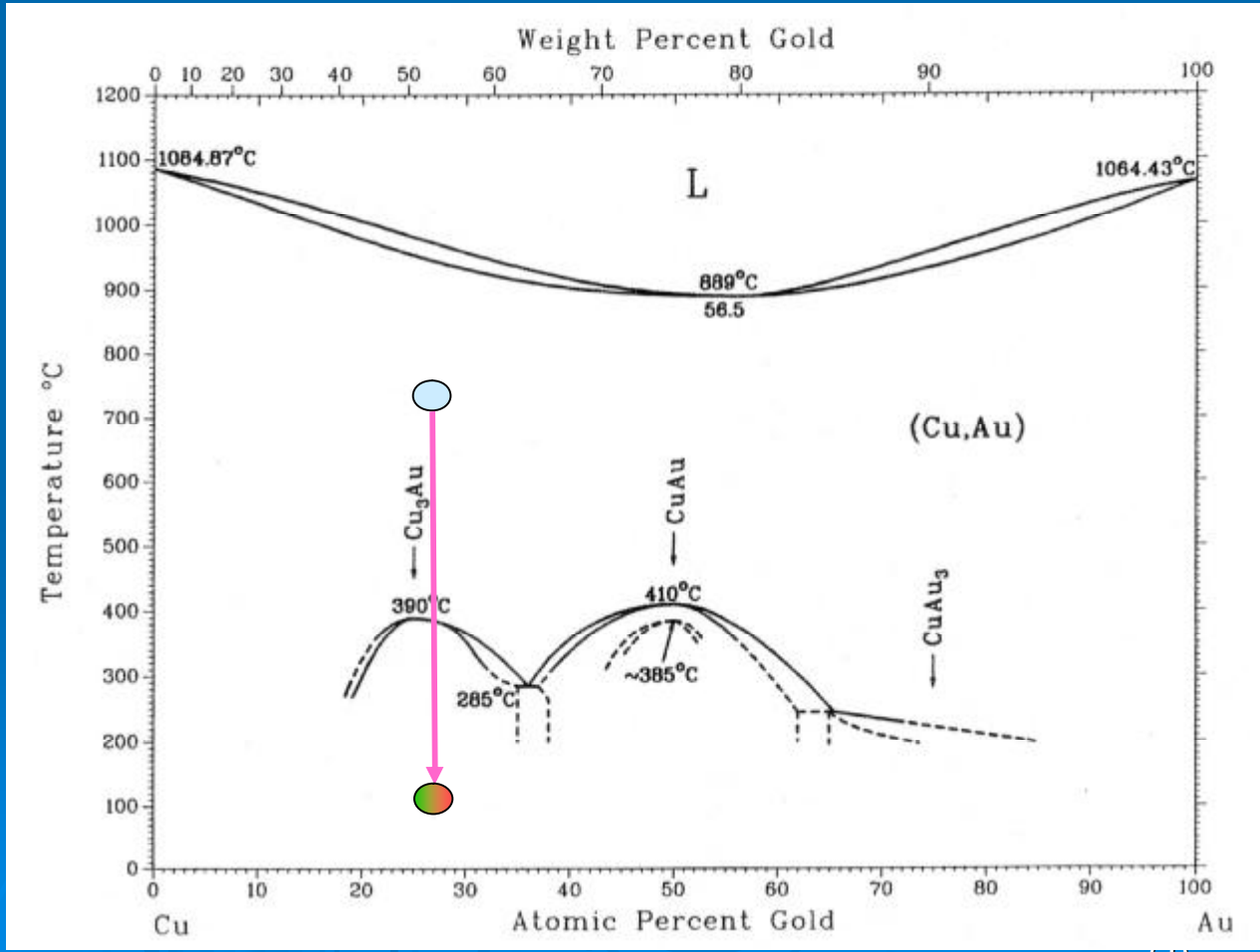

WPPM Application: APDs in Cu_3Au

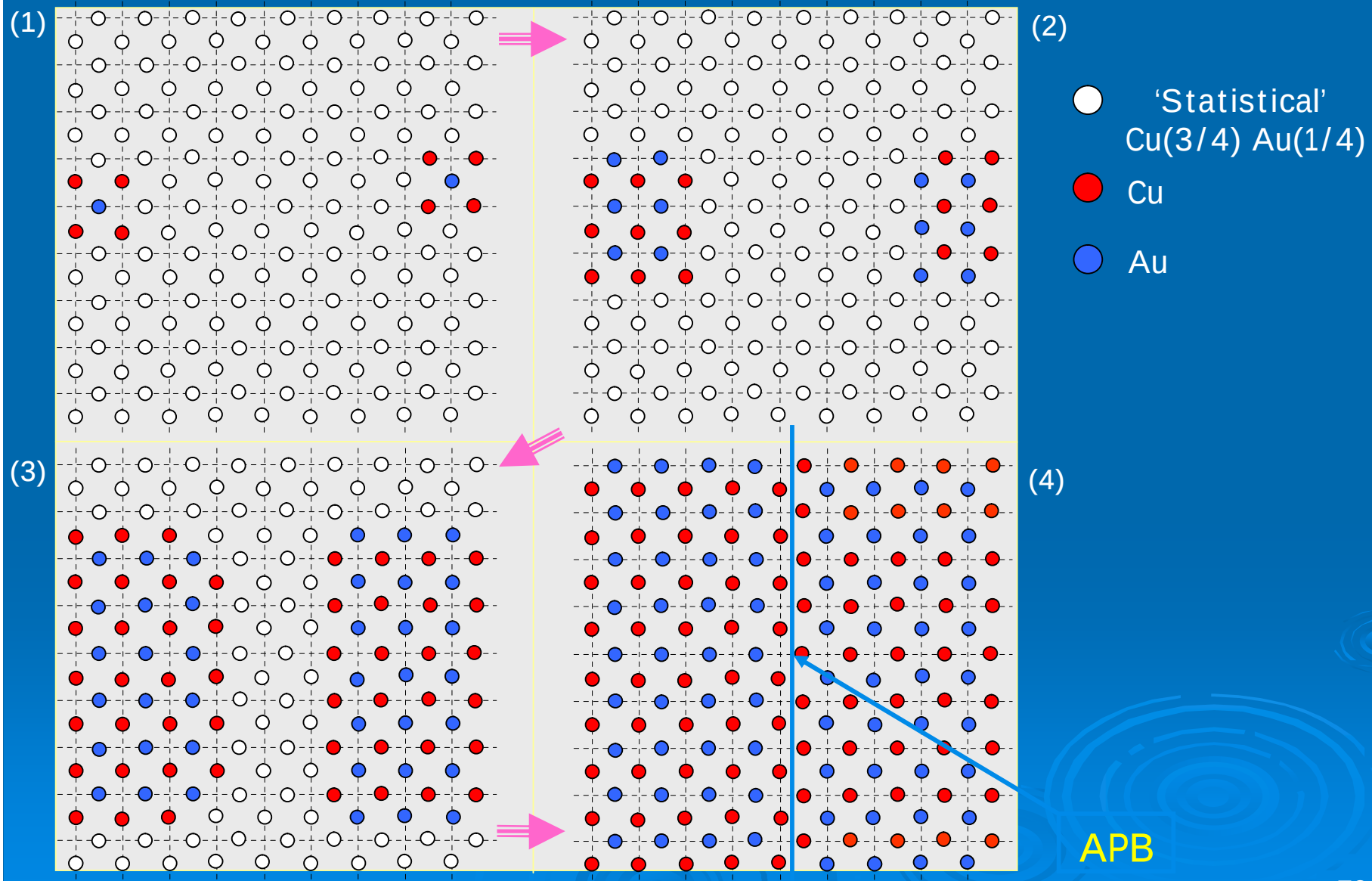

WPPM Application: APDs in Cu_3Au

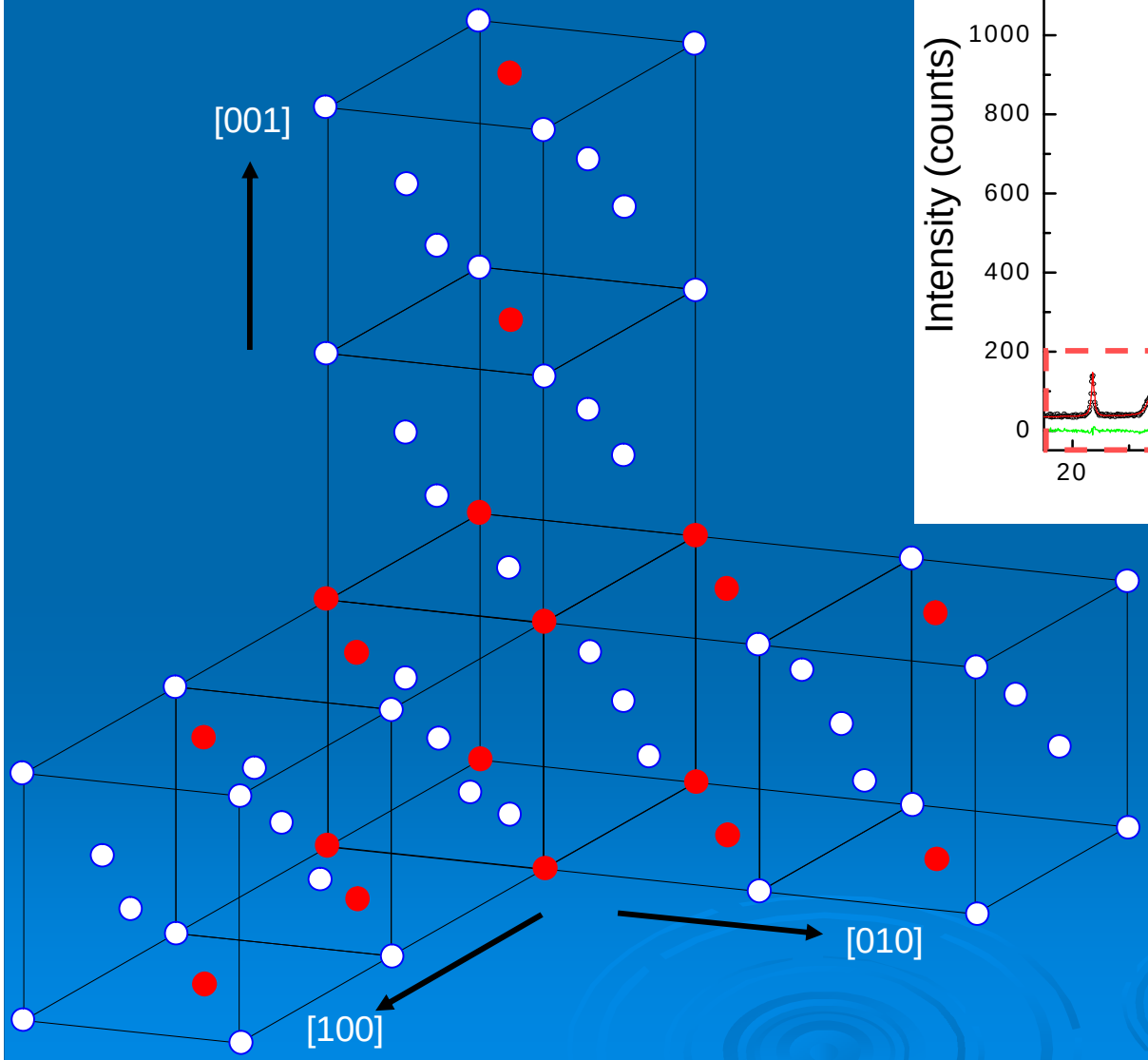

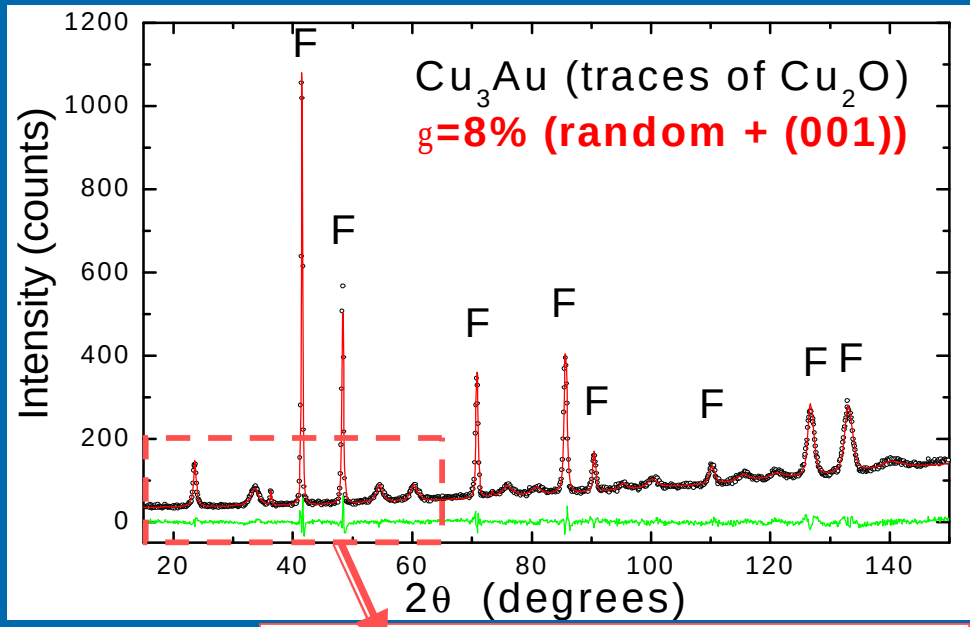

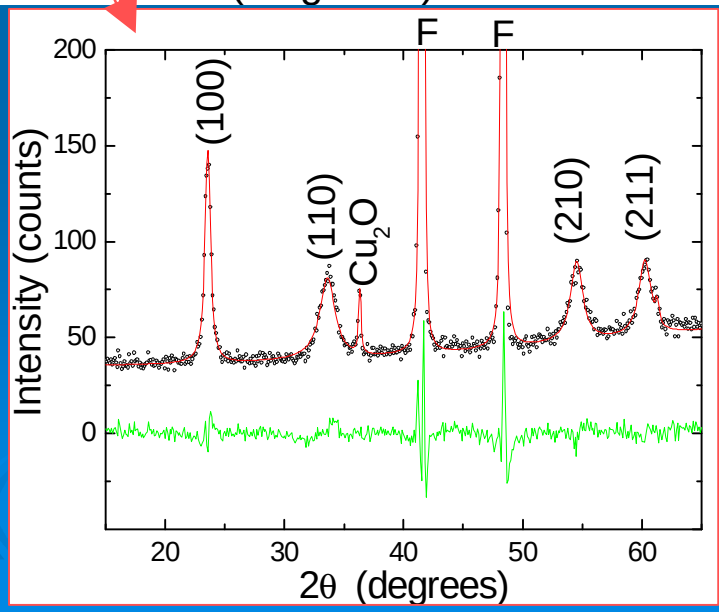

WPPM : conclusions

Main advantages of the WPPM with respect to traditional methods

- correct counting statistics is used;
- problem of peak overlapping is intrinsically solved: peak profiles across the whole pattern are simultaneously refined;
- instrumental profile component can be easily included as well as appropriate background functions;
- different line profile models (e.g., dislocation, faulting, APBs, etc.) can be tested together (parameter correlations can be evaluated);
- structural constraints can be easily implemented: the WPPM algorithm can host a Rietveld routine (or vice-versa) for a simultaneous structure-microstructure refinement
- multiple phase samples can be studied (considering different microstructures) including quantitative phase analysis